Technical Report No. AF-99

PARAMAGNETIC RELAXATION IN DILUTE POTASSIUM FERRICYANIDE

by

Andreas Rannestad

THE JOHNS HOPKINS UNIVERSITY
CARLYLE BARTON LABORATORY
BALTIMORE, MD.

CONTRACT NO. AF 33(616)-6753

DECEMBER 1962

Copy No.

ERRATA

P. 19, Fig. 2:	Delete "$s = 1/2$".
P. 24, line 3:	For "$\hbar$" read "$\bar{h}$".
P. 50, Fig. 12:	For "$T/0.2T$" reads "$1/0.2T$". The quantity equal to $(0.2T+0.01T^7+0.004T^9)^{-1}$ is T_1, not T.
P. 56, Table 2:	The numbers 3.5%, 0.51%, and 0.24% identify the samples and are <u>not</u> relative intensities.
P. 66, line 6:	For "$a(\nu, T)$" read "$a(\nu)T$".
P. 71, line 2:	For "limiting" read "slow".
P. 76, Line 2, 3, 4:	For "xy" read "ζ", for "yz" read "ξ", for "zx" read "η".
Line 4:	For "i" read "-1".
Line 9, 10, 11:	Delete "$\psi_\xi^\pm$", "$\psi_\eta^\pm$", "$\psi_\zeta^\pm$", "$\|\xi, \pm\rangle$", and "$\|\eta, \pm\rangle$".
P. 84, Table 6:	The matrix element in the first row, third column, should be "$V/2$" not "$\lambda/2$"; and that in the third row, third column, should be "$-\lambda/2$", not "$-\Delta/2$".
P. 87, line 6:	Multiply the expression by "$\vec{e}_j$".
P. 94, line 2:	The last formula should read "$\langle \psi^\pm \| x\rangle = -i\langle \psi^\mp \| x\rangle^*$".
P. 95, line 10:	The expression within the magnitude signs should be summed over i.
P. 100, line 1:	The sum should read $\sum_{ik} \| \langle \psi_o^- n_i n_k \| H^1 \| \psi_o^+ n_i - 1, n_k + 1\rangle \|^2$.

THE JOHNS HOPKINS UNIVERSITY
CARLYLE BARTON LABORATORY
BALTIMORE, MARYLAND

Technical Report No. AF-99

PARAMAGNETIC RELAXATION IN DILUTE POTASSIUM FERRICYANIDE

by

Andreas Rannestad

Program Element Code: 62405454
Technical Area: 760D
Task: 403601

Project Engineer:

1/Lt. W. F. H. Ring, Extension 33222
Aeronautical Systems Division
Wright-Patterson Air Force Base, Ohio

Contract No. AF 33(616)-6753 December 1962

ACKNOWLEDGMENT

The author wishes to thank Dr. P. E. Wagner of the Department of Electrical Engineering and Mr. J. M. Minkowski of the Carlyle Barton Laboratory for their many fine suggestions and excellent guidance in the preparation of this paper.

He is deeply indebted to Dr. Wagner for the many illuminating and fruitful discussions and the countless hours of his assistance in the design of equipment and the conduct of the experiment. Without Dr. Wagner's excellent guidance this work would not have been possible. Thanks are extended to Mr. J. M. Minkowski, Dr. A. Kiel, and other members of the Carlyle Barton Laboratory staff for many helpful discussions, and to Mr. J. W. Leight for growing all crystals used in the experiment. Thanks are also extended to the others members of the Department of Electrical Engineering Faculty, particularly Dr. Ferdinand Hamburger, Jr., and Professor Thorstein Larsen, for making the author's stay here so pleasant and fruitful. He thanks Mrs. Dolores A. Scholl for her careful typing of the paper, and Mr. C. M. LaPorte for his accurate preparation of the illustrations.

The author is indebted to Dr. J. G. Castle, Jr., and Dr. D. Feldman of the Westinghouse Research Laboratories for calibrating the temperature sensor. The generosity of the International Telephone and Telegraph Company in providing the X-band traveling wave tube, and the helpful advice of Mr. Arnold Hansen, are gratefully acknowledged.

TABLE OF CONTENTS

TABLE OF CONTENTS CONTD

LIST OF ILLUSTRATIONS

Page

ABSTRACT

The paramagnetic relaxation times for the ground state Kramers doublet of iron present as a dilute substitutional impurity in potassium cobalticyanide have been measured for iron concentrations from 0.24% to 3.5%, over the temperature range 1.25°K to 4.5°K. Measurements were performed at 1.8 Gc/s and at 8.5 Gc/s. The "Fast Passage-Recovery" method was used for the measurements, and a description of the microwave spectrometers and associated equipment is included.

A review of the relevant crystal field theory is given and includes a calculation of the energy levels for the three lowest Kramers doublets. The theory of spin-lattice relaxation is reviewed and compared with the experimental findings.

At low iron concentration the spin lattice times measured at 1.8 Gc/s are found to display a ninth-power temperature variation over five decades of time, in agreement with the theory of the Raman process. No change in the Raman rate is observed between 1.8 Gc/s and 8.5 Gc/s. At 8.5 Gc/s the linear temperature dependence for the direct relaxation process is also verified. The theoretical fourth-power frequency dependence of the direct process is not verified dir-

ectly by comparative measurements at the two frequencies, because the low frequency rates are dominated by the Raman process, even at the lowest temperature employed. The frequency dependence cannot, however, be much weaker than ν^4 and is definitely larger than ν^3.

At higher concentrations, added relaxation mechanisms appear and are tentatively attributed to: (1) cross relaxation from the main line to "extra" lines that are observable only at higher concentrations; and (2) cross relaxation from an isolated ion to ion pairs that are strongly coupled by exchange. At the highest concentrations a competing fast process is also observed, but is not fully understood.

I. INTRODUCTION

The now familiar phenomenon of paramagnetic resonance is of relatively recent origin. The first paramagnetic resonance experiment was performed in 1945 by Zavoisky (1). However, the closely related paramagnetic relaxation phenomenon was discussed by Waller (2) as early as 1932, and was first observed by Gorter (3) in 1936. Casimir and DuPré (4, 5) then developed a thermodynamic treatment; Kronig (6) extended Waller's treatment; and in 1939 - 40 a major advance was made by Van Vleck (7, 8).

Van Vleck, in agreement with Waller, considered two different relaxation mechanisms: the spin-lattice interactions, which give rise to the spin-lattice relaxation time T_1; and the spin-spin interactions, which give rise to the (usually) shorter spin-spin relaxation time T_2. More recently a third process, termed cross relaxation or spin diffusion, has been added.

Van Vleck and Waller also predicted two different spin-lattice relaxation processes, one predominant at low temperatures and the other at higher temperatures; but their interpretations of the underlying mechanisms were entirely different. Waller (2) postulated that the relaxation was due to phonon modulation of the magnetic dipolar interactions between ions, while Van Vleck (7, 8)

postulated a modulation of the crystalline electric field acting on the ions. The latter theory is in general accepted as being correct.

With the development of experimental methods for paramagnetic resonance measurement, relaxation phenomena in paramagnetic crystals have been studied more intensively, both theoretically and experimentally. The recent interest in solid state masers has also acted as a stimulant.

Most measurements of the relaxation time T_1 have been made on systems with complicated resonance spectra, so that the results are difficult to interpret. In the present work an ion-crystal combination having only a single resonance transition was used, namely Fe^{3+} present as a dilute substitutional impurity in $K_3Co(CN)_6$. Paramagnetic resonance data for this material have been reported by Baker et al. (9) and interpreted by Bleaney and O'Brien (10). There is only one line coming from the lowest Kramers doublet.

Recently the spin-lattice relaxation time for $K_3\left[Fe, Co\right](CN)_6$ was measured at about 9Gc/s by Paxman (11) and by Bray et al. (12). For crystals with an Fe^{3+} concentration of more than one-half per cent, the latter authors found the spectrum to be more complicated than might be expected. This is presumably due to exchange between iron ions and possibly to polytypism (13) as well.

A literature search reveals essentially no experimental studies of the dependence of T_1 on frequency. For the case in point the Van Vleck (8) theory indicates no dependence of $1/T_1$ on frequency in the high temperature "Raman" region and a fourth power dependence in the low temperature "direct" region.

To the author's knowledge, the only really systematic studies of a frequency dependence in any paramagnetic material have been made on an entirely different system, namely donor impurities in silicon, by Honig and Stupp (14), by Feher and Gere (15), and by Wilson and Feher (16).

In view of this, L- and X-band microwave spectrometers were constructed so that temperature and concentration dependence of T_1 could be examined at widely different frequencies. To avoid complications due to possible spin diffusion within the line, as reported by Bray et al. (12), and to be able to test for evidence of phonon imprisonment (17-21), the "Fast Passage-Recovery" method described by Castle et al. (19), was chosen instead of the experimentally simpler "Pulse Saturation-Recovery" method described by Davis et al. (23) and used by Paxman (11) and Bray et al. (12).

In keeping with the Van Vleck theory, the author anticipated a strong frequency variation in the direct region and none in the

Raman region; however the experimental results were complicated by a concentration dependent mechanism not contained in the Van Vleck theory and thus did not fully reflect the expected frequency variation.

II. THEORETICAL AND EXPERIMENTAL REVIEW

A. CRYSTAL FIELD THEORY

The energy levels of an ion situated in a crystal are modified by the crystalline surroundings. The predominant interactions in the free ion are the Coulomb forces between electrons and the nuclear charge and among the electrons themselves. These interactions can be divided into two parts, a spherically symmetric term ($\mathcal{H}_c$), which is estimated from atomic spectra to be of the order of 10^5 cm^{-1}, and a non-central term ($\mathcal{H}_{nc}$) of the order of $5 \cdot 10^3$ cm^{-1}. The spin-orbit interaction ($\mathcal{H}_{LS}$) between the electron spins and the orbital momenta must also be added and is of the order of 10^2 cm^{-1} for the iron group.

The strength of the crystalline field (V) can usually be treated in one of three limiting cases: the strong field, where $\mathcal{H}_c > V > \mathcal{H}_{nc}$; the medium field, $\mathcal{H}_{nc} > V > \mathcal{H}_{LS}$; and the weak field, $\mathcal{H}_{LS} > V$. The $K_3\left[Fe, Co\right](CN)_6$ crystal is an example of the first case.

Crystal field theory has been covered extensively by many authors (24-28), and will not be reviewed in detail. However, to provide an understanding of the origin of the ground-state Kramers doublet in $K_3\left[Fe, Co\right](CN)_6$, a simple outline of the theory pertaining to this case will be given.

Consider a positively charged paramagnetic ion residing in a near octahedron of negatively charged diamagnetic ions. Let the central ion have only one electron in the 3d-shell ($\ell = 2$, $s = 1/2$). Corresponding to the $(2\ell + 1)$ - fold orbital degeneracy there are five d-orbitals. From linear combinations of the angular functions for d-electrons, $e^{\pm 2i\phi} P_2^2(\cos\theta)$, $e^{\pm i\phi} P_2^1(\cos\theta)$, and $P_2^0(\cos\theta)$, one can form the wavefunctions $\frac{xy}{r^2}$, $\frac{yz}{r^2}$, $\frac{zx}{r^2}$, $\frac{x^2-y^2}{r^2}$, and $\frac{2z^2-x^2-y^2}{r^2}$ for the d-orbitals. The corresponding charge cloud distributions together with the wavefunctions are shown in Figure 1. For the free ion the energies corresponding to all the d-orbitals are the same. When a crystalline electric field of cubic symmetry is added some splitting occurs; the so-called "t" orbitals, $\frac{xy}{r^2}$, $\frac{yz}{r^2}$, and $\frac{zx}{r^2}$, split away from the "e" orbitals, $\frac{x^2-y^2}{r^2}$ and $\frac{2z^2-x^2-y^2}{r^2}$. Since the d-electrons will be repelled by negatively charged nearest neighbor ions, the negative charge clouds representing the orbitals will avoid negative ions, causing the average energy of the t-orbitals to be lower than that of the e-orbitals in the octahedral symmetry.

This example was used since it can easily be related to Fe^{3+} ions in $K_3Co(CN)_6$ crystal by substituting $(CN)^-$ dipoles for the negatively charged ions and by realizing that the total spin of Fe^{3+} in the strongly bound cyanide complex is 1/2. Since one can get a reduction in energy according to Hund's rule with all spins parallel, one expects a total spin of 5/2 rather than 1/2 for Fe^{3+}.

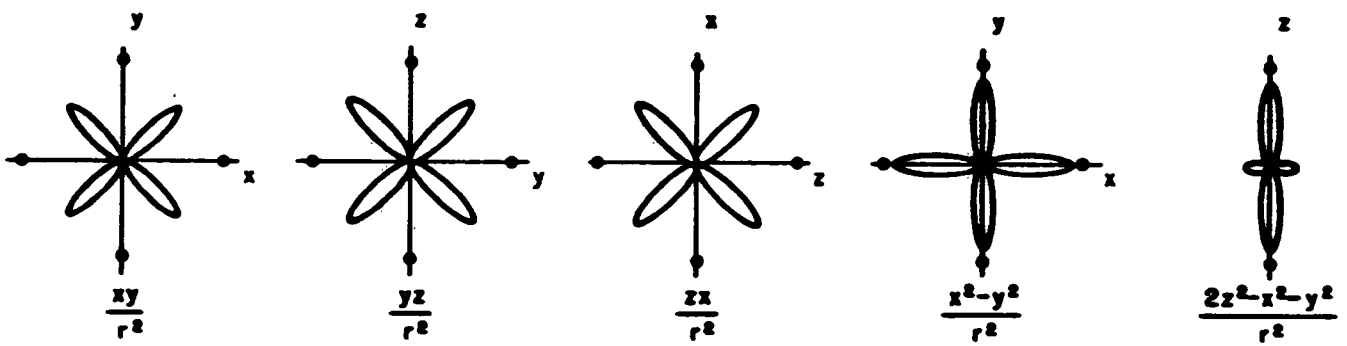

$$\psi_{xy} = \frac{1}{i\sqrt{2}}(|2,2\rangle - |2,-2\rangle) \qquad \psi_{zx} = \frac{1}{\sqrt{2}}(|2,1\rangle - |2,-1\rangle) \qquad \psi_{z^2} = |2,0\rangle$$

$$\psi_{yz} = \frac{i}{\sqrt{2}}(|2,1\rangle + |2,-1\rangle) \qquad \psi_{x^2-y^2} = \frac{1}{\sqrt{2}}(|2,2\rangle + |2,-2\rangle)$$

FIGURE 1: DIAGRAM OF THE CHARGE CLOUDS ASSOCIATED WITH THE d-ORBITALS OF A PARAMAGNETIC ION, AND THE ASSOCIATED WAVE FUNCTIONS.

However, to obtain a spin of 5/2 two electrons would have to occupy the much more energetic e-orbitals and thereby more than compensate for the lowering of energy due to parallel spins. Thus, the spin is 1/2 and the ground state manifold t_2^5 is complementary to t_2^1 (Appendix I).

In the iron-cyanide complex there is a distortion from cubic symmetry which can be treated formally as rhombic. If this distortion and the spin-orbit coupling are taken together as a joint perturbation on the cubic field model, one can show that the t-orbitals split into three distinct Kramers doublets. Kramers' theorem (29), which demands that a state made up from an odd number of electrons have at least a twofold degeneracy in the presence of an electrostatic field of time reversal symmetry, shows that no additional crystalline electrostatic field splitting can occur. Because the Zeeman Hamiltonian is not invariant under time reversal, addition of an external magnetic field will lift the Kramers degeneracy. Paramagnetic resonance can then be observed between the split members of the doublet.

The lowest electronic energy levels for a d^5 iron-cyanide complex are shown in Figure 2. A more detailed discussion of the crystal field theory is given in Appendix I.

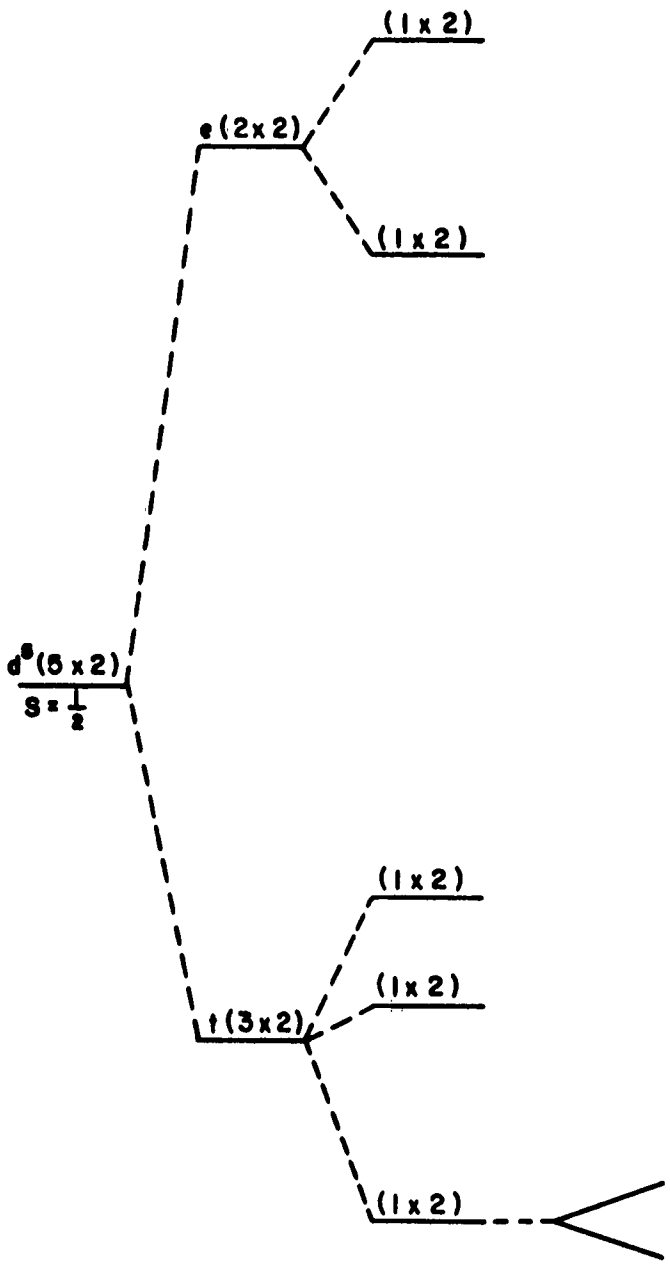

FIGURE 2: THE LOWEST ELECTRONIC ENERGY LEVELS FOR A d^5 CYANIDE COMPLEX.

B. RELAXATION EFFECTS

1. General

Paramagnetic relaxation had been observed by Gorter and other Dutch physicists (3, 30) long before any paramagnetic resonance had been seen. Relaxation times were obtained from dispersion measurements performed at audio or low radio frequencies. Since the apparatus was not very sensitive, concentrated rather than dilute crystals were used. In addition, the method could not distinguish between relaxation paths coming from different transitions in multilevel spin systems. For these reasons the results obtained cannot readily be compared with measurements made on dilute paramagnetic substances by resonance techniques.

Returning now to the iron-cyanide complex discussed in the last section, one notes that the occupancies of the different states follow the Boltzmann law

$$\exp(-E/kT) \quad ,$$

where E is the energy, k the Boltzmann constant, and T the temperature. At liquid helium temperatures only the lowest Kramers doublet is occupied. An applied radio frequency field induces magnetic dipole transitions between the two states with equal probability, and, as the lower state has a larger occupancy, a net absorption of radiation results. This absorption is in fact

the paramagnetic resonance and can be observed if, for example, the crystal is placed in a resonant cavity and the reflected power monitored as the Zeeman field is swept through its resonant value. Ideally, paramagnetic resonance would show up as a sharp line; but various mechanisms, for example, the spin-lattice, magnetic spin-spin, and exchange interactions, give rise to broadening. In the present study the spin-lattice time was too long to cause appreciable broadening at the temperatures of interest, and the other interactions are not the subject of the work.

The spin-lattice interaction gives a perturbed spin system a way to relax back to thermal equilibrium. The relaxation occurs through transfer of energy from the ions to vibrational modes of the crystal lattice. The spin-lattice relaxation time T_1 is a measure of the rate of the process and is defined for a single transition by,

$$\frac{d}{dt}(\Delta N - \Delta N_o) = -(1/T_1)(\Delta N - \Delta N_o) \quad ,$$

where

$\Delta N = n_1 - n_2$ = population difference between the two levels,

$\Delta N_o = n_{10} - n_{20}$ = population difference between the two levels at equilibrium,

and

$N = n_1 + n_2$.

If one considers two energy levels 1 and 2 at equilibrium;

$$\dot{n}_{10} = -W_{12} \cdot n_{10} + W_{21} \cdot n_{20} = 0 \quad .$$

where W_{12} and W_{21} are the probabilities of spin-lattice transitions from levels $1 \rightarrow 2$ and levels $2 \rightarrow 1$ respectively. But

$$\frac{n_{10}}{n_{20}} = e^{-\frac{(E_1 - E_2)}{kT}} = e^{-\frac{\hbar\omega_{12}}{kT}} ,$$

where $\hbar\omega_{12} = E_1 - E_2$; hence

$$\frac{W_{21}}{W_{12}} = \frac{n_{10}}{n_{20}} = e^{-\frac{\hbar\omega_{12}}{kT}} \cong 1 - \frac{\hbar\omega_{12}}{kT} ,$$

since $\hbar\omega << kT$, for cases considered herein.

By first applying a large radio frequency field pulse one can make the two populations equal and observe the relaxation afterwards with a much smaller radio frequency monitoring signal. If the monitoring signal is small enough to satisfy $W << W_{12}, W_{21}$, where W is the radio frequency transition probability, one can write

$$\dot{n}_1 = -W \cdot n_1 + W \cdot n_2 + W_{21} \cdot n_2 - W_{12} \cdot n_1$$

$$\dot{n}_2 = -W \cdot n_2 + W \cdot n_1 + W_{12} \cdot n_1 - W_{21} \cdot n_2$$

$$\dot{n}_1 - \dot{n}_2 = 2W (n_2 - n_1) - 2(W_{12} \cdot n_1 - W_{21} \cdot n_2)$$

$$\cong -2(W_{12} \cdot n_1 - W_{21} \cdot n_2) = -(W_{12} + W_{21})(\Delta N - \Delta N_o).$$

Thus,

$$\frac{d}{dt} (\Delta N - \Delta N_o) = -(W_{12} + W_{21})(\Delta N - \Delta N_o) ,$$

so that

$$1/T_1 = (W_{12} + W_{21}) \quad ,$$

which relates the observed spin-lattice relaxation time to the appropriate transition probabilities.

As mentioned earlier, two processes give rise to the spin-lattice relaxation time. The first, in which the ion absorbs a quantum of energy (phonon) from the lattice or imparts a quantum of energy to it, is called the "direct process" and is predominant at low temperatures. In the second process, called the "Raman process," the ion absorbs a phonon of one energy and scatters that of another. Because essentially the whole phonon spectrum can participate, the Raman process is dominant at high temperatures.

Recently a new mechanism, termed the "Orbach process", has been introduced (31-33). It can be observed when the crystal field splitting of the ground state free ion term is less than the Debye energy, so that phonon induced transitions can take place directly between energy levels of different Kramers doublets. The splitting of the ground state manifold for Fe^{3+} in $K_3Co(CN)_6$, as seen in Appendix I, is probably too large for this process to take place.

2. The Direct Process

From first order perturbation theory,

$$W_{+\rightarrow -} = \frac{1}{h^2} |\langle \psi^+ |H'| \psi^- \rangle|^2 \rho(\nu),$$

where $|\psi,^+\rangle$ and $|\psi,^-\rangle$ are the two states of the Kramers doublet, and $\rho(\nu)$ is the density of states. According to Kramers' theorem the matrix element must be zero unless time reversal symmetry is lifted. Addition of an external magnetic field, which removes time reversal symmetry, will lift the Kramers degeneracy so that one-phonon relaxation can take place.

Appendix I, which gives a more detailed review of the theory, shows that if one considers the orbit-lattice interaction as the perturbing Hamiltonian and uses wave functions that are themselves corrected to first order for Zeeman mixing, one obtains the following relationship for the spin-lattice relaxation time:

$$1/T_{1D} = a\nu^4 T$$

where "a" is a constant, ν is the frequency, and T the temperature.

3. The Raman Process

To second order, use of the Zeeman mixed wave functions gives the relaxation time

$$1/T_{1R} = b\nu^2 T^7 \quad .$$

Another second order process can also give a contribution because of the fact that the absorbed and emitted phonons differ in energy by the Zeeman energy. In this case, as shown in Appendix I,

$$1/T_{1R} = cT^9.$$

4. Remarks

Since all of the rate processes are additive,

$$1/T_1 = a\nu^4 T + b\nu^2 T^7 + cT^9$$

The analogous result for a non-Kramers transition turns out to be

$$1/T_1 = a'\nu^2 T + b'T^7 \quad .$$

Two factors of frequency are missing in the "a" and "b" terms because there is no need to mix states via the Zeeman field. The "c" term is negligible in non-Kramers salts.

For comparison with experiment it would be desirable to compute the various numerical coefficients a, b, c; however, this turns out to be impossible for reasons discussed in the Appendix.

One should also note that the theory reviewed does not consider any effects due to the exchange interaction, although exchange can in principle couple the paramagnetic ion to the lattice

vibrations (34, 35). Unfortunately there is not enough information to make any quantitative estimates of this process; however, the experimental data obtained are very likely governed by some kind of exchange effect, as will be considered in more detail in Chapter V.

C. EXPERIMENTAL REVIEW

Since the data obtained by Paxman (11) and Bray et al. (12) for $K_3[Co, Fe](CN)_6$ will be compared with the data of the present work, a short review of their results will first be given. Paxman (11) worked at a frequency of 9.375 Gc/s and over a temperature range $1.6^{\circ}K$ to $4.2^{\circ}K$. His Zeeman field was oriented along the b-axis of the crystal. He used crystals with Fe^{3+} dilutions 1.7%, 3.2%, and 6.6%, and found that the relaxation times for temperatures greater than $2.8^{\circ}K$ were approximately proportional to T^{-7} while below $2.4^{\circ}K$ they were approximately proportional to T^{-1}. A small concentration dependence was also observed. He concluded that the measured relaxation times were in agreement with the Van Vleck theory. He also concluded that the model proposed by Waller (2) and Altshuler (36), in which relaxation is due to modulation of the dipolar interaction between ions, did not apply, owing to the large concentration dependence required by this theory. The results obtained by Paxman are shown in Figure 3.

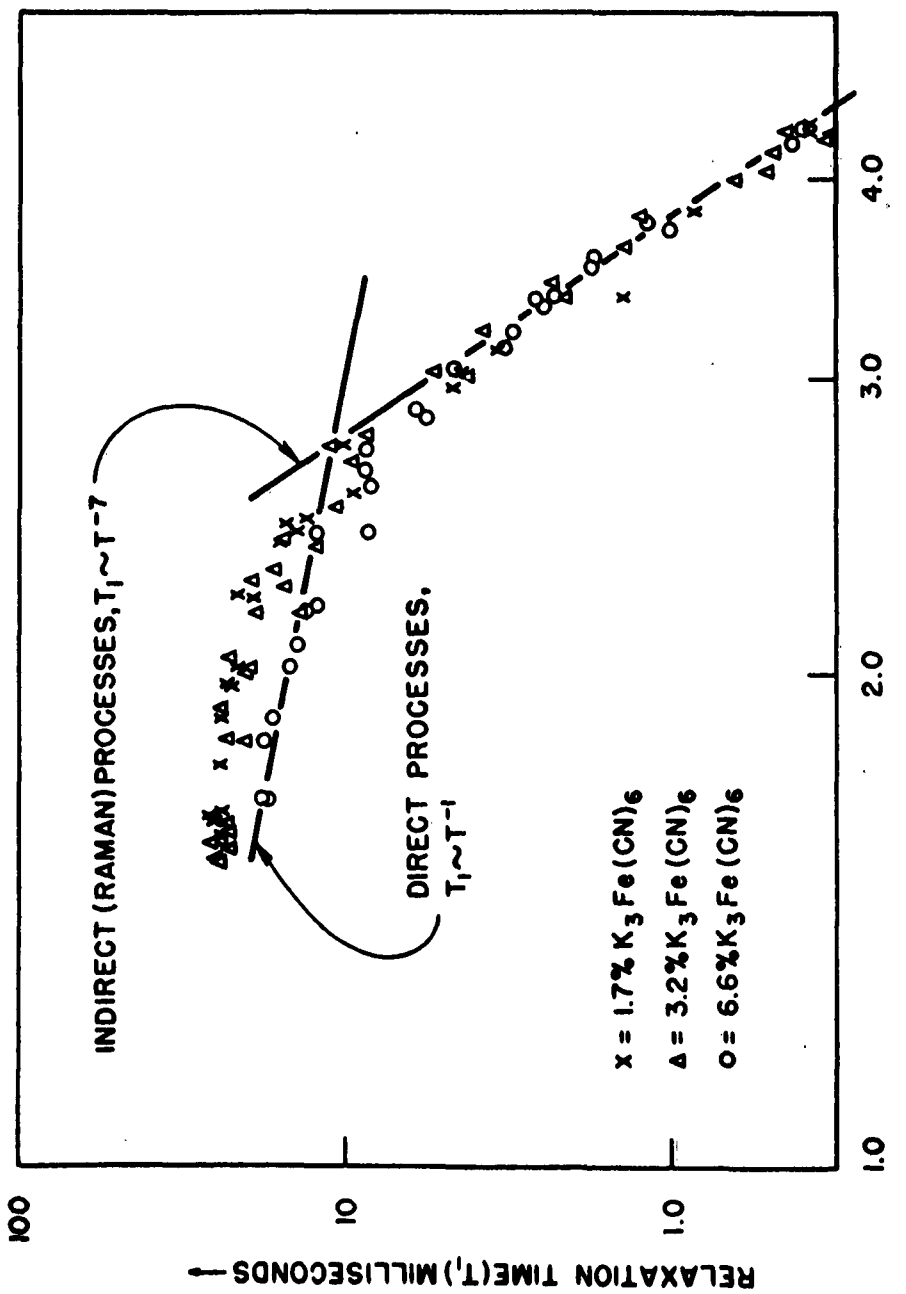

FIGURE 3: RELAXATION TIME VERSUS TEMPERATURE (PAXMAN (11)).

Bray et al. (12) performed their experiment at 8.750 Gc/s in the temperature range 1.6°K to 4.2°K with the H_o field oriented in the a-b plane of the crystal. The Fe^{3+} ion concentration was varied from 0.1% to 3.0%. Their results could be fitted by the empirical relation

$$1/T_1 = 5.4T + 0.0054T^9$$

and are plotted in Figure 4. They found no appreciable concentration dependence. By an adaptation of Van Vleck's calculation for Ti^{3+}, they calculated the following values for the spin-lattice relaxation time:

$$1/T_1 \cong 15T + 0.1T^9 \quad ,$$

which, in view of the uncertainties in the calculation, does not disagree seriously with their experimental findings. They also concluded that the concentration dependence reported by Paxman might be due to the "exchange pocket" mechanism (34) introduced by Van Vleck. Bray et al. also found that the spectra for the more concentrated crystals were suprisingly complex, and showed in one case as many as 57 different lines, .

Some experimental studies of the magnetic field and/or frequency dependence of T_1 have been made (14-16, 20, 21, 35). With one exception all of these studies were carried out on entirely different ion-crystal systems, so that the results

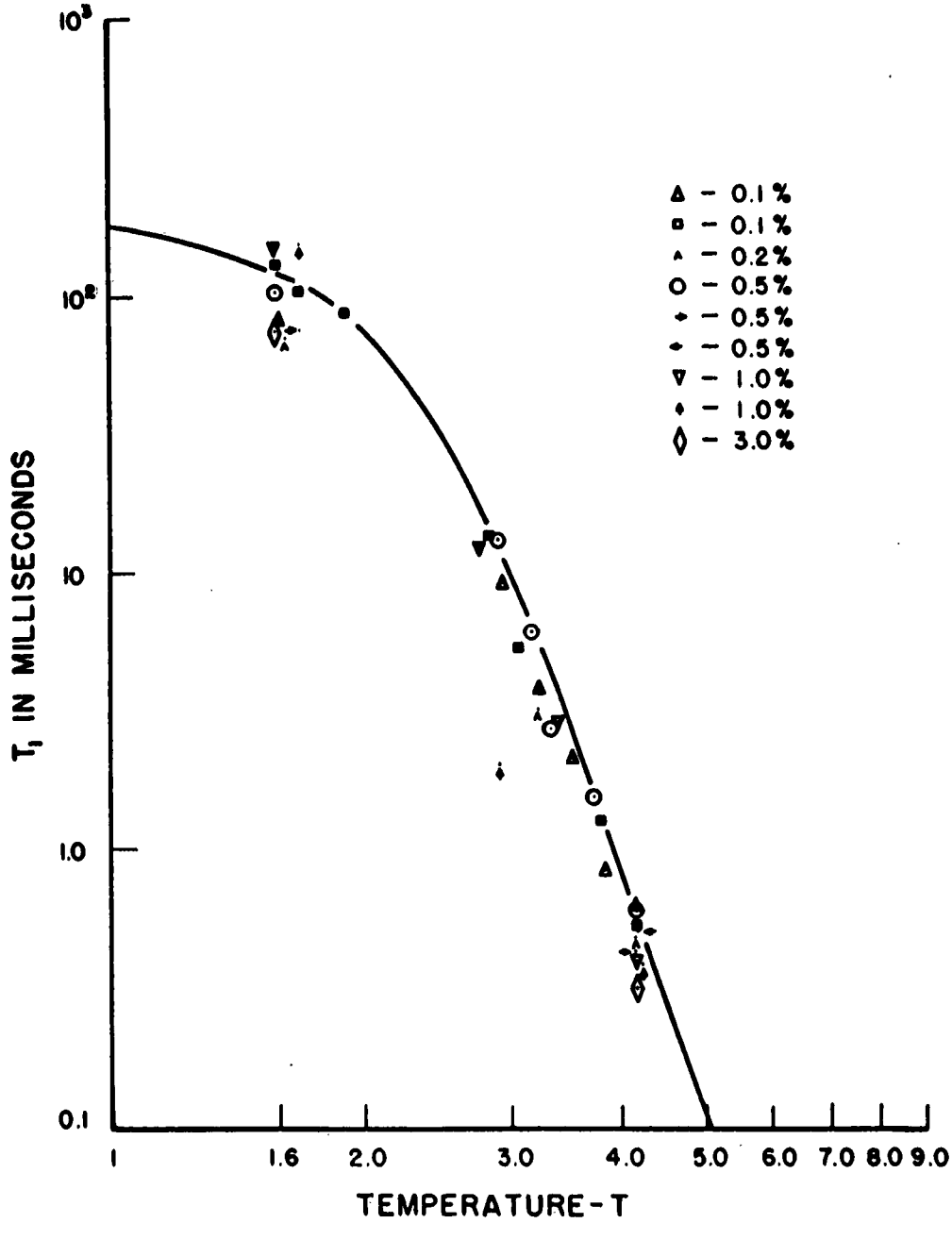

FIGURE 4: RELAXATION TIME VERSUS TEMPERATURE (BRAY et al. (12)).

cannot be compared with those obtained by the author. The exception is a remark made by J. S. Thorp (35). The remark concerns relaxation in ferricyanide, but it is too brief to be useful.

III. EXPERIMENTAL TECHNIQUES AND APPARATUS

A. GENERAL CONSIDERATIONS

The development of microwave tubes for use in radar made electron paramagnetic resonance experimentation possible. As microwave tubes and components have been improved over the years, the early rather primitive microwave spectrometers have evolved into much more sensitive and sophisticated devices (22).

A microwave spectrometer consists basically of a magnet, an oscillator, a microwave path through the sample, and a suitable detector. The sample of paramagnetic material is usually placed in a cavity of resonant frequency ν, and, when subjected to a magnetic field H and an RF field of frequency ν, is found to absorb RF energy, provided the resonance condition is met. In many cases, and certainly for Kramers' doublets in moderate magnetic fields, the condition can be written

$$h\nu = g\beta H$$

where h is Planck's constant, g the effective spectroscopic splitting factor, and β the Bohr magneton. The consequent change in power reflected from the cavity is detected, and the absorption is seen on an oscilloscope or a recorder. The simplest detector uses a straightforward crystal rectifier. An improvement in sensitivity is gained by the introduction of superheterodyne techniques.

B. TECHNIQUES FOR RELAXATION MEASUREMENTS

The apparatus mentioned above is generally sufficient for routine electron paramagnetic resonance measurements, but one usually needs additional apparatus for relaxation measurements. The simplest experimental technique, termed the "CW Saturation" method (37), was originally developed for nuclear relaxation. With this method one measures the magnitude of the resonance absorption as a function of the microwave power incident on the sample. An increase in microwave power will tend to equalize the populations of the ground state Kramers pair, and thus reduce the net resonance absorption.

From a plot of resonance signal versus microwave power, one can in principle find the spin-lattice relaxation time. However, since the nature of the line broadening influences the results, the deduction of the correct relaxation time can become rather difficult.

A second method, called "Pulse Saturation-Recovery" (23), involves the application of an intense microwave pulse at the resonant frequency in order to saturate the line. After removal of the pulse a low monitoring signal is used to measure the recovery as a function of time. This method has many advantages over CW techniques; however, since the saturation pulse is applied only at the center of the resonance line, complications may occur with inhomogeneously broadened lines (38). The saturation energy

will be applied only to those spins whose local fields satisfy the resonance condition, and spin diffusion to the rest of the line may occur. In addition, care must be exercised to avoid partial saturation of the transition by the monitoring signal. Measurements may therefore be a combination of spin-lattice relaxation, spin-diffusion, and saturation effects. These effects can usually be separated if one uses extreme care in taking the measurements.

The technique giving the fewest ambiguities in interpretation is the "Fast Passage-Recovery" method (19, 39, 40), in which the magnetic field is held slightly away from the resonant value and at some time is swept through it. Application of a microwave pulse concurrent with the sweep will in principle invert the level populations, provided the pulse is well above the saturation level and the line is swept through in a time short compared to the relaxation time, (40). In practice the line is not always inverted, but at least is uniformly excited. By use of a delayed field sweep, without the microwave pulse, one can subsequently measure the signal as it recovers its equilibrium value.

The main advantage of this method is that microwave excitation can be applied to the whole line so that spin-diffusion is no longer a problem. One may also use somewhat larger monitoring power since the resonant condition only occurs for short times. Another advantage is that when inversion is obtained, a sensitive test for phonon imprisonment (17-21) is provided.

C. APPARATUS

Figure 5 shows a block diagram of the L-band microwave spectrometer used in the present work. Both "Pulse Saturation-Recovery" and "Fast Passage-Recovery" methods can be used: however, only the latter was actually employed. With relatively minor changes in the apparatus, duplicate measurements can be taken at X-band.

The spectrometer is of the superheterodyne type, and a synchronous detection system can be substituted to obtain standard CW spectrometric measurements.

Since the general design is fairly conventional (19, 22), only a brief description will be given in this section. A more detailed description of the different components is given in Appendix II.

The L-band frequency used varied from 1.81 to 1.82 Gc/s. Since the cavity had no provisions for tuning, corrections could not be made for this slight change in resonant frequency with temperature. Since the change amounted to only about 1/2%, any effect on the results was negligible. Provisions for variable coupling were made, and a slight undercoupling was used throughout the experiment.

A similar frequency shift, from about 8.500 to 8.535 Gc/s, occurred at X-band, but the effect on the results was again negligible.

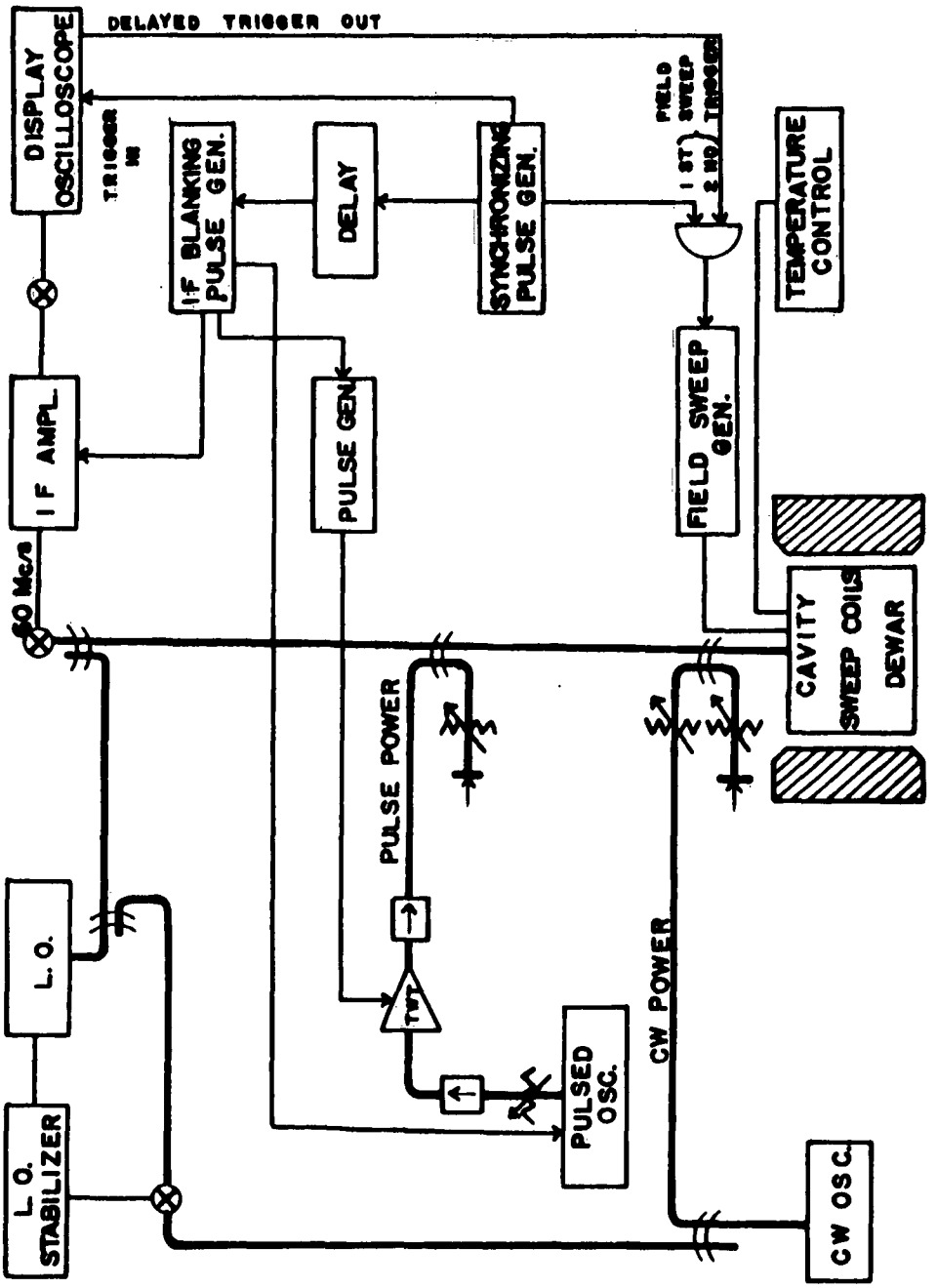

FIGURE 5: MICROWAVE SPECTROMETER.

Since at X-band there was no provision for changing coupling during a "run", the coupling was preset at room temperature to obtain slight undercoupling at helium temperatures.

The cavities, of rectangular coaxial type for L-band and regular rectangular type for X-band, were made of epoxy resin and silver plated. A pair of Helmholtz coils was attached to each cavity to obtain the requisite field sweep. A current of 1/4 amp through the coils effected a field sweep of about 50 Gauss.

At both frequencies the monitoring power was usually held to submicrowatt levels, while the pulsed power level was about 7 watts, as measured at the entrance to the cavity.

The time sequence adopted for the fast passage is shown in Figure 6. The duration of the field sweep could be changed from about 4 to 100 μsec in the increasing direction and from about 1 to 200 μsec in the decreasing direction. An upsweep of about 50 to 100 μsec was used for most measurements. By observing during the down sweep, one could measure the recovery at approximately 50 μsec after inversion. Delaying the second sweep allowed continuous measurements from about 150 μsec out to arbitrarily long times. Pulse power was applied only to every second pair of field sweeps, and the oscilloscope was triggered so as to superpose the perturbed line on the equilibrium absorption signal.

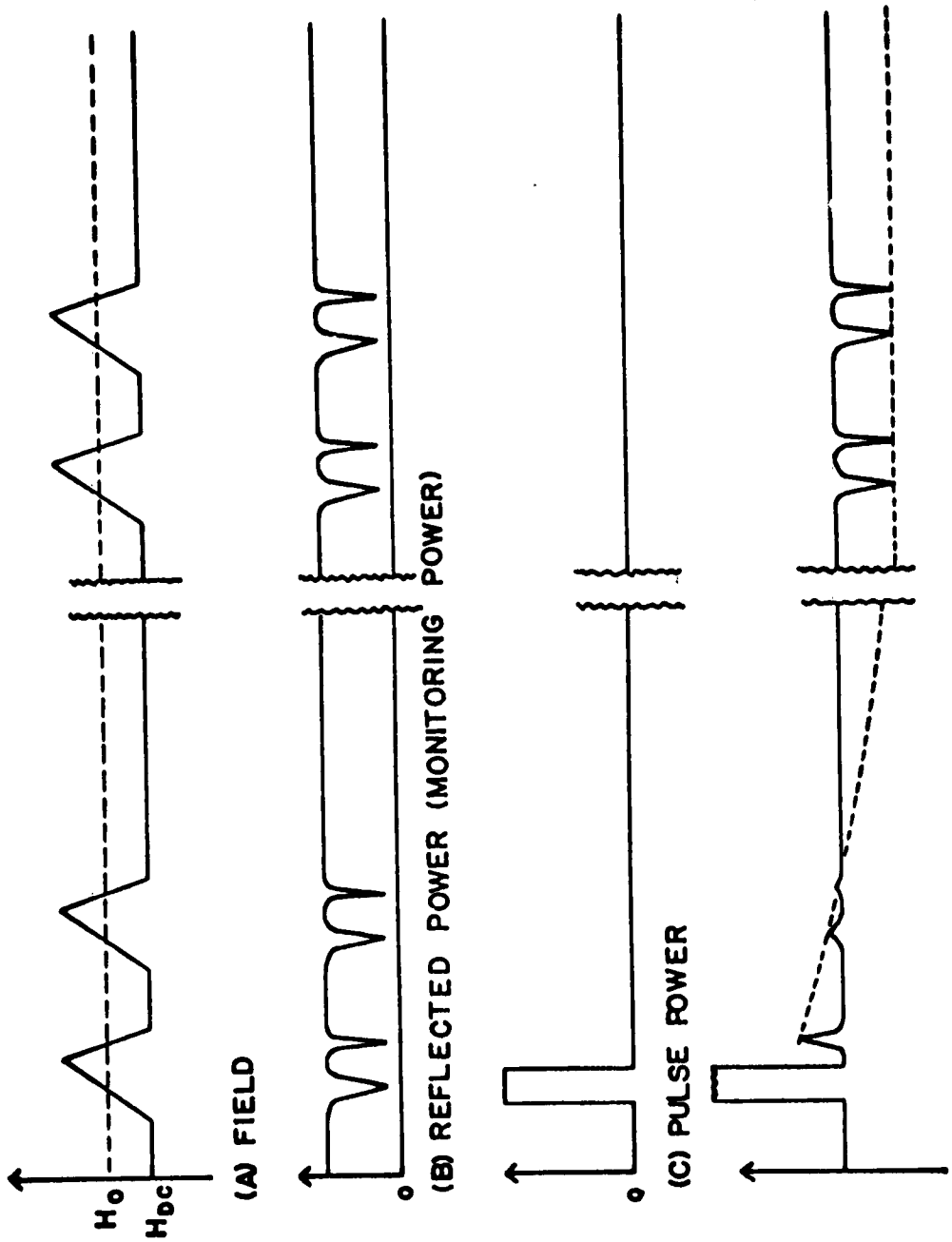

FIGURE 6: TIME SEQUENCE USED FOR FAST PASSAGE RELAXATION TIME MEASUREMENTS.

Two complete field sweeps were used to avoid the heat from current through the coils that would otherwise have flowed during the interval between inversion and inspection.

The temperature was altered by pumping on the liquid helium bath and stabilized by a servo system which added a controlled amount of heat to the bath. A calibrated carbon resistor was used for temperature measurements.

During the experiments, it was noticed that when the liquid helium level had fallen below the cavity one could still maintain a constant temperature and useful measurements could be made. At the same time an increase in signal to noise ratio by a factor of 5-10 was found. This observation suggests that it is in general preferable to exclude liquid helium from the cavity and to maintain thermal contact by means of the vapor.

IV. EXPERIMENTAL OBSERVATIONS

A. THE EXPERIMENT (41)

The spin-lattice relaxation measurements were carried out in the temperature range approximately $1.3^{\circ}K$ to $4.5^{\circ}K$. To permit comparison with the data of Bray et al. (12), the H_o field was oriented in the a-b plane, parallel to the a-axis. The $K_3[Co, Fe](CN)_6$ crystals were grown from a saturated aqueous solution by slow evaporation at a constant temperature. The Fe^{3+} concentrations, as determined from spectrochemical analysis[1] of the actual crystals used in the experiment, were: 0.24%, 0.51%, 1.0%, 1.7%, and 3.5%, where

$$\%Fe^{3+} = \frac{\text{Number of } Fe^{3+} \text{ ions}}{\text{Number of } Fe^{3+} + Co^{3+} \text{ ions}}$$

The crystal size was made large enough to ensure sufficient sensitivity, but small enough to fit well within the Helmholtz coils and also to preclude possible radiation damping (42).

B. RESULTS

1. Spin-Lattice Relaxation Times

A representative recovery curve obtained by means of the sequence shown in Figure 6 is shown in Figure 7. The output of the spectrometer, which is proportional to the deviation

---

[1] The analyses were performed by Spectrochemical Laboratories, Inc. Pittsburgh, Pennsylvania.

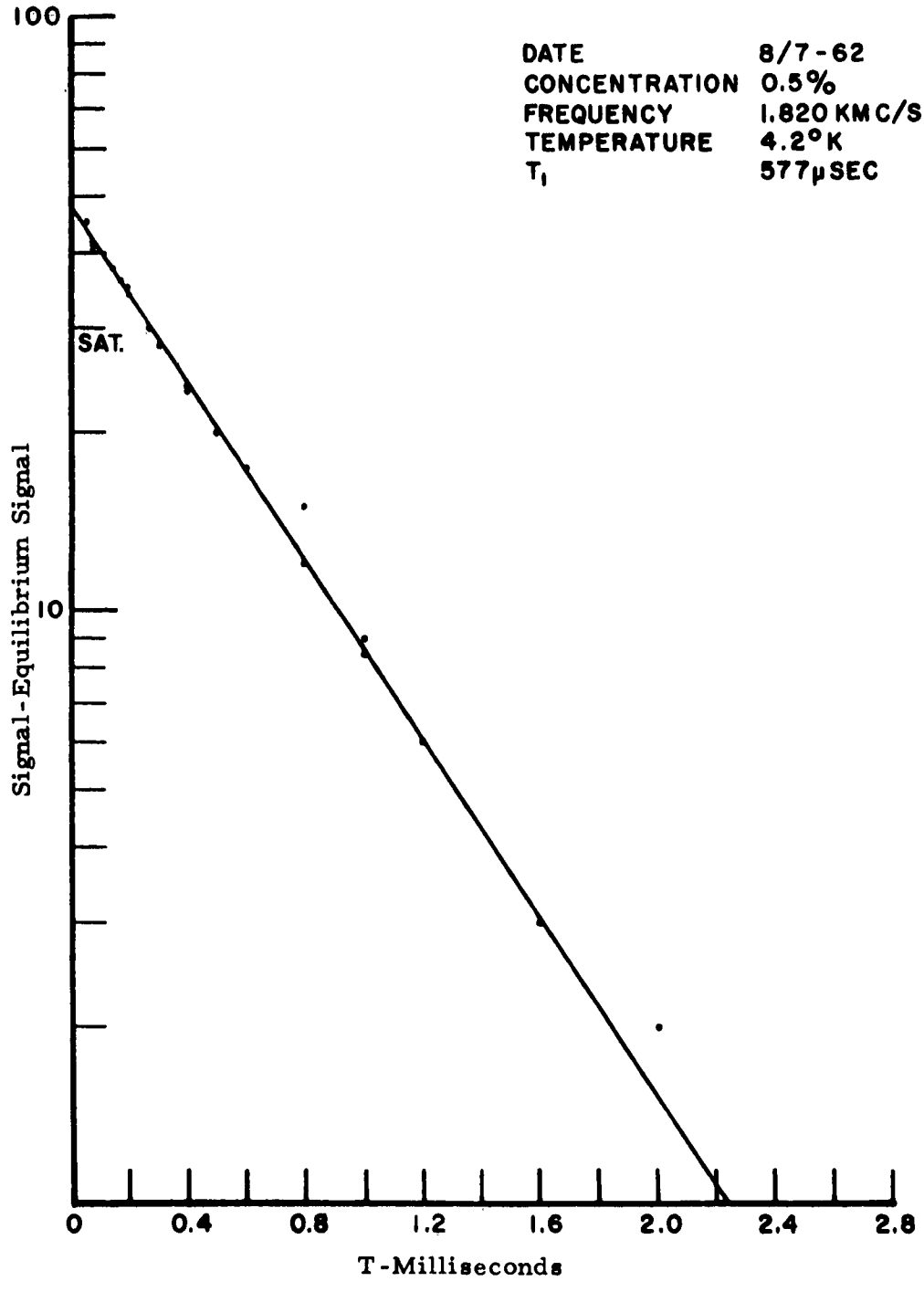

FIGURE 7: TYPICAL DECAY CURVE.

of the peak absorption from its equlibrium value, is plotted semilogarithmically as a function of time after inversion. For this particular curve, an initial (extrapolated) inversion of 62% was obtained. At temperatures below $2^{\circ}K$ it was found that excessive monitoring power, too rapid an overall repetition rate and/or operation in the nonlinear region of the IF amplifier and detector, resulted in a curved recovery (on semilogarithmic plots). As a result some caution had to be observed to obtain data that were independent of these factors.

Figure 8 shows an oscilloscope picture of an inverted line superposed on the equilibrium signal. The picture was taken 300μsec after inversion in the 1.0% Fe^{3+} crystal at $1.36^{\circ}K$. The time base was 20μsec per major division. The inverting pulse was applied for 60 μsec while the field was swept through approximately 50 Gauss in 50μsec.

All the data obtained for the various samples, at both L-band and X-band frequencies, are given in Table 1, and a master plot of log T_1 versus log T is shown in Figure 9. The data obtained for the different concentrations are plotted separately in Figures 10-14. The interpretation given in the next section is based almost wholly on these plots. Reproducibility was very good except for a rather large difference at the very low temperatures for data taken two

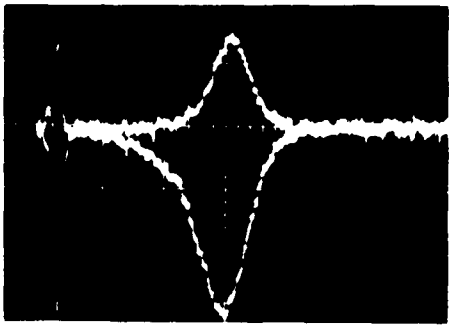

FIGURE 8: INVERTED LINE SUPERPOSED ON THE EQUILIBRIUM SIGNAL.

TABLE 1

Results of Spin-Lattice Relaxation Time Measurements

Concentration	Freq.	Temp. (^{o}K)	T_1
0.24%Fe^{3+}	1.8Gc/s	4.26	655 ±30 μs
		4.25	460 ±20 μs
		4.25	460 ±20 μs
		3.12	7.9 ± 0.4ms
		2.64	35 ± 1.5ms
		2.11	310 ±15 ms
		1.98	680 ±10 ms
		1.69	2.5 ± 0.1s
		1.47	6.5 ± 0.5s
		1.41	9.3 ± 0.5s
		1.32	16.8 ± 0.6s
		1.32	18.0 ± 0.6s
	8.5Gc/s	4.25	440 ±50 μs
		2.00	120 ± 5 ms
		1.52	206 ± 5 ms
		1.32	223 ± 5 ms
0.51 %Fe^{3+}	1.8Gc/s	4.50	307 ±20 μs
		4.40	447 ±20 μs
		4.29	463 ±10 μs
		4.22	530 ±20 μs
		~4.20	541 ±20 μs
		~4.20	567 ±10 μs
		~4.20	577 ±10 μs
		~4.20	593 ±20 μs
		4.19	530 ±20 μs
		4.19	620 ±20 μs
		3.82	1.21 ± 0.1ms
		3.41	3.23 ± 0.1ms
		3.11	6.25 ± 0.1ms
		2.77	3.83 ± 0.1ms
		2.51	37.4 ± 2.0ms
		1.98	232 ± 5.0ms
		1.88	530 ±40 ms
		1.80	650 ±50 ms

TABLE 1 CONTD

Concentration	Freq.	Temp. (^{o}K)	T_1
-.51% Fe^{3+}	1.8Gc/s	1.69	1.14 ± 0.1 s
		1.64	1.10 ± 0.2 s
		1.56	1.70 ± 0.2 s
		1.52	2.60 ± 0.2 s
		1.45	3.10 ± 0.4 s
		1.41	3.40 ± 0.4 s
		1.40	2.60 ± 0.3 s
		1.37	2.70 ± 0.2 s
		1.34	3.40 ± 0.3 s
		1.25	9.85*± 0.2 s
	8.5Gc/s	4.25	425 ±20 μs
		4.25	475 ±20 μs
		4.25	500 ±20 μs
		2.26	63 ±10 ms
		2.12	87 ±10 ms
		1.70	170 ±20 ms
		1.40	205 ±20 ms
		1.34	221 ±10 ms
1.04% Fe^{3+}	1.8Gc/s	~4.18	535 ±10 μs
		4.18	540 ±20 μs
		2.38	50.8 ± 2 ms
		2.15	120 ± 5 ms
		2.13	193 ±10 ms
		1.91	428 ±20 ms
		1.72	930 ±50 ms
		1.48	1.7 ± 0.25s
		1.44	1.92 ± 0.2 s
1.7 % Fe^{3+}	1.8Gc/s	4.18	540 ±20 μs
		2.82	17.6 ± 1 ms
		2.28	54 ± 5 ms
		1.90	119* ±15 ms
		1.54	130* ±20 ms
		1.40	158* ±15 ms
		1.39	162* ±10 ms

* Non-exponential decay; asymptotic time constant (slightly curved).

TABLE 1 CONTD

Concentration	Freq.	Temp. (°K)		T_1
1.7%Fe^{3+}	8.5Gc/s	4.30	400	±20 μs
		4.30	420	±20 μs
		2.62	19	± 2 ms
		2.06	66	± 5 ms
		1.79	124*	±10 ms
		1.50	146*	±10 ms
		1.30	163*	±20 ms
		1.28	171*	±10 ms
~ 3.5%Fe^{3+}	1.8Gc/s	4.26	400	±20 μs
		3.49	2.33	± 0.1ms
		2.90	8.8	*± 0.3ms
		2.12	55	†± 5 ms
		1.67	130	†±10 ms

* Non-exponential decay; asymptotic time constant (slightly curved).
† Badly non-exponential decay; asymptotic time constant.

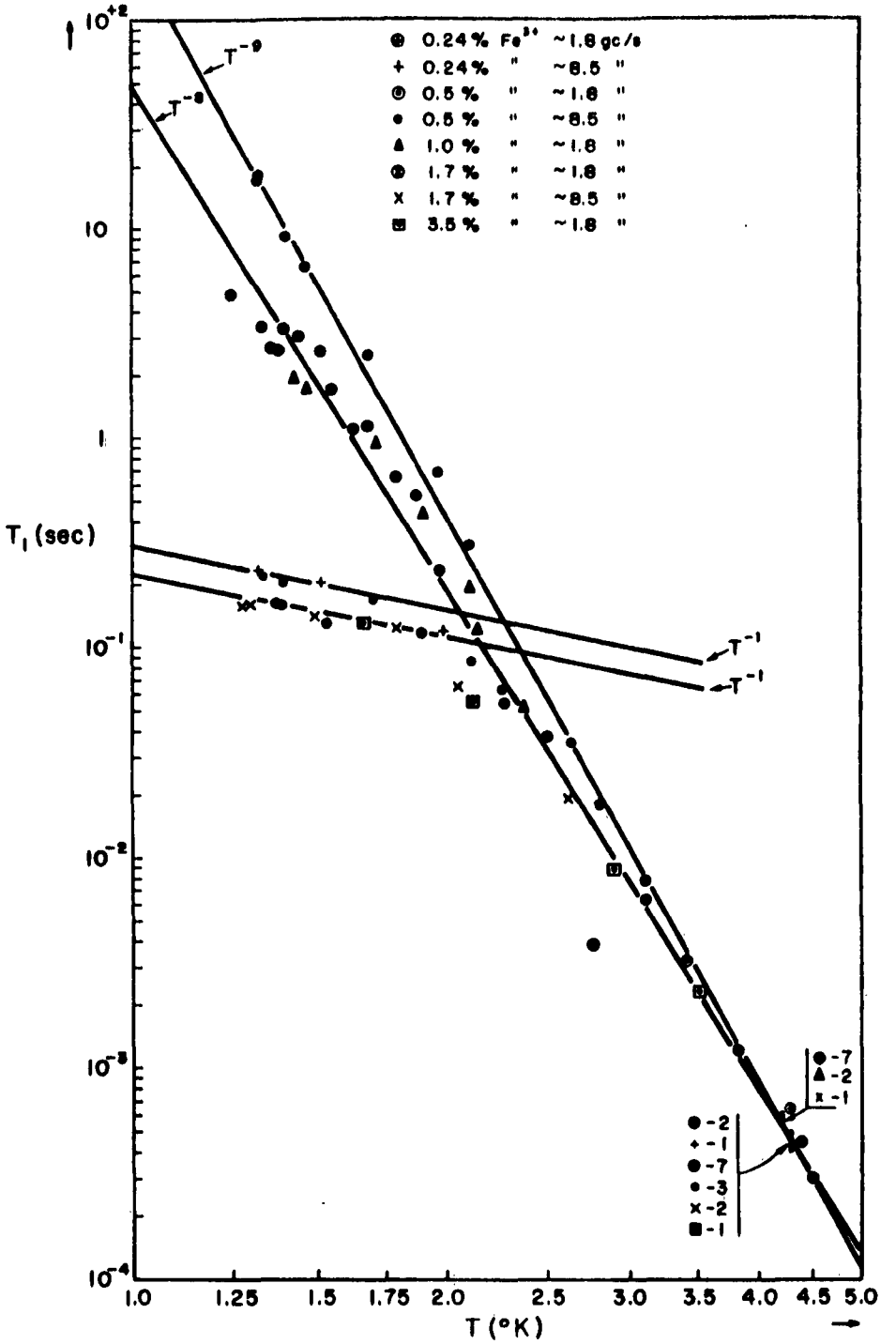

FIGURE 9: SPIN-LATTICE RELAXATION TIME VERSUS TEMPERATURE (ALL DATA).

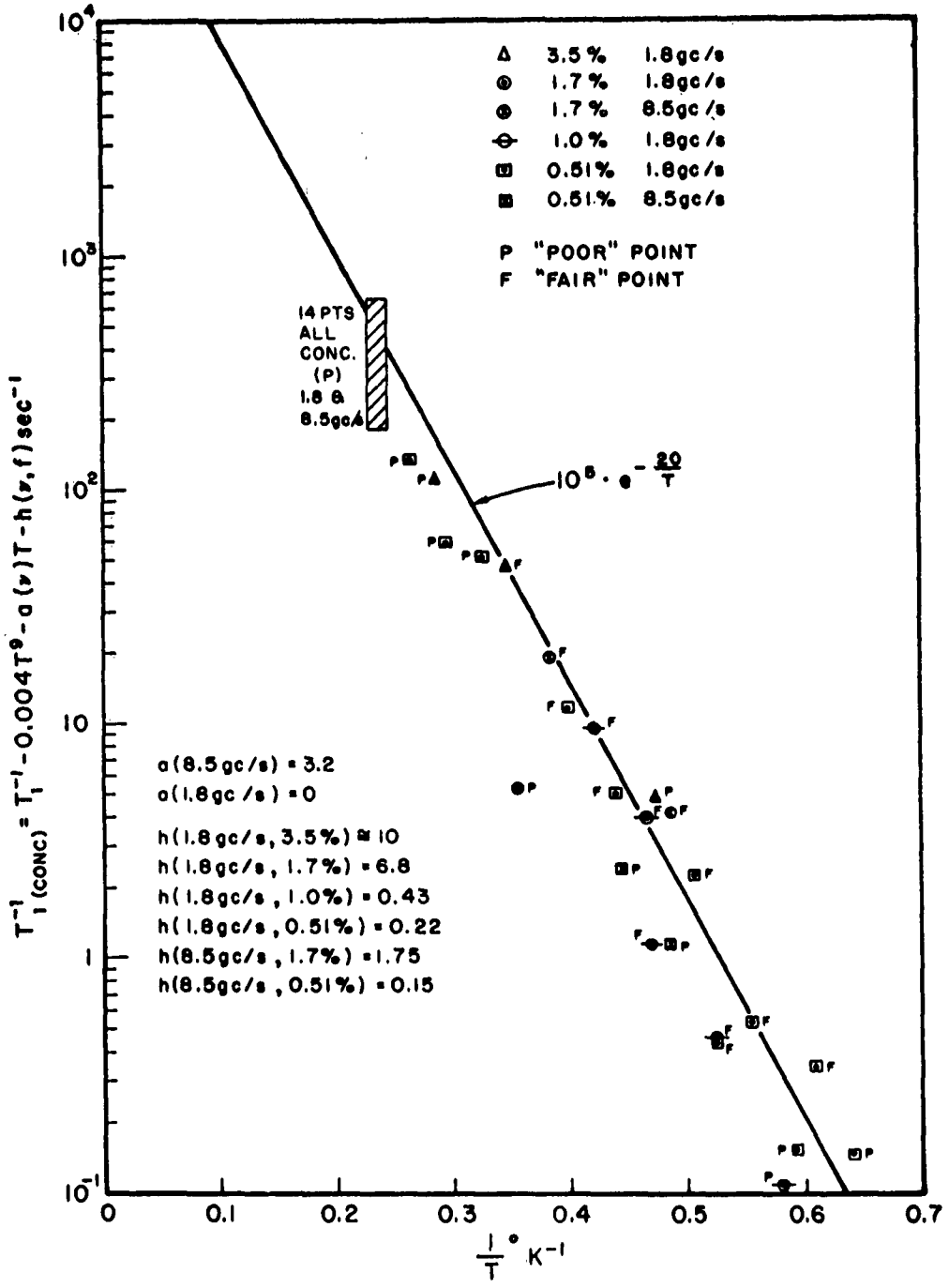

FIGURE 9a: CONCENTRATION DEPENDENT RELAXATION RATE VERSUS 1/T (ALL CONC.).

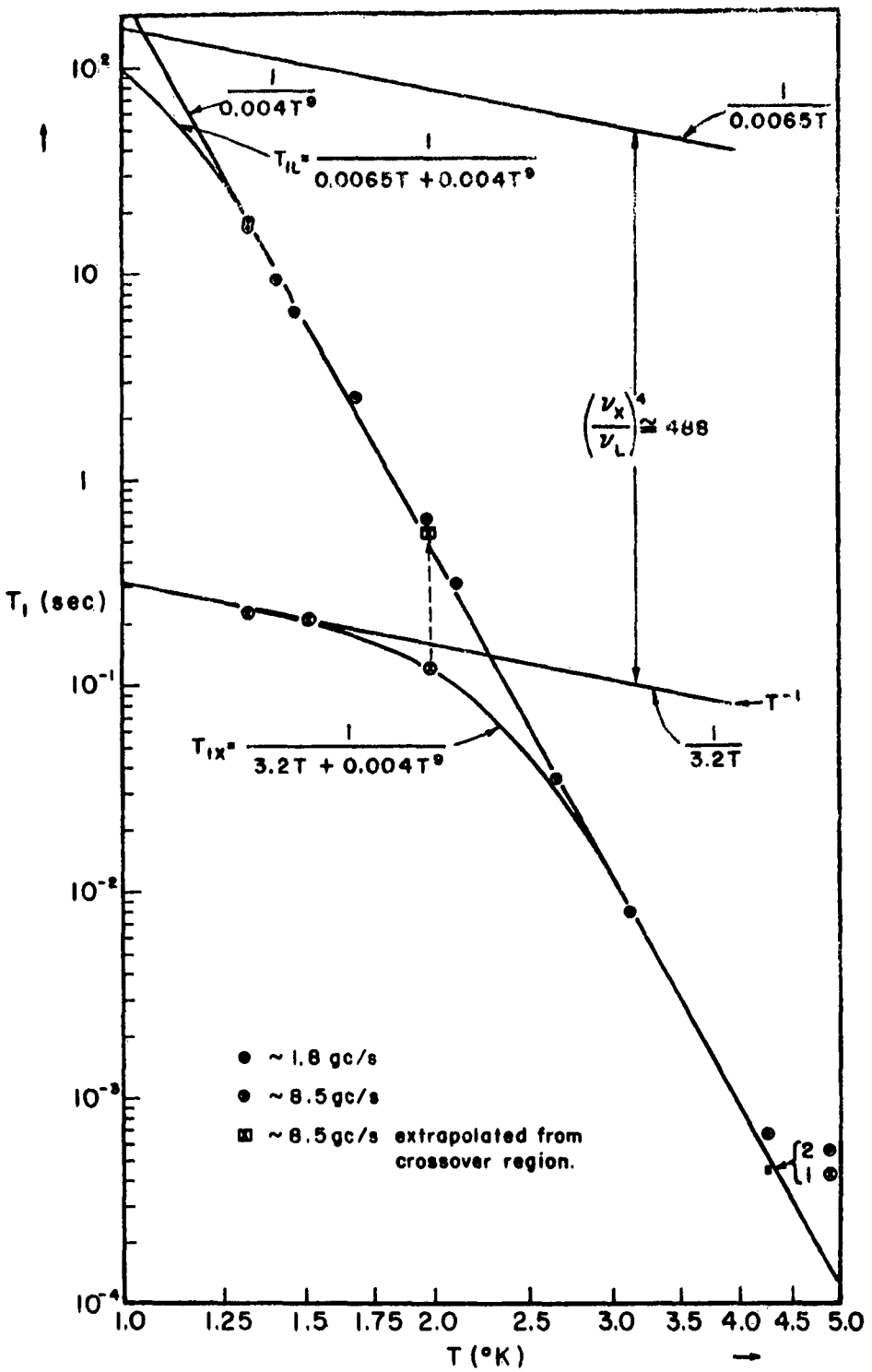

FIGURE 10: SPIN-LATTICE RELAXATION TIME VERSUS TEMPERATURE (0.24%).

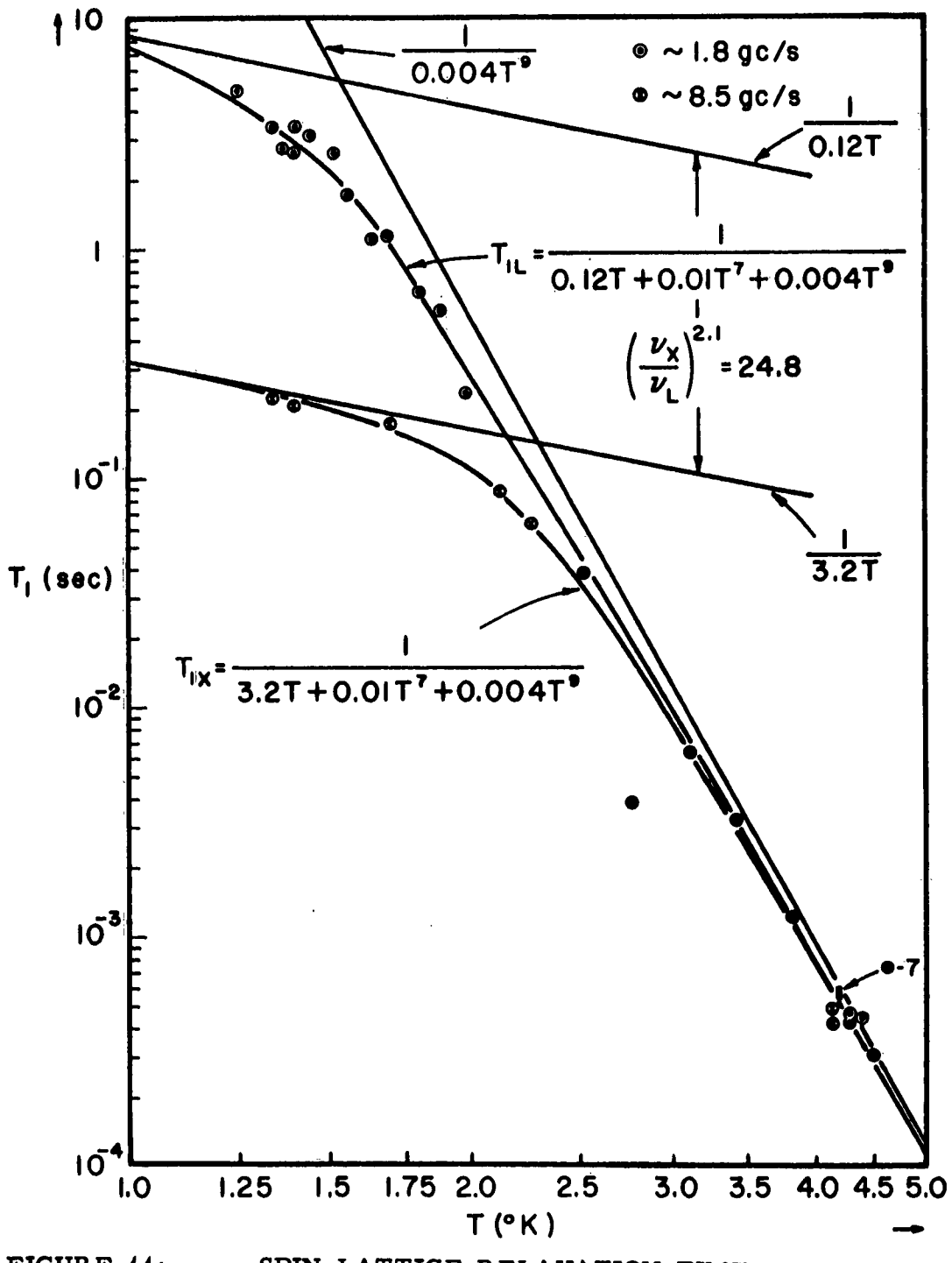

FIGURE 11: SPIN-LATTICE RELAXATION TIME VERSUS TEMPERATURE (0.51%).

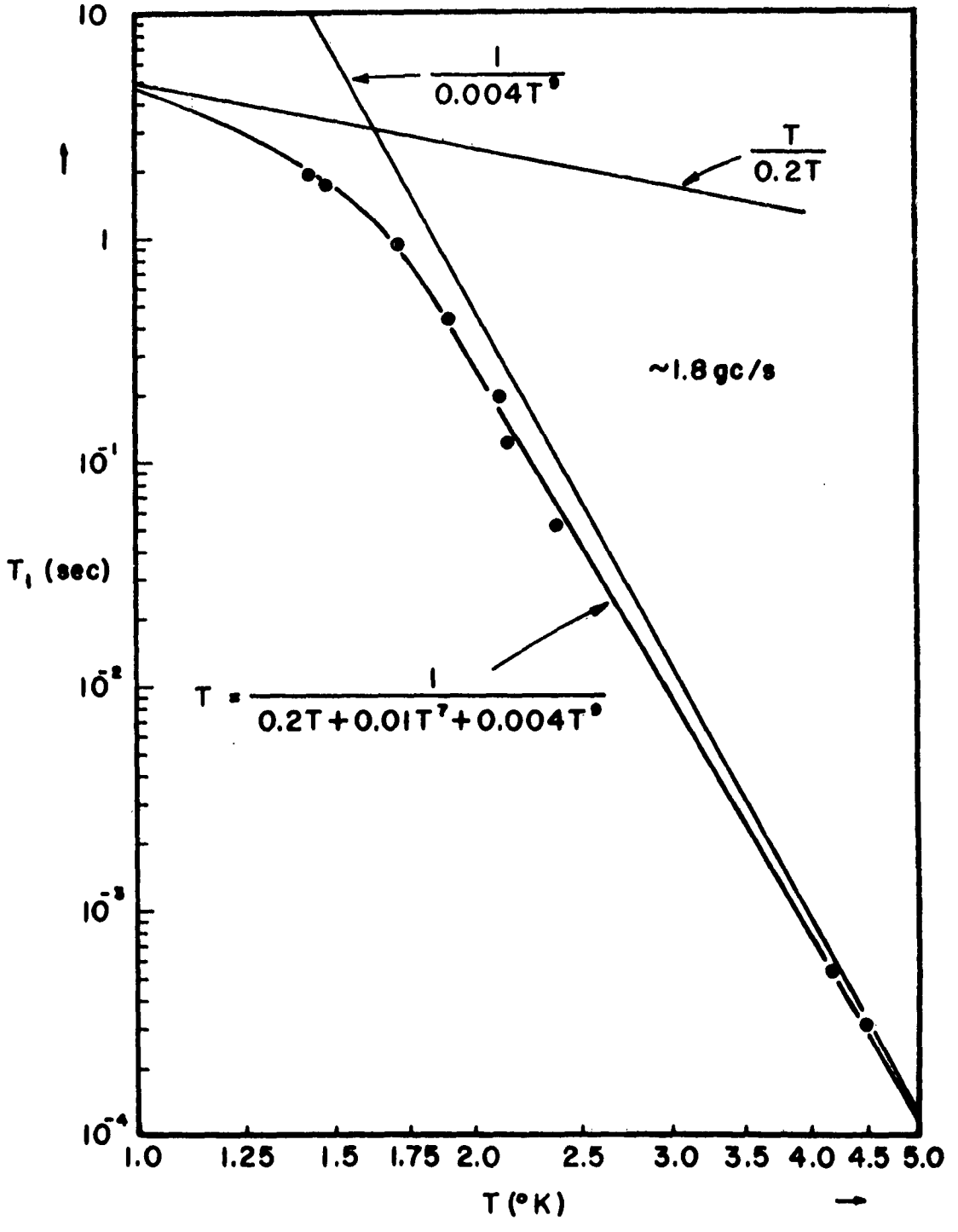

FIGURE 12: SPIN-LATTICE RELAXATION TIME VERSUS TEMPERATURE (1.0%).

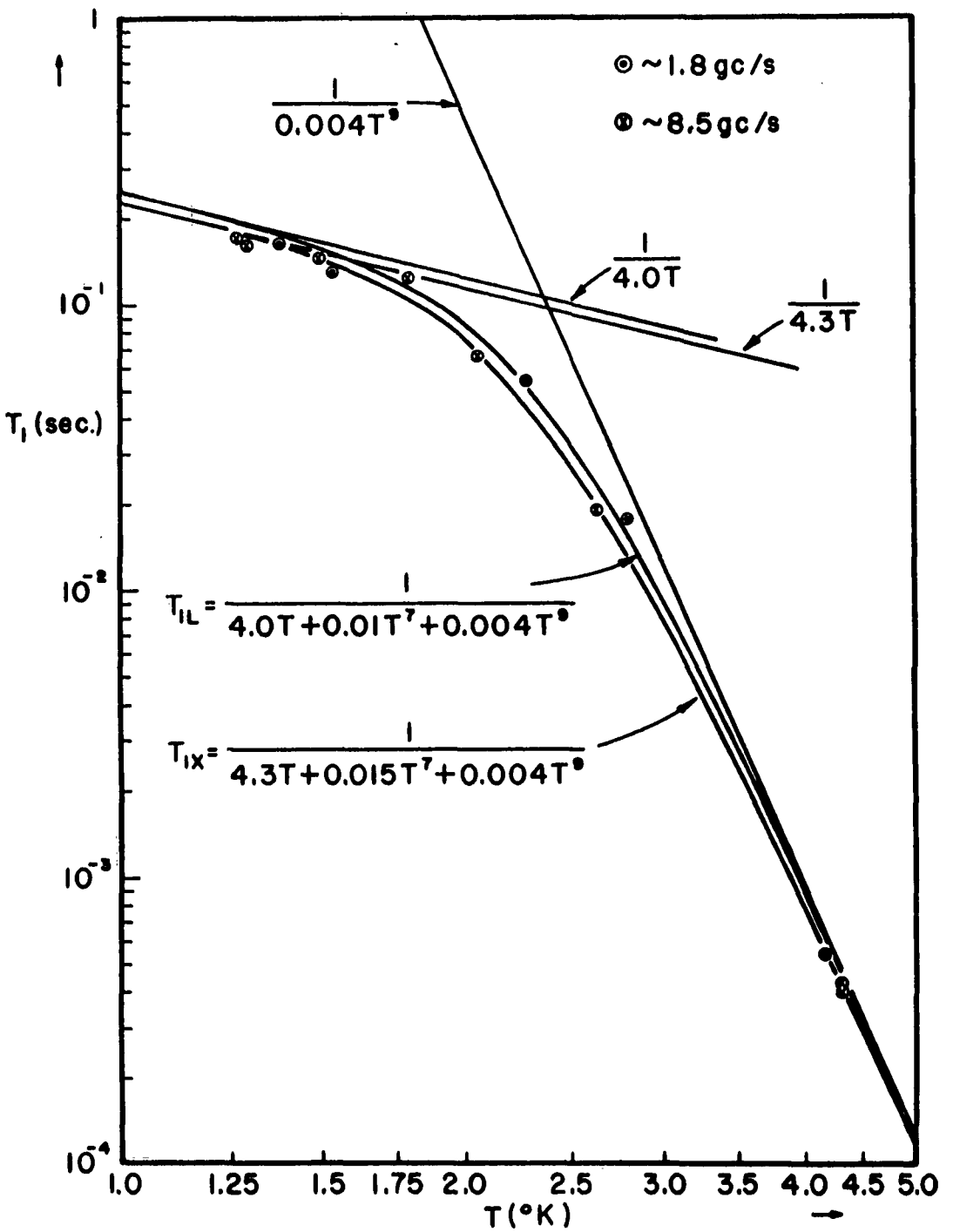

FIGURE 13: SPIN-LATTICE RELAXATION TIME VERSUS TEMPERATURE (1.7%).

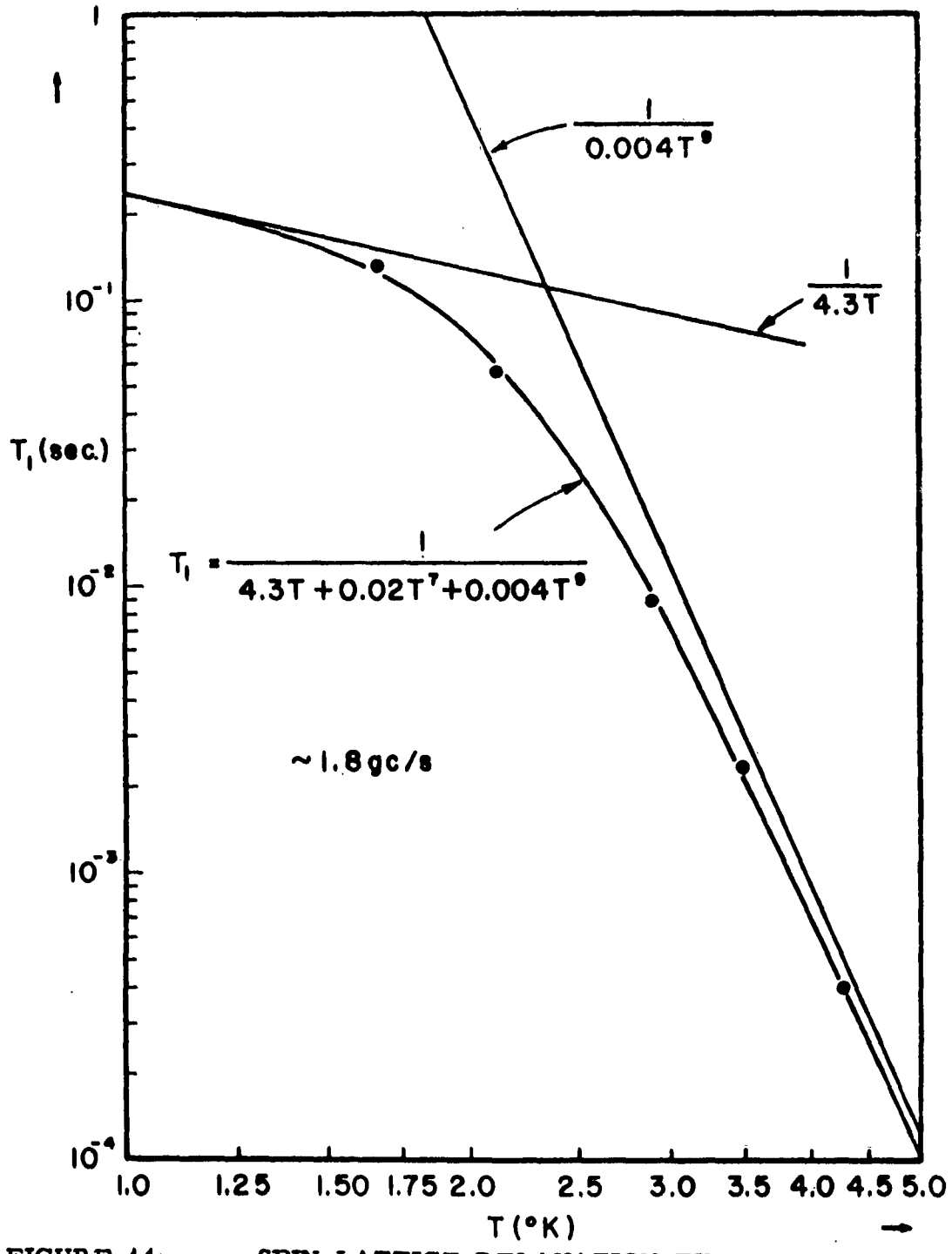

FIGURE 14: SPIN-LATTICE RELAXATION TIME VERSUS TEMPERATURE (3.5%).

months apart on the 0.51% sample. The experimental error given is estimated from the uncertainty in logarithmic slopes of the recovery curves.

Some of the data for the 1.7% and 3.5% samples require added comment. With the former, slight curvature was encountered in the semilogarithmic decay plots at low temperatures, despite all attempts to adjust the repetition rate, monitoring power, and receiver gain. The curvature became much more pronounced with the 3.5% specimen at low temperatures. The curves were found to be independent of the above variables over relatively wide limits, so that the effect was evidently inherent. Figure 15 shows a typical curved decay plot. For reasons to be discussed below, the asymptotic slope was believed to represent the genuine spin-lattice time and was the value plotted in Figures 9, 13, and 14.

The lowest temperature obtained was about 1.25^{o}K. It would have been desirable to obtain still lower temperatures but the capacity of the vacuum pump was the limiting feature. A somewhat lower concentration would also have been desirable; however, the signal-to-noise ratio became unacceptably small.

2. Paramagnetic Spectra

Conventional measurements of the absorption spectra were made on several samples at approximately 1.8 Gc/s

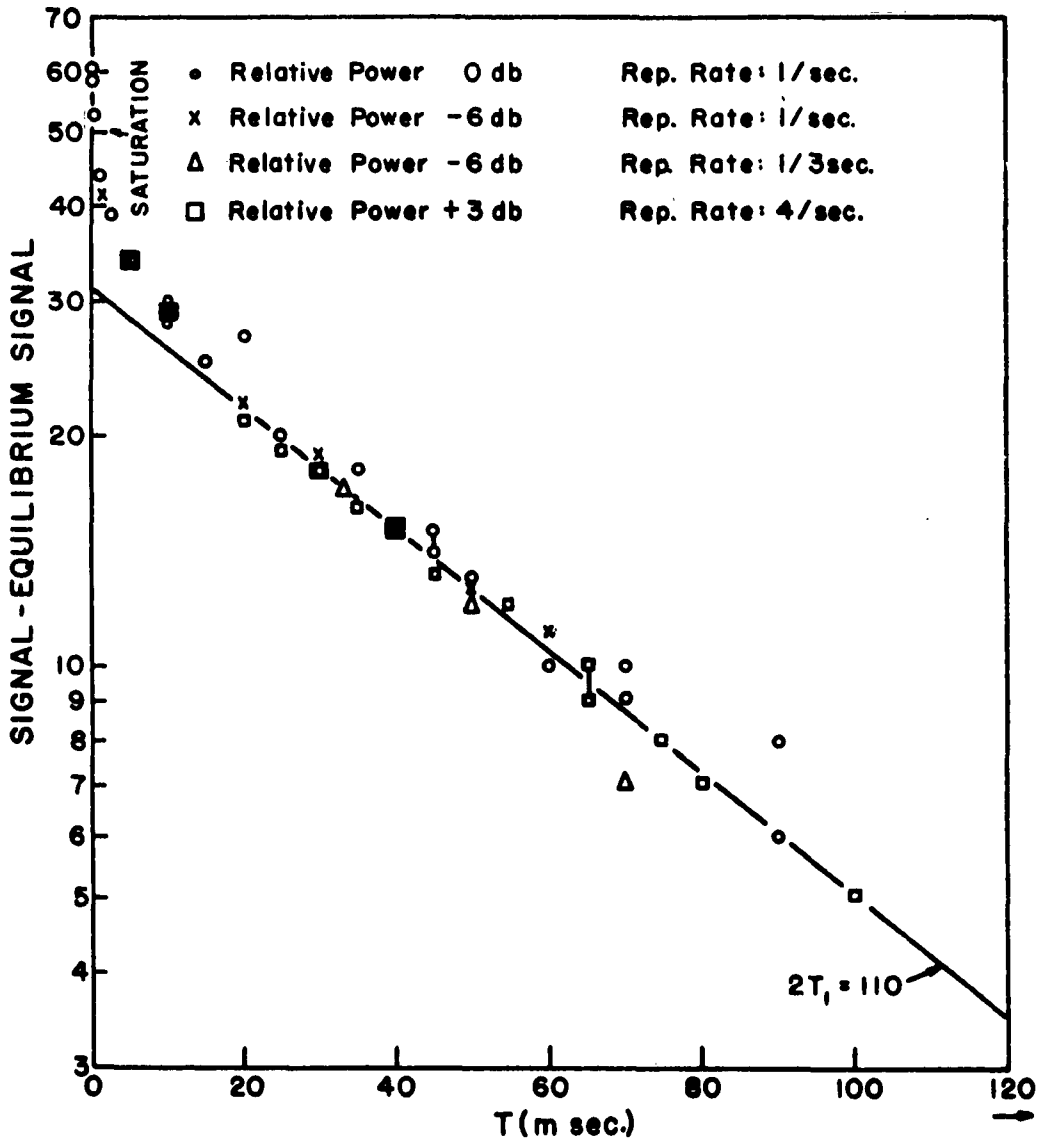

FIGURE 15: CURVED DECAY PLOT FOR 3.5% CONCENTRATION.

and 2°K. The same a-axis orientation used in the relaxation measurements was used in recording the spectra. The spectra of the 0.51% and the 3.5 % samples are listed in Table 2. They turned out to be rather complicated. None of the additional lines, even at 3.5 % concentration, had an intensity of more than about two percent of that of the main line.

No additional lines were found in the spectrum of the 0.24 % Fe^{3+} sample although lines having peak-to-peak derivatives 3×10^{-5} that of the main line could have been seen. With this sample, when the magnetic field was oriented slightly away from the a-axis, two pairs of lines appeared instead of just two lines. Each pair represented one of the magnetic complexes, and the splitting within the pairs is believed to be due to polytypism, as discussed by Artman, et al. (13). Figure 16 shows the derivative of the main absorption line for the 0.51% crystal at 4.2°K and 8.596 Gc/s. This curve is included only for illustrative purposes and was not used in the computation of Table 2. None of the satellite structure is apparent at this sensitivity.

TABLE 2

Paramagnetic Resonance Spectra of $K_3[Co, Fe](CN)_6$ Crystals (L-band ~ 1.8 Gc/s)

H_o in gauss.	Relative Intensity 3.5 %	0.51 %	0.24 %	
240	1.0			~20 gauss wide
280	0.25			
309	0.25			
360	1.0			
390	2.0			
472	1.5			
562		1.10^{-4}		
595	100			Main Line 3.5 % ~15 gauss wide
621		100		Main Line 0.51 % ~ 7.5 gauss wide
625			100	Main Line 0.24 % ~ 6 gauss wide
642	1.5			
725		1.10^{-4}		
764	1.0			
828	1.5			

1. Peak to peak derivative signal between inflection points.
2. At 0.51 %, some additional lines having absorption derivatives $\lesssim 10^{-6}$ that of the main line were seen but their positions were not recorded.
3. At 0.24 % lines having absorption derivatives 3×10^{-5} that of the main line would have been observed.

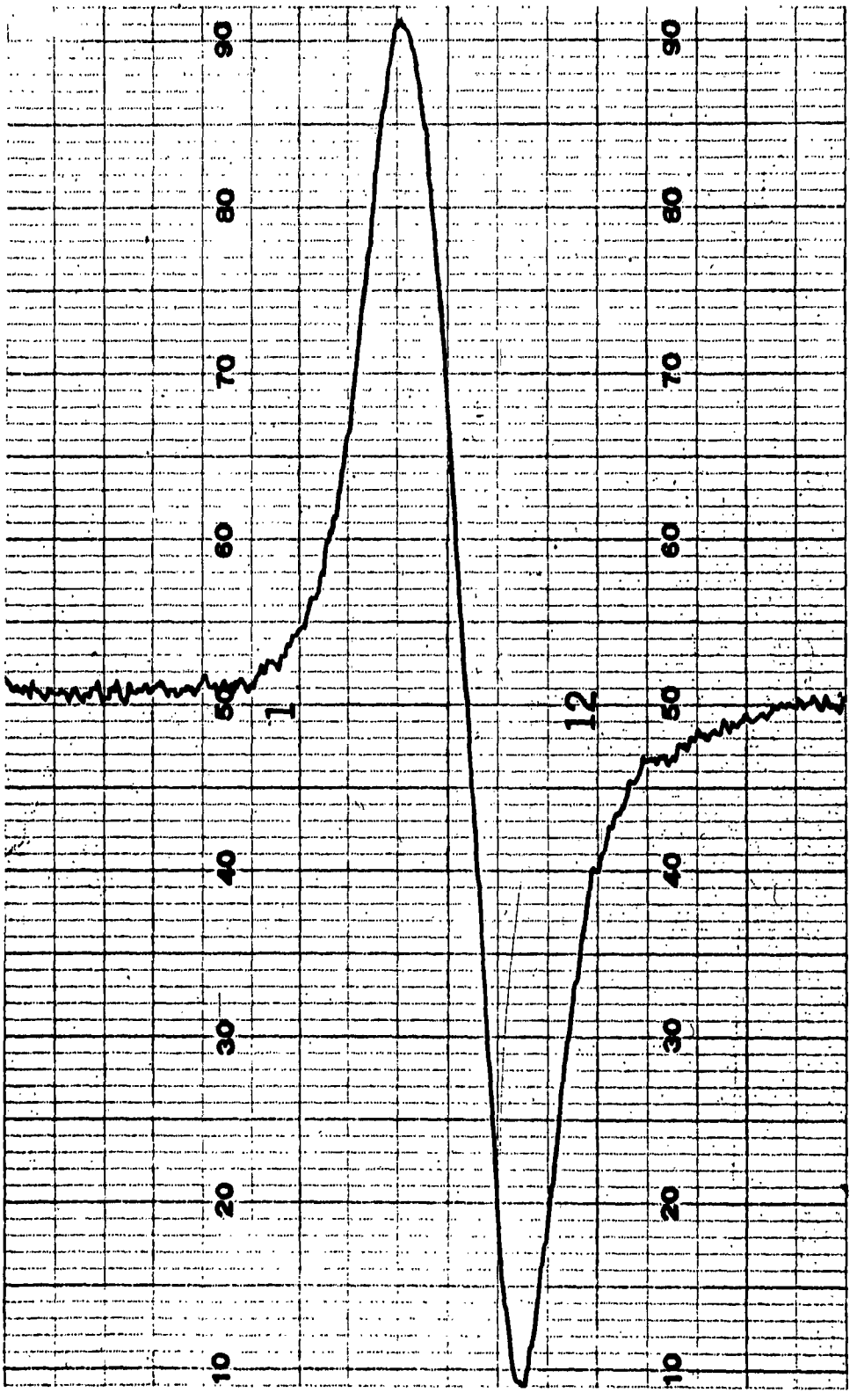

FIGURE 16: MAIN ABSORPTION LINE.

V. DISCUSSION

A. LOW CONCENTRATION (0.24% Fe^{3+})

The experimental relaxation times obtained at both L-band and X-band are plotted versus temperature on a log-log scale in Figure 10, page 48. The X-band results could be fitted to the empirical relation,

$$T_{1X}^{-1} = 3.2T + 0.004T^9 \ \text{sec}^{-1} \ .$$

Down to the lowest temperature of measurement the L-band results accurately fitted the relationship

$$T_{1L}^{-1} = 0.004T^9 \ \text{sec}^{-1} \ .$$

At the minimum attainable temperature the direct process had not yet appeared at L-band. It should also be noted that only one point was measured in the Raman region for X-band, and one point was extrapolated from the crossover region. The latter was obtained by subtracting the extrapolated direct rate from the observed rate. Since both points agree with the T^9 dependence observed at L-band, there evidently is no strong change of the Raman rate when the frequency is changed by a factor of five.

One may therefore conclude that the predicted T^9 dependence in the Raman region is confirmed over five decades of time at L-band, and is consistent with the X-band results. The linear temperature variation expected in the direct region is also consistent with the X-band measurements.

It is interesting to speculate on the frequency shift of the direct process, that would be expected between 8.5 Gc/s and 1.8 Gc/s. Since

$$T_{1X}^{-1} = 3.2T \quad \text{sec}^{-1}$$

$$T_{1L}^{-1} = 3.2 \left(\frac{\nu_L}{\nu_X}\right)^4 T \cong 0.0065T \quad \text{sec}^{-1} \ .$$

As indicated in Figure 10, this process would have halved the observed time constant at a temperature of 1.05°K, and it is unfortunate that the choice of L-band frequency and the lowest attainable temperature did not permit observation of the effect. One can, however, see from the results that a dependence much weaker than ν^4 is not possible.

Thus, one may conclude that the entire low concentration study does not contradict the theoretical predictions and, at least for the Raman region, is in excellent agreement with theory. One may also add that the author's findings at X-band agree with those of Bray et al. (12) at 4.18°K (as can be seen from Figure 4, page 29), but that nearly all other relaxation times for 0.1% and 0.2% Fe^{3+} concentration measured by Bray et al. are systematically shorter.

They used the "Pulse Saturation-Recovery" method, and saturation and/or spin diffusion effects would affect their measurements in the right direction.

A conventional paramagnetic spectrum was taken of the sample, but, as shown in Table 2, any lines other than the main transition would have to be extremely feeble.

B. HIGHER CONCENTRATIONS (0.51% to 3.5%Fe^{3+})

1. Features of the Data

Inspection of Figures 9-14, pages 46-52, indicates certain qualitative trends in the data that are clear. In the low temperature region, there appears to be a small increase in the X-band relaxation rate with increasing iron concentration, between 0.24% and 1.7%. At L-band there is a pronounced concentration dependence, the low temperature rate increasing from values too slow to measure (because of the competing Raman process) up to values equal to the X-band rate at 1.7 % concentration.

By the time a concentration of 3.5% is reached, a non-exponential relaxation is observed and becomes more pronounced in recovery curves taken below 3.5°K at L-band (See Figure 15, page 54). The fast decay rate is of the order of milliseconds and was subtracted out from the values given for T_1.

There is no evidence of phonon imprisonment from any of the data. While it was observed that the lines obtained in concentrated samples were more difficult to invert, consistently with the imprisonment mechanism, no increase in relaxation times occurred with increasing concentration, as would also be required by this process.

At higher temperatures, the data can be described qualitatively as showing a weak decrease in the exponent n of $T_{1R} \sim T^{-n}$ at concentrations above 0.24%. For example, the L-band data at 0.51% and 1.0% concentrations can be fitted rather well for $T \geq 1.7^{\circ}K$ by a curve with n = 8.3. By including the direct process $T_{1D} \sim T^{-1}$, one can in fact fit all curves over the whole temperature range, using $8 \leq n \leq 9$.

Alternatively, one can characterize the Raman data by adding an extra decay process that appears only above 0.24% concentration and has a temperature dependence other than T^9. As is discussed below, the author has tried this approach, using various functions of temperature for the added rate.

2. Heat Contact

It is possible to raise the objection that all data are distorted by poor heat contact between the sample and the bath. If the sample were hotter than the surroundings, the measured time constants would be characteristic of temperatures higher than the assigned values; moveover the discrepancy would increase with higher concentrations, because more energy would be stored in the more concentrated samples.

This argument can be rejected on two counts. In the first place, inadequate heat contact would be expected to give rise to a discontinuity in a plot of T_1 versus T at the λ-point. This behavior was never observed. Secondly, if the sample were

heated by the decaying magnetization to a temperature greater than ambient but more or less constant during a given relaxation time measurement one would expect a dependence of relaxation time on repetition rate. The only observed effect of this kind took place when the magnetization was not allowed to recover fully between pulses, so that a false equilibrium signal was used for the decay plots. This effect disappeared at lower repetition rates.

3. Data Reduction

a. General

At L-band, the Raman relaxation rate was established rather satisfactorily with the 0.24% sample as

$$T_{1R}^{-1} = 0.004T^9 \text{ sec}^{-1},$$

and one or two spot checks were made at X-band to show that there was no strong frequency shift.

At X-band the low concentration direct rate was relatively well fixed by data on the 0.24% and 0.51% crystals as

$$T_{1D}^{-1} = 3.2\ T\ ,$$

and the L-band direct rate was too slow to be seen.

The remainder of the data were examined for an added concentration dependent relaxation rate. As a first step, the quantity

$$T_1^{-1}(\text{conc.})_L = T_1^{-1} - 0.004\,T^9$$

was computed for the L-band data, and

$$T_1^{-1}(\text{conc.}) = T_1^{-1} - 0.004T^9 - 3.2\,T$$

was computed for the X-band data.

b. Power Series Expansion

In this reduction of the data, the author sought an added decay process of the form

$$d(\nu, f)\,T + b(\nu, f)T^7\,,$$

where ν is the Zeeman frequency and f the concentration. These particular terms were used instead of a general power series in T for reasons to be discussed below. Two methods were employed in finding "d" and "b". In the first, $T_1^{-1}(\text{conc.})$ was plotted on a log-log scale versus temperature. In the second, functions of the form

$$T_{1L}^{-1} = dT + bT^7 + 0.004T^9$$

and

$$T_{1X}^{-1} = (3.2 + d)T + bT^7 + 0.004T^9$$

were plotted on the experimental data, using "d" and "b" as parameters separately adjustable for each concentration and frequency. The two methods agreed within the accuracy of either one.

The curves are shown in Figure 11-14. The constants obtained are given in the following table.

f	d(1.8Gc/s,f)	3.2+d(8.5Gc/s,f)	b(1.8Gc/s,f)	b(8.5Gc/s,f)
0.24%	?	3.2	~0	~0
0.51%	~0.12	3.2	0.01	0.01
1.0 %	~0.2	not studied	0.01	not studied
1.7 %	4	4.3	?	0.01
3.5 %	~4.3	not studied	0.02	not studied

The coefficients of the linear term not marked as approximate are thought to be reliable with ± 10%, while the "b" values are perhaps good to within a factor of three. It should be noted, however, that the curves of Figures 11-14 are deceptive, as they are rather insensitive to the choice of coefficients. One would demand much more refined measuring apparatus (or much better statistics) to improve the accuracy, owing to the overriding T^9 term

c. Exponential Decay Process

In this decomposition, the data were tested for a concentration dependent rate,

$$T_{1\,(conc.)}^{-1} \sim e^{-\Delta/kT} ,$$

as proposed independently by Bloembergen and Pershan, by Van Vleck, and by Gill and Elliott (35). During the data reduction it became evident that a universal curve could be obtained for $T_{1(conc.)}^{-1}$ as a function of T for <u>all</u> samples (other than the 0.24% sample) by plotting

$$T_{1(conc.)}^{-1} = T_1^{-1} - 0.004\,T^9 - a(\nu,T) - h(\nu,f)$$

on a semilogarithmic scale versus T^{-1}. In this, $a(\nu)T$ is the direct rate at low concentration, so that

$$a(1.8\text{Gc/s}) \cong 0$$

and

$$a(8.5\text{Gc/s}) = 3.2 \quad .$$

The parameter $h(\nu,f)$ was rather well established in the data plots, that is, no reasonable curves could be constructed without it.

The results are shown in Figure 9a, page 47. They can be fitted by an exponential

$$T_{1(conc.)}^{-1} = 10^5\, e^{-20/T}\ \text{sec}^{-1}.$$

The values for the additive constant $h(\nu,f)$ in sec^{-1} are

$h(1.8\text{Gc/s},\ 3.5\%) \cong 10$

$h(1.8\text{Gc/s},\ 1.7\%) = 6.8$ $\qquad$ $h(8.5\text{Gc/s},\ 1.7\%) = 1.75$

$h(1.8\text{Gc/s},\ 1.0\%) = 0.43$

$h(1.8\text{Gc/s},\ 0.51\%) = 0.22$ $\qquad$ $h)8.5\text{Gc/s},\ 0.51\%) = 0.15$

In view of the fact that the values of $T_{1(conc.)}^{-1}$ represent small differences between large numbers of the same order of magnitude, it is remarkable that the plot shows any systematic trend at all. To give some indication of the reliability of the data, the symbol "F" (fair) was attached when the net rate constant was greater than 20% of the observed decay rate; and "P" (poor) was used to denote smaller differences.

An attempt to test for a linear concentration dependence in the coefficient of the exponential term

$$T_{1(conc.)}^{-1} \sim e^{-\Delta/kT}$$

was made by dividing the rates by the corresponding concentrations, but the results were inconclusive, owing to the large scatter in Figure 9a.

4. Interpretation

From the above analysis one sees that, even after subtraction of the low concentration direct and Raman rates, a concentration dependence is present.

Among the various choices for phenomenological characterization of the effect, three will now be discussed.

In the first, the exponent of the T^9 term was taken to decrease, and the coefficient of the T^{-1} term to increase, with increasing concentration. Since there does not appear to be any straightforward model for such behavior, this approach will not be pursued.

In the second method, concentration dependent T^7 and T^1 terms were added to the low concentration rates. To fit the data both terms must increase with increasing concentration, and the added T^1 term must be much more effective at L-band than at X-band. The reason for choosing only the exponents one and seven was to test a possible model that involved a concentration dependent decay process. As shown in Appendix I, both linear and seventh power temperature dependences could appear. The difficulty here is that the added direct rate decreases with increasing frequency, while one would expect an increase of at least the square of the frequency from the phonon density of states alone. Further speculations were abandoned in favor of the model presented below.

One model has been proposed by several authors (35) and is capable of explaining,at least qualitatively, the behavior of $T_{1(conc.)}^{-1}$ The model involves the decomposition of $T_{1(conc.)}^{-1}$ into the sum of an exponential function of temperature and a temperature independent term, as shown in Figure 9a.

The part of $T_{1(conc.)}^{-1}$ that varies exponentially with T^{-1} is consistent with a model proposed by Bloembergen and others (35). One considers cross relaxation between an isolated ion and a nearby pair, the latter being strongly coupled by exchange. If the pair $\vec{S}_1$, $\vec{S}_2$ is in its triplet state, transitions

$\Delta M(\vec{S}_1, \vec{S}_2) = \pm 1$ will be nearly coincident in frequency with the main absorption line of the single ion. (The departure from perfect coincidence would be due only to crystal field effects). Cross relaxation can therefore be very effective. Let the triplet state lie above the singlet by an energy $\Delta >> kT$, and let the relaxation rate between the triplet and the singlet be sufficiently fast to maintain Boltzmann equilibrium among the populations of the triplet and singlet levels. In view of the studies of Gill and Elliott (35) and Weber et al. (49) this assumption is not unreasonable.

Starting from the rate equations one can easily show that under these conditions

$$T_1^{-1} = (T_1^{-1})_{\text{all other processes}} + 2\omega_x N(\Delta) ,$$

where ω_x is the cross relaxation rate normalized to one ion and one pair, and $N(\Delta)$ is the number of pairs in the triplet state. Since

$$N(\Delta) = N\, e^{-\Delta/kT} ,$$

where N is the number of pairs, the relaxation rate of interest is just

$$2\omega_x N\, e^{-\Delta/kT} .$$

In a private communication J. M. Minkowski has indicated that an excited pair concentration of the order of $2 \cdot 10^{15}/cm^3$ could give a cross relaxation rate of the order of magnitude observed at 4^oK, with an ion concentration of 1% ($2 \cdot 10^{19}/cm^3$). From the slope of the curve in Figure 9a one finds $\Delta \sim 15^o$ to 20^oK, so that on this model a value of $N \sim 2 \cdot 10^{17}$ would be required.

In using the model one must assume that the effect appears rather suddenly between concentrations of 0.24% and 0.51% Fe^{3+}, and thereafter displays a dependence on concentration that is too weak to be revealed in the data. Although the coefficient associated with the exponential term of Figure 9a was taken to be constant, it is questionable whether a variation as fast as the first power of concentration could have been distinguished.

The constant term $h(\nu, f)$ could well result from residual cross relaxation between the main line and the "extra" lines (see Table 2). Such an effect would increase with increasing concentration and, at fixed concentration, would decrease with increasing magnetic field. Both trends were observed. While the origin of the extra lines is not clear, they could result from exchange coupling between more remote neighbors having $\Delta \sim h\nu$. There is precedent for this assumption in the work

of Rimai et al. (48). In this case, as opposed to the one discussed above, the cross relaxation rate could be limiting, because the lines did not coincide in frequency with the main transition.

The fast component of the decay curves for the more concentrated samples could perhaps be due to spin diffusion to the wings of the main line, as would occur if the field sweep were insufficient to span them. Indeed, at the highest concentration the wings were found to be disproportionately broad compared to the linewidth between inflection points. This explanation, however, is not very satisfying, as the diffusion time should be much less than milliseconds at this concentration. A more acceptable explanation has not been found.

In summary, the concentration dependence of T_1 can be ascribed to a "resonant" cross relaxation process between the main line and ion-pairs that are antiferromagnetically coupled by an exchange energy of the order of $20^{o}K$, and to a "non-resonant" cross relaxation between the single ion line and weakly coupled exchange pairs. It is of course tempting to assign the strong exchange to nearest neighbors pairs and the weak exchange to second, third, etc. nearest neighbor pairs.

VI. CONCLUSIONS

The main objective of this experimental study was to examine the temperature dependence of T_1 at different frequencies in order to test the theory developed by Van Vleck (7, 8), and in addition to test for any possible dependence of T_1 on concentration.

One may conclude that the low concentration results are consistent with the theoretical predictions, and, at least for the Raman region, are in excellent agreement with theory. A T^9 dependence was observed over five decades of T_1 at 1.8 Gc/s, and the same results were found at X-band. The linear temperature dependence predicted for the direct region was established at X-band, but was not observed at 1.8 Gc/s, as the Raman process was dominant even at the lowest temperatures attained. The predicted ν^4 dependence in the direct region was not established, but any frequency dependence much weaker than ν^4 would have been seen; in fact, the variation definitely had to be faster than ν^3. The author feels confident that the frequency dependence could easily be established by additional measurements at 3-4 Gc/s or at 12-18 Gc/s.

The data obtained at higher concentrations are much more complicated than theory would predict, but do not in any way contradict the theory. The data can be characterized by first

assuming additive rate processes that vanish in the low concentration limit, and then plotting the difference between the observed rates and their low concentration counterparts as a function of temperature. When this is done a universal curve is obtained, which fits all data (except those of the lowest concentration) with only one adjustable parameter.

While this curve may be deceptive, owing to the scatter in the data, it nevertheless can be interpreted in terms of two plausible processes. The first mechanism is postulated to be cross relaxation to the "extra" lines that appear at higher concentrations. The second process is taken to be cross relaxation from an isolated ion to a nearby pair that is strongly coupled by exchange and is also tightly coupled to the lattice. A third effect was also observed at the highest concentrations but was subtracted out from the data. The origin of this process is not fully understood.

In view of these findings it would seem extremely profitable to perform the same measurements at 3-4 Gc/s and above X-band within the concentration range of approximately 0.1% to 5% Fe^{3+}. It is probable that the ν^4 dependence of the direct process can be established directly for the lowest concentrations; in fact the requirements on concentration might be relaxed

at higher frequencies, where the direct process becomes faster than its concentration dependent competitors. In this respect it is noteworthy that the fourth-power variation predicted so long ago has, to the authors knowledge, never been verified for an iron group or rare earth ion in a diamagnetic host.

Once the direct process has been clearly verified, it would also be of interest to study the relaxation mechanisms that depend on concentration in a more detailed way than was possible with the present apparatus. The role of exchange-coupled pairs, for example, might be clarified by a careful study of the absorption spectra, in the manner used so successfully by the Raytheon group (48, 49) to study pairs in ruby.

APPENDIX I. THEORETICAL CONSIDERATIONS

A. CRYSTAL FIELD SPLITTING

The development of the crystal field splitting calculations given below is based on the theory developed by Griffith (27) and the calculations performed by Kiel et al. (12), with some modifications.

In this section we shall show the origin of the ground state Kramers doublet. The crystalline field has predominantly cubic symmetry, which splits the e and t orbitals by about $10^4 cm^{-1}$. One therefore has to consider only the t orbitals. The ground manifold for octahedral symmetry can be written t_2^5, in accordance with the notation used by Griffith (27). Since Fe^{3+} has one empty t orbital and Ti^{3+} in the same symmetry has one filled t orbital, the t_2^1 manifold is complementary to the t_2^5 manifold with respect to the filled t_2^6 manifold. One may therefore use the much simpler t_2^1 manifold for the calculations, and, remembering that one really has a "hole" instead of an electron, change the appropriate signs at the end of the calculation.

From the angular functions for the d-electrons, $e^{\pm 2i\phi}P_2^2(\cos\theta)$, $e^{\pm i\phi}P_2^1(\cos\theta)$ and $P_2^o(\cos\theta)$, one easily constructs the Cartesian wave functions,

$i\frac{xy}{r^2}$, $i\frac{yz}{r^2}$, and $\frac{zx}{r^2}$ for the t orbitals; and

$\frac{x^2-y^2}{r^2}$, $\frac{2z^2-x^2-y^2}{r^2}$ for the e orbitals.

The associated wavefunctions are:

$$\left.\begin{aligned} \psi_{xy} &= \frac{1}{i\sqrt{2}}(|2,2\rangle - |2,-2\rangle) \\ \psi_{yz} &= \frac{i}{\sqrt{2}}(|2,1\rangle + |2,-1\rangle) \\ \psi_{zx} &= \frac{i}{\sqrt{2}}(|2,1\rangle - |2,-1\rangle) \end{aligned}\right\} \text{t orbitals}$$

$$\left.\begin{aligned} \psi_{x^2-y^2} &= \frac{1}{\sqrt{2}}(|2,2\rangle + |2,-2\rangle) \\ \psi_{z^2} &= |2,0\rangle \end{aligned}\right\} \text{e orbitals} \quad .$$

For convenience one uses the following wave functions instead of the t wave functions:

$$\psi_{\xi}^{(\pm)} = |2,1,\pm 1/2\rangle \quad = |1,\pm\rangle = |\xi,\pm\rangle$$

$$\psi_{\eta}^{(\pm)} = |2,-1,\pm 1/2\rangle \quad = |-1,\pm\rangle = |\eta,\pm\rangle$$

$$\psi_{\zeta}^{(\pm)} = \frac{1}{i\sqrt{2}}(|2,2,\pm 1/2\rangle - |2,-2,\pm 1/2\rangle) = |\zeta,\pm\rangle = \frac{1}{i}|\zeta_1,\pm\rangle \quad .$$

where the signs refer to the spin orientation.

The rhombic distortion and the spin orbit coupling split the cubic ground state into three Kramers doublets. Since the magnitudes of these interactions relative to one another are not known, but both are presumably small compared to the cubic field, one treats them together as a perturbation. A general wavefunction, with unknown coefficients, can be written for a Kramers doublet.

$$|\psi^+\rangle = A|1,+\rangle + B|\zeta_1,-\rangle + C|-1,+\rangle$$
$$|\psi^-\rangle = A|-1,-\rangle - B|\zeta_1,+\rangle + C|+1,-\rangle$$

where $\langle x|\psi^+\rangle = i\langle x|\psi^-\rangle^*$, for all x. A, B, C are real constants, and $A^2 + B^2 + C^2 = 1$.

Assuming that there is a single orbital g-factor, k, that may differ from unity, as proposed by Bleaney and O'Brien (10), one has the Zeeman Hamiltonian

$$\mathcal{H} = \beta\vec{H} \cdot (k\vec{L} + 2\vec{S})$$
$$= \beta \{H_x(kL_x+2S_x) + H_y(kL_y+2S_y) + H_z(kL_z+2S_z)\}$$

One should note that covalent bonding in the host crystal is only considered insofar as it is included in the orbital reduction factor k, and in the reduction of the spin-orbit coupling factor λ. The only non-vanishing matrix elements of $\mathcal{H}$ are

$$\langle\psi^\pm|\tfrac{k}{2}(L^+ + L^-) + (S^+ + S^-)|\psi^\pm\rangle = \sqrt{2}\,k\,B(C-A) + (2AC - B^2)$$
$$\langle\psi^\pm|\tfrac{k}{2}(L^+ - L^-) + (S^+ - S^-)|\psi^\pm\rangle = \pm\tfrac{1}{i}\{\sqrt{2}kB(C+A) + (2AC+B^2)\}$$
$$\langle\psi^\pm|kL_z+2S_z)|\psi^\pm\rangle = \pm\{k(A^2-C^2) + (A^2-B^2+C^2)\} \quad ,$$

and one can write down the Zeeman matrix between the wavefunctions of the Kramers doublet, as shown in Table 3. This matrix applies to any of the three Kramers doublets but each of them will have different values for the constants A, B, and C. The same matrix can be written down in terms of a rhombic "spin Hamiltonian", with an effective spin of 1/2:

$$\mathcal{H} = \beta\vec{H} \cdot g \cdot \vec{S} = \beta(g_x H_x S_x + g_y H_y S_y + g_z H_z S_z),$$

from which one may calculate g for any arbitrary direction of H.

$$g = \sqrt{g_x^2 \sin^2\theta \cos^2\phi + g_y^2 \sin^2\theta \sin^2\phi + g_z^2 \cos^2\theta}$$

The values of A, B, C, and k can therefore be found empirically from experimental g-values. Baker et al. (9) measured $g_x = 2.35$, $g_y = 2.10$ and $g_z = 0.915$.

The relationship between the principal axes of g and the orthorhombic axes of the crystal is shown in Table 4, and Figure 17. Due to the presence of two magnetic complexes, $K_3Co(CN)_6$ has two sets of principal axes. The right handed principal axes will be used throughout this section.

	ψ^+	ψ^-
ψ^+	$\left[k(A^2-C^2)+(A^2-B^2+C^2)\right]\beta H_z$	$\left[\sqrt{2}kB(C-A)+(2AC-B^2)\right]\beta H_x$ $+\frac{1}{i}\left[\sqrt{2}kB(C+A)+(2AC+B^2)\right]\beta H_y$
ψ^-	$\left[\sqrt{2}kB(C-A)+(2AC-B^2)\right]\beta H_x$ $-\frac{1}{i}\left[\sqrt{2}kB(C+A)+(2AC+B^2)\right]\beta H_y$	$-\left[k(A^2-C^2)+(A^2-B^2+C^2)\right]\beta H_z$

Table 3: Matrix Elements Between the Wavefunctions of The Kramers Doublet.

Orthorhombic axis \ Principal Axis	Direction Cosines			Orientation of Principal Axes				
	x	y	z	x'	x	y'	y	z
a	0.866	0.500	0.000	30°	330	300	60°	90°
b	±0.500	∓0.866	0.000	300°	240°	210°	330°	90°
c	0.00	0.00	1.000	90°	90°	90°	90°	0°

Table 4: Relationship Between the Orthorhombic Axes (a, b, c) and the Principal Axes (x, y, z). (The Direction Cosines are Taken from Baker et al. (9)).

Orthorhombic axis \ Octahedral Axis	Direction Cosines			Orientation of Octahedral Axes					
	α	β	γ	α''	α'	β''	β'	γ''	γ'
a	0.45	-0.63	0.63	63°	297°	231°	129°	51°	309°
b	±0.89	±0.32	∓0.32	333°	207°	109°	71°	289°	251°
c	0.00	0.71	0.71	90°	90°	45°	45°	45°	45°

Table 5: Relationship Between the Orthorhombic Axes (a, b, c) and the Two Cyanide Octahedral Axes (α, β, γ). (The Direction Cosines are Taken From Baker et al (9)).

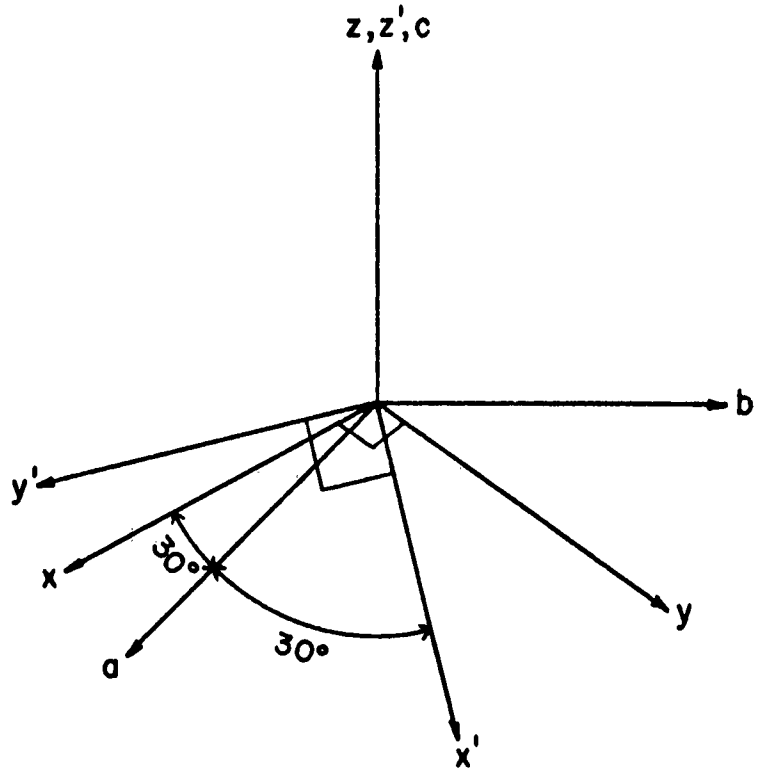

FIGURE 17: RELATIONSHIP BETWEEN THE ORTHORHOMBIC AXES (a, b, c) AND THE PRINCIPAL AXES (x, y, z).

The orthorhombic axes are in turn related to the two cyanide octahedral axes as shown in Table 5 and Figure 18.

Separating the matrix given in Table 3 into the x, y, and z components, finding the eigenvalues, and using the spin Hamiltonian, we have the following relationships between the experimental g values and the constants A, B, C, and k.

$$g_x = 2\left[2kB(C-A) + (2AC-B^2)\right] = \pm (2.35 \pm 0.02)$$
$$g_y = 2\left[2kB(C+A) + (2AC+B^2)\right] = \pm (2.10 \pm 0.02)$$
$$g_z = 2\left[k(A^2-C^2) + (A^2-B^2+C^2)\right] = \pm (0.915 \pm 0.01)$$
$$A^2 + B^2 + C^2 = 1 \quad .$$

Since one cannot experimentally determine the signs of the g-values, the above equations do not have a unique solution. Bleaney and O'Brien (10) found a best fit with experiment by assuming all g-values negative and using $k = 0.875$. Using $k = 0.87$, Kiel (43) found that for g_x and g_z negative and g_y positive, the best fit was for $A = 0.35$, $B = 0.86$, and $C = -0.05$.

One finally has the following wavefunctions for the ground state Kramers doublet.

$$|\psi_o^+\rangle = 0.35|1,+\rangle + 0.86|\zeta_1,-\rangle - 0.05|-1,+\rangle$$
$$|\psi_o^-\rangle = 0.35|-1,-\rangle - 0.86|\zeta_1,+\rangle - 0.05|+1,-\rangle.$$

The spin-orbit interaction $\lambda(\vec{L} \cdot \vec{S})$ has the following non-zero matrix elements.

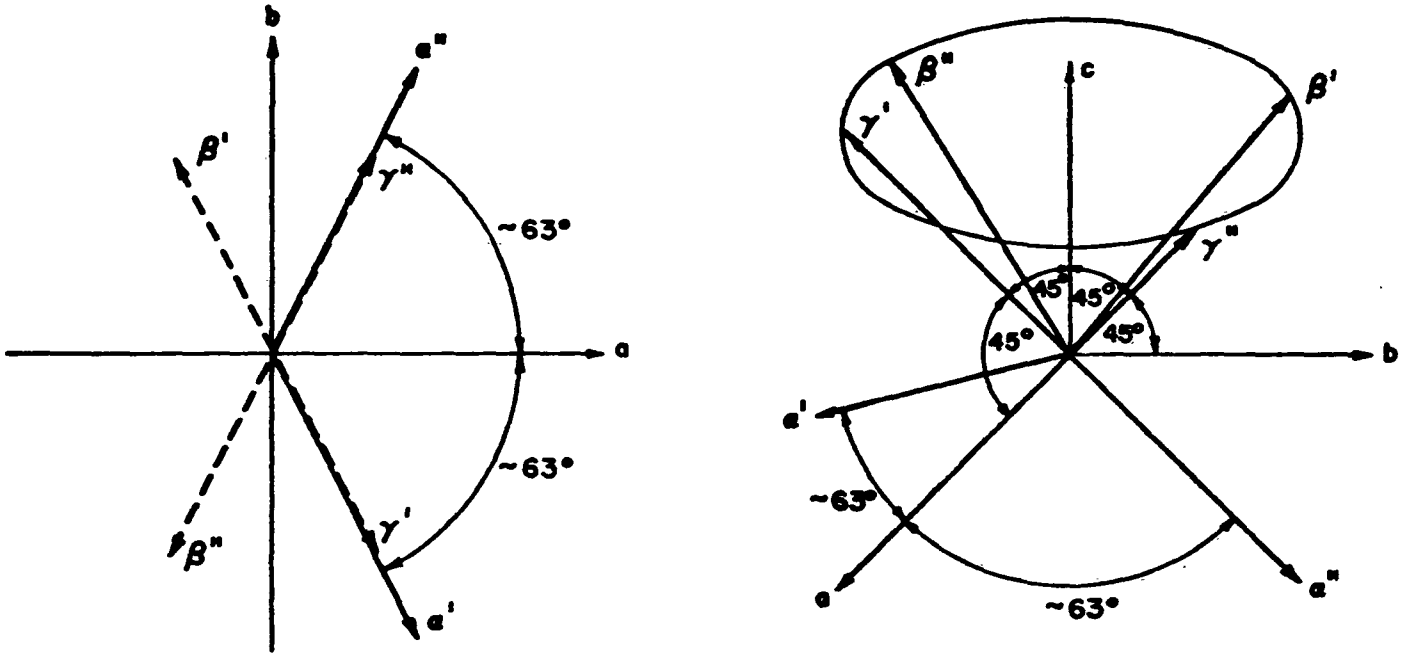

FIGURE 18: RELATIONSHIP BETWEEN THE ORTHORHOMBIC AXES (a, b, c) AND THE TWO CYANIDE OCTAHEDRAL AXES (α, β, γ).

$$\langle 1,+|\lambda(L_zS_z)|1,+\rangle = \frac{\lambda}{2} = \langle -1,-|\lambda(L_zS_z)|-1,-\rangle$$

$$\langle -1,+|\lambda(L_zS_z)|-1,+\rangle = \frac{\lambda}{2} = \langle 1,-|\lambda(L_zS_z)|1,-\rangle$$

$$\langle \zeta_1,-|\lambda(L_xS_x+L_yS_y)|-1,+\rangle = \frac{\sqrt{2}}{2}\lambda = \langle -(\zeta_1,+)|\lambda(L_xS_x+L_yS_y)|-1,-\rangle$$

$$\langle 1,+|\lambda(L_xS_x+L_yS_y)|\zeta_1,-\rangle = \frac{\sqrt{2}}{2}\lambda = \langle -1,-|\lambda(L_xS_x+L_yS_y)|-(\zeta_1,+)\rangle .$$

Using the energy level for the t orbitals in a cubic field as a reference, one has the new energy levels, due to the rhombic field, at

$$E_\xi = (1/2)V$$

$$E_\eta = -(1/2)V$$

$$E_\zeta = \Delta \quad .$$

One may now write down the two conjugate submatrices for the joint spin-orbit coupling and rhombic distortion within the t_2^1 manifold, as shown in Table 6.

The secular equations associated with Table 6 are

$$(\frac{\lambda}{2} - E)A + \frac{\sqrt{2}}{2}\lambda B + \frac{1}{2}VC = 0$$

$$\frac{\sqrt{2}}{2}\lambda A + (\Delta - E)B + 0 = 0$$

$$\frac{1}{2}VA + 0 + (-\frac{\lambda}{2} - E)C = 0 \quad ,$$

where A, B, and C are as defined earlier and E is the energy of the ground state doublet $|\psi_o^{\pm}\rangle$. Using A, B, C as obtained from the experimental g-values Bray et al. (12) found the following values for the unknowns E, Δ, and V(E is of course, superfluous).

$E\lambda^{-1} = 2.31$

$\Delta\lambda^{-1} = 2.02$

$V\lambda^{-1} = -0.81$.

	$\lvert 2, 1, +\frac{1}{2}\rangle$ $\lvert \zeta, -\frac{1}{2}\rangle$ $\lvert 2, -1, +\frac{1}{2}\rangle$	
	$\lvert 2, -1, -\frac{1}{2}\rangle - \lvert \zeta, +\frac{1}{2}\rangle \lvert 2, 1, -\frac{1}{2}\rangle$	
$\lvert 2, 1, +\frac{1}{2}\rangle$ or $\lvert 2, -1, -\frac{1}{2}$	$\frac{1}{2}\lambda$ $\quad$ $\frac{\sqrt{2}}{2}\lambda$ $\quad$ $\frac{1}{2}\lambda$	
$\lvert \zeta_1, -\frac{1}{2}\rangle$ or $\lvert \zeta, +\frac{1}{2}\rangle$	$\frac{\sqrt{2}}{2}\lambda$ $\quad$ Δ $\quad$ 0	
$\lvert 2, -1, +\frac{1}{2}\rangle$ or $\lvert 2, 1, -\frac{1}{2}\rangle$	$\frac{1}{2}V$ $\quad$ 0 $\quad$ $-\frac{1}{2}\Delta$	

where $\lvert \zeta_1, \pm 1/2\rangle = i\lvert \zeta, \pm 1/2\rangle = \frac{-1}{\sqrt{2}} (\lvert 2, 2\pm 1/2\rangle - \lvert 2\text{-}2, \pm 1/2\rangle)$

Table 6: Matrix of the Rhombic Field and the Spin Orbit Coupling Within t_2^1.

Finally one can write down the determinental equation for the energy levels, remembering that since one has been working with the t_2^1 manifold instead of the t_2^5 manifold, the signs of λ, V, and Δ must now be changed.

$$\begin{vmatrix} (-\frac{\lambda}{2} - E) & -\frac{\sqrt{2}}{2}\lambda & -\frac{1}{2}V \\ -\frac{\sqrt{2}}{2}\lambda & (-\Delta - E) & 0 \\ -\frac{1}{2}V & 0 & (+\frac{\lambda}{2} - E) \end{vmatrix} = 0$$

Using $\lambda = 280\ cm^{-1}$ as found by Bleaney and O'Brien (10), Bray et al (12) found the energy levels,

$$E_o = -640\ cm^{-1}$$
$$E_1 = -110\ cm^{-1}$$
$$E_2 = 190\ cm^{-1},$$

which give the energy separations between Kramers doublets,

$$\Delta_{10} = 530\ cm^{-1}$$
$$\Delta_{20} = 830\ cm^{-1}$$
$$\Delta_{21} = 300\ cm^{-1} \quad .$$

Thus the ground doublet is well isolated from the others and is the only one occupied at helium temperatures; moreover the first excited doublet is separated from the ground state by an energy that is probably well above the Debye value.

B. THE OSCILLATING CRYSTAL FIELD

1. Lattice Vibrations

The mechanism for coupling the ion to the lattice vibrations is taken to be the oscillating crystal field, whose Hamiltonian depends on both the ionic and lattice coordinates. The theory of lattice vibrations has been considered by many authors (7, 44, 45); however, since it is basic to the entire theory of relaxation effects in crystals, a short summary will be given.

The displacement from equilibrium $\vec{U}(\vec{r}_n)$, due to the oscillating crystal field, of an ion "n" of the nearest neighbor complex, located an average distance $\vec{r}_n$ from the paramagnetic ion, can, in the quantized version, be written (44, 45)

$$\vec{U}(\vec{r}_n) = \sum_j \left[\frac{2h}{M\omega_j}\right]^{1/2} \cdot \vec{e}_j \cdot \left[q_j^+ + q_j^-\right] \cos\left[\vec{k}_j \cdot \vec{r}_n - \delta_j\right] \quad ,$$

where $\vec{k}_j$ is the wave vector, $\vec{e}_j$ the unit polarization vector, ω_j the angular frequency, and M the total mass of the sample. The subscript "j" labels a particular lattice wave, and the phase is given by δ_j. q^+ and q^- are quantum mechanical raising and lowering operators satisfying the relationship,

$$\left[q^+, q^-\right] = 1 \quad .$$

In the number representation, the only nonvanishing matrix elements of q^+ and q^- are

$$\langle n_j + 1 | q_j^+ | n_j \rangle = \langle n_j | q_j^- | n_j + 1 \rangle = \sqrt{n_j + 1} \quad ,$$

where n_j is the occupation number of lattice mode "j". The frequency of vibration is related to the velocity of sound, $\vec{v}_j$, by

$$\vec{v}_j = \omega_j \frac{\vec{k}_j}{k_j^2} \quad .$$

Since the wavelengths $2\pi/|\vec{k}_j|$ are long compared to the dimensions of the complex $|\vec{r}_n|$ for frequencies used in this experiment,

$$\vec{k}_j \cdot \vec{r}_n = \omega_j \frac{\vec{k}_j \cdot \vec{r}_n}{\vec{k}_j \cdot \vec{v}_j} << 1 ,$$

and one may use the approximation,

$$\cos(\vec{k}_j \cdot \vec{r}_n - \delta_j) \cong \vec{k}_j \cdot \vec{r}_n \sin \delta_j = \omega_j \frac{\vec{k}_j \cdot \vec{r}_n}{\vec{k}_j \cdot \vec{v}_j} \sin \delta_j .$$

Thus

$$\vec{U}(\vec{r}_n) \cong \sum_j \left[\frac{2h\omega_j}{M}\right]^{1/2} \cdot \vec{e}_j \left[q_j^+ + q_j^-\right] \cdot \frac{\vec{k}_j \cdot \vec{r}_n}{\vec{k}_j \cdot \vec{v}_j} \sin \delta_j$$

$$= \sum_j a_{nj} \cdot \omega_j^{1/2} \left[q_j^+ + q_j^-\right]$$

where the constants a_{nj} do not depend on frequency.

2. Vibrations of the Cyanide Complex

We consider a paramagnetic ion at the center of the complex of nearest neighbors. Let the Hamiltonian due to the modulation of the crystal field by thermal vibrations be

$$\mathcal{H}^1 = \sum_{i,i'} \frac{\partial V}{\partial Q_i} Q_i + 1/2 \frac{\partial V}{\partial Q_i} \frac{\partial V}{\partial Q_{i'}} \cdot Q_i \cdot Q_{i'} + \ldots ,$$

where V is the local crystalline potential and the Q_i are vibrational normal modes of the complex (not the lattice), which are to be regarded as operators. One should note that the cyanide complex has a center of symmetry, so that one may classify the

vibrations as even or odd with respect to inversion, and only the even vibrations need be considered. Another simplifying factor in octahedra of 6-fold coordination is that only one vibration of a given symmetry need be considered. The 6 normal modes which remain are shown in Figure 19. A more complete discussion is given by Van Vleck (7) and Kiel (45).

The Q_i's are defined by taking certain linear combinations of the components $U_d(\vec{r}_n)$ of the displacement vector $\vec{U}(\vec{r}_n)$ of the nearest neighbors, that is

$$Q_i = \sum_{nd} C^i_{nd} \, U_d \, (\vec{r}_n) \, ,$$

which can be written

$$Q_i = \sum_j b_{ij} \, \omega_j^{1/2} \left[q^+ + q^- \right]$$

where

$$b_{ij} = \sum_{n,d} C^i_{nd} \, a_{nj}$$

and b_{ij} is not a function of frequency. Due to the orthogonality of the q_j's one finds

$$|\langle n_j+1 | Q_i | n_j \rangle|^2 = \sum_j |b_{ij}|^2 \omega_j |\langle n_j+1 | q_j^+ + q_j^- | n_j \rangle|^2$$

where $|b_{ij}|^2$ has now been averaged over phase and propagation in the manner given by Van Vleck (8).

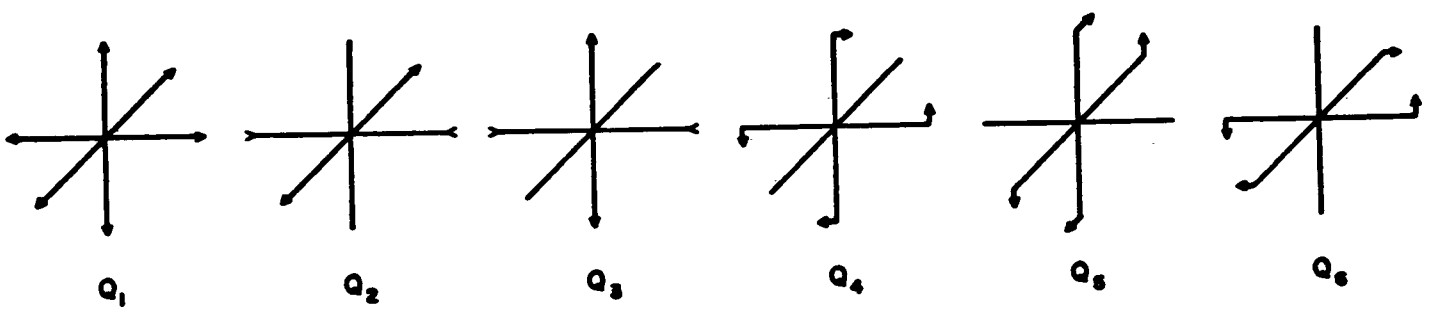

FIGURE 19: EVEN MODES OF VIBRATION FOR AN OCTAHEDRAL COMPLEX.

$$|b_{ij}|^2 = \frac{r^2\hbar}{60Mv_l^2} \quad \text{(longitudinal)}$$

$$= \frac{r^2\hbar}{80Mv_t^2} \quad \text{(transverse)}$$

Thus apart from any frequency dependence of the n_j's, one factor of frequency is found in the squared matrix element of the phonon operators.

C. SPIN-LATTICE RELAXATION

1. General Considerations

The development of the spin-lattice relaxation theory given below is based on the approach developed by Orbach (32), with some modifications. Since the dependence of T_1 on frequency and temperature in a Kramers salt is the subject of the present experiment, this section attempts mainly to demonstrate these features. The exchange interaction, although it is probably important in explaining the experimental results, has not been treated theoretically and will not be considered; however, some discussion will be included in Chapter V.

2. The Direct Process

Considering the system shown in Figure 20, we now calculate the transition probability for the process in which one resonant phonon is emitted or absorbed. The appropriate perturbation formula for emission is

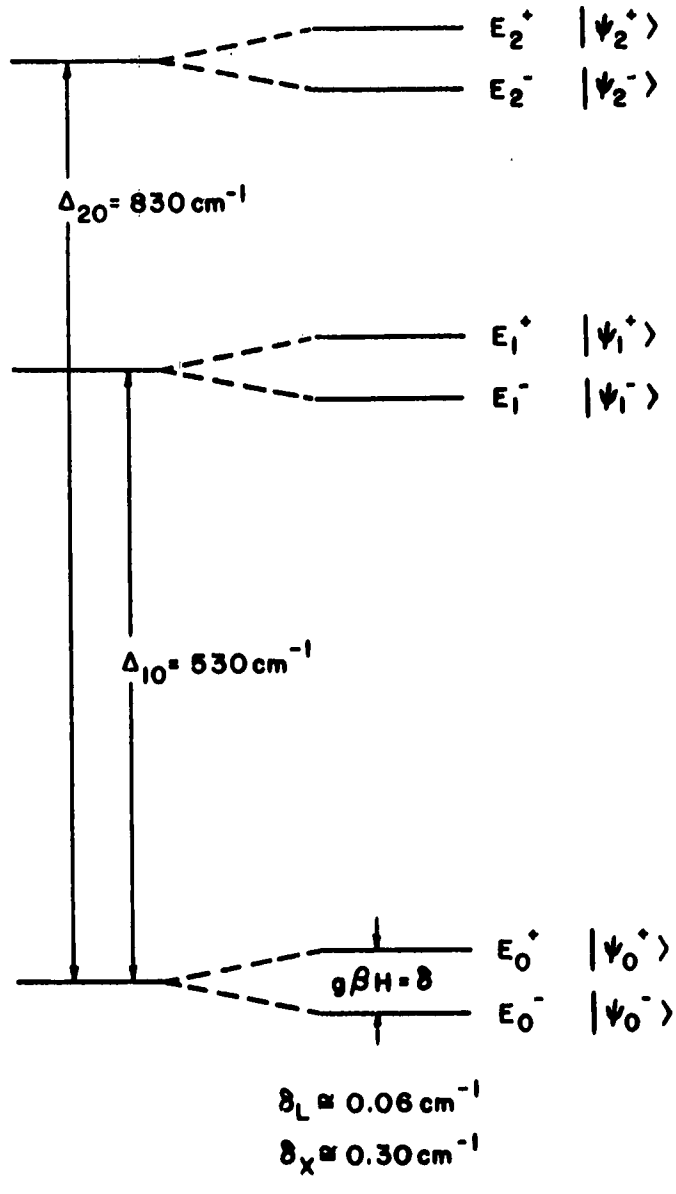

FIGURE 20: ENERGY LEVEL DIAGRAM FOR THE KRAMERS DOUBLETS.

$$W_{+\rightarrow -} = \frac{1}{\hbar^2} \left| \langle n(E) + 1, \psi_o^- | H' | n(E), \psi_o^+ \rangle \right|^2 \cdot \rho(\nu),$$

where n(E) means that only the phonons with energy $E = h\nu$, where ν is the frequency separation between $|\psi_o^-\rangle$ and $|\psi_o^+\rangle$, take part in the transition. The quantity

$$\rho(\nu) = 4\pi V \left(\frac{1}{v_\ell^3} + \frac{2}{v_t^3} \right) \nu^2 = \frac{12\pi V}{v_{avg.}^3} \nu^2$$

is the density of phonon states. One should note that in obtaining the above expression for $\rho(\nu)$ one has assumed a Debye spectrum and summed over the two transverse and one longitudinal modes.

Using the first term in the expansion of H' one has

$$W_{+\rightarrow -} = \frac{\pi^2 r^2}{3\hbar v^5} \cdot \frac{V}{M} \left| \sum_i \langle \psi_o^- | \frac{\partial V}{\partial Q_i} | \psi_o^+ \rangle \sum_j \langle n(E)+1 | q_j^+ + q_j^- | n(E) \rangle \right|^2 \nu^3.$$

In the case of thermal equilibrium one may replace n_j by its statistical average, the Bose-Einstein factor

$$\bar{n}_j = \left[e^{h\nu_j/kT} - 1 \right]^{-1}$$

$$\bar{n}_j + 1 = \left[1 - e^{-h\nu_j/kT} \right]^{-1} .$$

For this particular case only the modes "j" for which $\nu_j = \nu$ are to be summed over.

Substituting into the above formula one then has

$$W_{+\to -} = \frac{\pi^2 r^2}{3h\nu^5} \cdot \frac{V}{M} \left| \sum_i \langle \psi_o^- | \frac{\partial V}{\partial Q_i} | \psi_o^+ \rangle \right|^2 \cdot \nu^3 \left[1 - e^{-h\nu/kT} \right]^{-1}$$

Since the states $|\psi_o^-\rangle$ and $|\psi_o^+\rangle$ are time conjugates of one another, the matrix elements should be zero because $\frac{\partial V}{\partial Q_i}$ is invariant under time reversal. Addition of an external magnetic field, whose Hamiltonian does not have time reversal symmetry, will cause admixture of excited states into the zeroth order states. If one writes,

$$\mathcal{H}_z = \beta \vec{H} \cdot (k\vec{L} + 2\vec{S})$$

as described in Section A, the corrected wave functions become

$$|\psi_o^+\rangle = |\psi_o^+\rangle - \frac{\beta \vec{H}}{\Delta} \cdot \langle \psi_1 | \vec{O} | \psi_o^+ \rangle |\psi_1\rangle$$

$$|\psi_o^-\rangle = |\psi_o^-\rangle - \frac{\beta \vec{H}}{\Delta} \cdot \langle \psi_1 | \vec{O} | \psi_o^- \rangle |\psi_1\rangle ,$$

where $k\vec{L} + 2\vec{S}$ has been abbreviated by the operator $\vec{O}$, and the fact that $|\psi_1\rangle$ is a Kramers doublet has not been indicated explicitly. One may now write down the matrix element between the Zeeman corrected wavefunctions.

$$\langle \psi_o^- | \frac{\partial V}{\partial Q_i} | \psi_o^+ \rangle = - \frac{\beta \vec{H}}{\Delta} \{ \langle \psi_o^- | \frac{\partial V}{\partial Q_i} | \psi_1 \rangle \langle \psi_1 | \vec{O} | \psi_o^+ \rangle + \langle \psi_o^- | \vec{O} | \psi_1 \rangle \langle \psi_1 | \frac{\partial V}{\partial Q_i} | \psi_o^+ \rangle \} ,$$

where one has used the fact that

$$\langle \psi_o^- | \frac{\partial V}{\partial Q_i} | \psi_o^+ \rangle = 0 .$$

Since one is dealing with Kramers doublets

$$\langle x|\psi^{\pm}\rangle = i\,\langle x|\psi^{\mp}\rangle^{*}, \text{ hence } \quad \langle \psi^{=}|x\rangle = -\langle \psi^{\mp}|x\rangle^{*}.$$

Thus

$$\langle \psi_o^-|\vec{\sigma}|\psi_1\rangle\langle\psi_1|\frac{\partial V}{\partial Q_i}|\psi_o^+\rangle = -i^2\langle\psi_o^+|\vec{\sigma}|\psi_1\rangle^*\langle\psi_1|\frac{\partial V}{\partial Q_i}|\psi_o^-\rangle^*$$

and one may write

$$\langle \psi_o^-|\vec{\sigma}|\psi_1\rangle\langle\psi_1|\frac{\partial V}{\partial Q_i}|\psi_o^+\rangle = \langle\psi_1|\vec{\sigma}^{\,*}|\psi_o^+\rangle\langle\psi_o^-|\frac{\partial V}{\partial Q_i})^*|\psi_1\rangle .$$

Since both $\vec{\sigma}$ and $\frac{\partial V}{\partial Q_i}$ are Hermitian, one has

$$\langle \psi_o^-|\vec{\sigma}|\psi_1\rangle\langle\psi_1|\frac{\partial V}{\partial Q_i}|\psi_o^+\rangle = \langle\psi_o^-|\frac{\partial V}{\partial Q_i}|\psi_1\rangle\langle\psi_1|\vec{\sigma}|\psi_o^+\rangle .$$

Hence one may write the simplified expression

$$\langle\psi_o^-|\frac{\partial V}{\partial Q_i}|\psi_o^+\rangle = -\frac{2\beta\vec{H}}{\Delta}\cdot\langle\psi_o^-|\frac{\partial V}{\partial Q_i}|\psi_1\rangle\langle\psi_1|\vec{\sigma}|\psi_o^+\rangle .$$

Thus, the transition probability becomes

$$W_{+\to -} = \frac{4\pi^3 rh}{3v^5\Delta^2}\cdot\frac{V}{M}\Big|\sum_i \frac{\vec{H}}{gH}\cdot\langle\psi_o^-|\frac{\partial V}{\partial Q_i}|\psi_1\rangle\langle\psi_1,|\vec{\sigma}|\psi_o^+\rangle\Big|^2\cdot\nu^5\left[1-e^{-h\nu/kT}\right]^{-1},$$

where the two additional factors of ν come from the Zeeman perturbation, and the g value to be used is that of the ground state.

For the reverse process $W_{-\to +}$ one gets the same expression except that

$$n(E) = \left[e^{h\nu/kT}-1\right]^{-1}$$

appears instead of n(E) + 1. But the measured relaxation time is

$$1/T_1 = W_{+\rightarrow -} + W_{-\rightarrow +},$$

which is proportional to

$$2\bar{n}(E) + 1 = \left[e^{h\nu/kT} + 1 \right] \left[e^{h\nu/kT} - 1 \right]^{-1}$$

For the frequencies and temperatures used in this experiment, $h\nu \ll kT$, so that

$$2\bar{n}(E) + 1 \cong 2kT/h\nu \quad .$$

Thus

$$1/T_{1D} \cong \frac{8\pi r^2 k}{3v^5 \Delta^2} \cdot \frac{V}{M} \left| \frac{\vec{H}}{gH} \cdot \langle \psi_o^- | \frac{\partial V}{\partial Q_i} | \psi_1 \rangle \langle \psi_1 | \vec{\sigma} | \psi_o^+ \rangle \right|^2 \nu^4 T \ ,$$

where D indicates the direct process. Since the matrix elements are not a function of frequency and temperature, one has the important result (8, 32)

$$1/T_{1D} = a\nu^4 T \quad .$$

In this expression, two factors of frequency and one of temperature came from the phonon matrix elements, while two powers of frequency came from the (required) Zeeman mixing of Kramers doublets.

Unfortunately, reliable calculations of the coefficient "a" cannot be performed since the wavefunctions of the excited states are not known; moreover the result depends critically on

parameters that are not accurately known, namely on the velocity of sound and the splitting between different Kramers doublets. By analogy to the case of Ti^{3+} in alum, a rough numerical estimate can be made by using the appropriate matrix elements calculated by Van Vleck (7.8). This was done by Bray et al. (12) who arrived at the result, (for $\nu = 8.7$ Gc/s)

$$1/T_{1D} \cong 15T \text{ sec}^{-1}.$$

This value should not be taken too seriously because Van Vleck's matrix elements cannot really be carried directly over to the present case.

One may add that for a non-Kramers salt direct transitions would have been possible between the two lowest energy levels, without admixture by the Zeeman field. From the development one can easily see that this would have given the relationship,

$$1/T_{1D} \sim \nu^2 T \quad .$$

3. The Raman Process

For the direct process the interaction Hamiltonian was expanded only to terms linear in Q_i and was used with first order perturbation theory. In the Raman process there are two possibilities. In the first the term linear in Q_i is used with second order perturbation theory, and in the second, the term quadratic in Q_i is used to first order with Zeeman-mixed wave-functions. In both cases one finds the creation and destruction of two phonons whose difference in energy equals the splitting of the participating spin state.

Using the term linear in Q_i with second order perturbation theory, one may write down the following matrix element, (neglecting the highest Kramers doublet):

$$\langle \psi_o^-, n_i, n_k | H' | \psi_o^+, n_i', n_k' \rangle =$$

$$\sum_{j,\ell''} \frac{1}{E_o' - E''} \langle \psi_o^-, n_i, n_k | \frac{\partial V}{\partial Q_j} Q_j | \psi_1, n_i'', n_k'' \rangle \langle \psi_1, n_i'', n_k'' | \frac{\partial V}{\partial Q_\ell} Q_\ell | \psi_o^+, n_i', n_k' \rangle ,$$

where E_o', E'' are the total energies of the initial and intermediate states. Before developing this matrix further one can write down the different possibilities that satisfy the restriction that energy must be conserved. For a Raman process,

$$n_i' = n_i - 1 \qquad n_k' = n_k + 1 \qquad h\nu_i - h\nu_k = h\nu_o = g\beta H$$
$$n_i' = n_i + 1 \qquad n_k' = n_k - 1 \qquad h\nu_k - h\nu_i = h\nu_o = g\beta H$$

are the only possibilities. In these cases one phonon is created and another is destroyed. Since $\nu_i > \nu_k$ and $\nu_k > \nu_i$ for the first and second cases respectively, one sees that they are really the same, and only one of them has to be retained.

Using

$$n_i' = n_i - 1 \qquad n_k' = n_k + 1 \ ,$$

one may write down the simplified matrix element,

$$\langle \psi_o^-, n_i, n_k | H' | \psi_o^+, n_i-1, n_k+1 \rangle =$$

$$\sum_{j,\ell} \{ \frac{1}{(E_o^+ - E_1^+ - h\nu_i)} \langle \psi_o^- | \frac{\partial V}{\partial Q_j} | \psi_1^+ \rangle \langle \psi_1^+ | \frac{\partial V}{\partial Q_\ell} | \psi_o^+ \rangle \langle n_i | Q_j | n_i-1 \rangle \langle n_k | Q_\ell | n_k+1 \rangle$$

$$+ \frac{1}{(E_o^+ - E_1^- + h\nu_k)} \langle \psi_o^- | \frac{\partial V}{\partial Q_j} | \psi_1^- \rangle \langle \psi_1^- | \frac{\partial V}{\partial Q_j} | \psi_o^+ \rangle \langle n_k | Q_\ell | n_k+1 \rangle \langle n_i | Q_j | n_i-1 \rangle \} .$$

Taking the time and transposed conjugate of the matrix element

$$\langle \psi_o^- | \frac{\partial V}{\partial Q_\ell} | \psi_1^- \rangle \langle \psi_1^- | \frac{\partial V}{\partial Q_j} | \psi_o^+ \rangle$$

and demanding it to be Hermitian, one finds that

$$\langle \psi_o^- | \frac{\partial V}{\partial Q_\ell} | \psi_1^- \rangle \langle \psi_1^- | \frac{\partial V}{\partial Q_j} | \psi_o^+ \rangle = - \langle \psi_o^- | \frac{\partial V}{\partial Q_j} | \psi_1^+ \rangle \langle \psi_1^+ | \frac{\partial V}{\partial Q_\ell} | \psi_o^+ \rangle .$$

In spite of this change of sign, the sum will not vanish, due to the difference in energy denominators ("Van Vleck cancellation") (32). The denominators can be rewritten,

$$E_o^+ - E_1^+ - h\nu_i = -\Delta_{10} + (g_o - g_1) \frac{\beta H}{2} - h\nu_i$$

$$E_o^+ - E_1^- + h\nu_k = -\Delta_{10} + (g_o + g_1) \frac{\beta H}{2} + h\nu_k .$$

Hence

$$\langle \psi_o^-, n_i, n_k | H' | \psi_o^+, n_i-1, n_k+1 \rangle =$$

$$\sum_{j,\ell} \langle \psi_o^- | \frac{\partial V}{\partial Q_i} | \psi_1^+ \rangle \langle \psi_1^+ | \frac{\partial V}{\partial Q_\ell} | \psi_o^+ \rangle \langle n_i | Q_j | n_i-1 \rangle \langle n_k | Q_\ell | n_k+1 \rangle \left\{ \frac{h(\nu_i + \nu_k)}{\Delta_{10}^2 - h\nu_i h\nu_k} \right\}$$

where

$$h(\nu_i - \nu_k) = g_o \beta H$$

has been used (energy conservation), and

$$g_o \beta H,\ g_1 \beta H << h\nu_i$$

is assumed. On making the substitution

$$Q_j = \sum_m b_{jm}\, \omega_m^{1/2} \left[q_m^+ + q_m^- \right]$$

$$Q_k = \sum_n b_{kn}\, \omega_n^{1/2} \left[q_n^+ + q_n^- \right]$$

and summing over m, n one finds

$$\langle n_i | Q_j | n_i - 1 \rangle = b_{ji}\, \omega_i^{1/2}\, n_i^{1/2}$$

$$\langle n_k | Q_\ell | n_k + 1 \rangle = b_{\ell k}\, \omega_k^{1/2} \sqrt{n_k + 1}$$

so that

$$\langle \psi_o^-, n_i, n_k | H' | \psi_o^+, n_i - 1, n_k + 1 \rangle =$$

$$\sum_{j\ell} \langle \psi_o^- | \frac{\partial V}{\partial Q_j} | \psi_1^+ \rangle \langle \psi_1^+ | \frac{\partial V}{\partial Q_\ell} | \psi_o^+ \rangle b_{ji} b_{\ell k}\, \nu_i^{1/2} \cdot \nu_k^{1/2} \cdot \frac{1}{2\pi} \sqrt{n_i}\, \sqrt{n_k + 1}\, \frac{h(\nu_i + \nu_k)}{\Delta_{10}^2 - h^2 \nu_i \nu_k}$$

At this point one assumes that the Debye energy $k\Theta$ is small compared to Δ_{10}, so that $h^2 \nu_i \nu_k << \Delta_{10}^2$. Also the difference between ν_i and ν_k can be neglected, and one can sum over all possible ν_i, ν_k.

$$\sum_{ik} | \langle \psi_o^-, n_i, n_k | H' | \psi_o^+, n_i - 1, n_k + 1 \rangle =$$

$$\int_{\nu=0}^{\nu = k\Theta/h} d\nu \, \rho(\nu)\rho(\nu) \frac{\nu^2}{4\pi^2} \left(\frac{2h\nu}{\Delta_{10}^2} \right)^2 \left(\frac{1}{e^{h\nu/kT} - 1} \right) \left(\frac{e^{h\nu/kT}}{e^{h\nu/kT} - 1} \right)$$

$$\times \Big| \sum_{j\ell} \langle \psi_o^- | \frac{\partial V}{\partial Q_j} | \psi_1^+ \rangle \langle \psi_1^+ | \quad \frac{\partial V}{\partial Q_\ell} | \psi_o^+ \rangle \Big|^2 \cdot \left(\frac{\pi r^2 h}{36 M v^2} \right)^2$$

where the density of states has been put in twice (once for i and once for k), thermal equilibrium occupation numbers have been used, and the b_{ij}'s have been replaced by their average values, as was done for the direct process. Assuming, as before, that $W_{+\to -} \cong W_{-\to +}$, one has the expression for the spin-lattice relaxation time,

$$1/T_{1R} = \frac{8\pi^4 h^2 r^4 V^2}{9 v^{10} \Delta^4 M^2} \int_0^{\Theta k/h} \nu^8 \, e^{h\nu/kT} \left[e^{h\nu/kT} - 1 \right]^{-2} d\nu$$

$$\times \Big| \sum_{j\ell} \langle \psi_o | \frac{\partial V}{\partial Q_j} | \psi_1 \rangle \langle \psi_1 | \frac{\partial V}{\partial Q_\ell} | \psi_o \rangle \Big|^2,$$

where R indicates the Raman process. At low temperatures $T \ll \Theta$, and one may make the approximations:

$$\Theta k/h \to \infty$$

$$e^{h\nu/kT} \left[e^{h\nu/kT} - 1 \right]^{-2} \to e^{-h\nu/kT}$$

and the standard integral

$$I_n = \int_o^\infty \nu^n e^{-h\nu/kT}\, d\nu = n!\ (kT/h)^{n+1}$$

can be used. For the present case n = 8, and the relaxation time is given by

$$1/T_{1R} = \frac{8\cdot 8!\,\pi^4 h^2 r^4}{9\, v^{10}\, \Delta_{10}^4} \cdot \left(\frac{V}{M}\right)^2 \cdot \left(\frac{k}{h}\right)^9 \Big| \sum_{jl} \langle \psi_o^- | \frac{\partial V}{\partial Q_j} | \psi_1^+ \rangle \langle \psi_1^+ | \frac{\partial V}{\partial Q_l} | \psi_o^+ \rangle \Big|^2 \cdot T^9.$$

Since the matrix elements are not a function of temperature and/or frequency, one has the important result (8.32).

$$1/T_{1R} \sim T^9.$$

Using the term quadratic in Q with first order perturbation theory and the Zeeman corrected wavefunctions given in Part 2, one may perform an analysis similar to that used for the direct process. This leads to the following relationship for the relaxation time

$$1/T_{1R} \sim \nu^2 T^7$$

For a non-Kramers salt, the T^9 term is negligible and the T^7 term is no longer a function of ν because transitions are possible without Zeeman mixing.

Orbach (32), in referring to the $\nu^2 T^7$ term, concludes that is may have considerable effect on the relaxation time if the excited state Kramers doublets are close to one

another ; but in the present case $\Delta_{21} \cong 300\text{cm}^{-1} >> kT$, so that the $\nu^2 T^7$ term is probably negligible.

The possibility of making numerical calculations of the Raman relaxation time is even smaller here then was the case for the direct region, due to the increased dependence on the velocity of sound and the crystal field splitting, the lack of knowledge of the excited state wavefunctions, and the added complication of two possible mechanisms. By using the analogy to Ti^{3+}, Bray et al. (12) performed a rough numerical estimate and found,

$$\frac{1}{T_{1R} \cdot T^9} \cong 0.01 \text{ to } 0.1 \text{ sec}^{-1} \text{ (degrees K)}^{-9} .$$

APPENDIX II: DESCRIPTION OF THE MICROWAVE SPECTROMETER

A. THE MICROWAVE SYSTEM

1. L-Band

A block diagram of the L-band spectrometer is shown in Figure 5, page 35. The microwave circuit is self explanatory except for certain features which are described below.

A General Radio Unit Oscillator (type 1218-A), which used a 5675 pencil triode as its oscillator tube, served as the CW oscillator. The frequency range was 0.9 - 2.0 Gc/s with an output power of approximately 200 mw into a 50 ohm load. The frequency drift after two hours of operation was quoted to be 2.10^{-7} per minute.

A 6BM6 klystron in an AMERAC type 198-A cavity was used as a local oscillator. The frequency range was 0.9-2.1 Gc/s, and the output power, 50-100 mw.

The local oscillator was "locked" to the CW oscillator with a Hallicrafters SA-27A FM receiver used as an IF amplifier and discriminator, followed by a DC amplifier whose output was applied to the reflector of the klystron. A schematic of the DC amplifier is shown in Figure 21.

Because the IF frequency in the spectrometer was close to the sound carrier of television Channel 2, it was necessary to

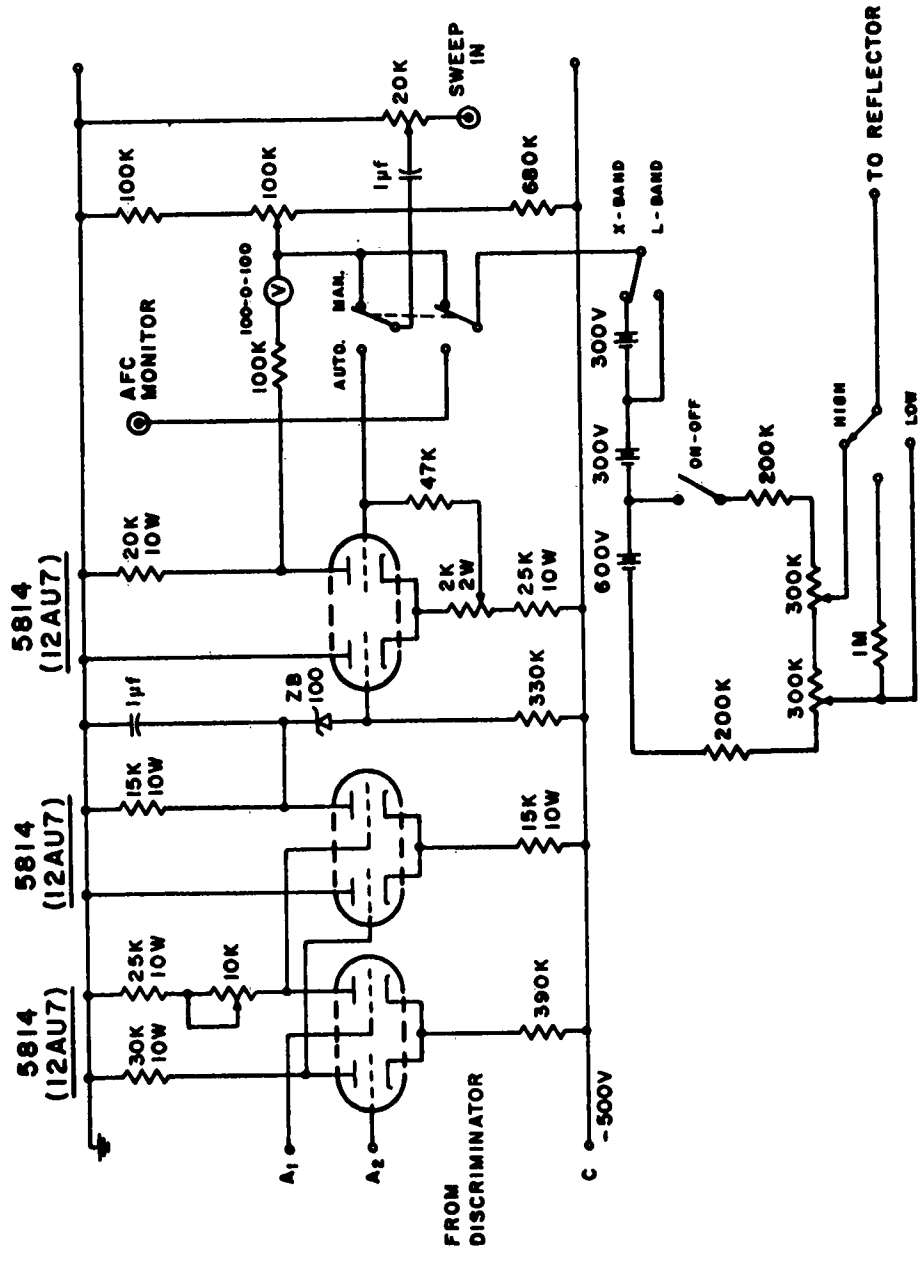

FIGURE 21: LOCAL OSCILLATOR STABILIZATION CIRCUIT.

realign the IF amplifier to 63 Mc/s, where the interference was found to be small.

A 2C36 triode in an AMERAC type 192B5 cavity was used as the driver for the pulse power. The output power was approximately 100 mw in the frequency range 1.5 - 1.9 Gc/s. A schematic of the pulsing circuit is shown in Figure 22.

The output from the pulsed triode was amplified in an ITT traveling wave tube amplifier (type F6868), with a nominal output power of about 20w in the frequency range 1.8 - 2.4 Gc/s. The traveling wave tube was also pulsed by applying approximately 450 volts to its current controlling electrode. The pulsing circuit is shown in Figure 23. A 25 volt power supply and a IN649 diode were provided to allow adjustment of the bias voltage on the traveling wave tube for minimum helix current in its "on" condition. A separate pulsed source, rather than the CW oscillator itself, was used to obtain pulse power, due to the relatively large leakage through the traveling wave tube amplifier in its "off" condition.

To be able to reduce the power incident on the mixer crystal and IF amplifier during the pulse, a bucking arrangement was used. The microwave circuit consisted of a 3db bidirectional coupler, a variable attenuator, and a sliding short circuit. A similar bucking arrangement was used in the CW monitoring circuit, to allow separation of absorption and dispersion. Here, a 15 db bidirectional coupler was used.

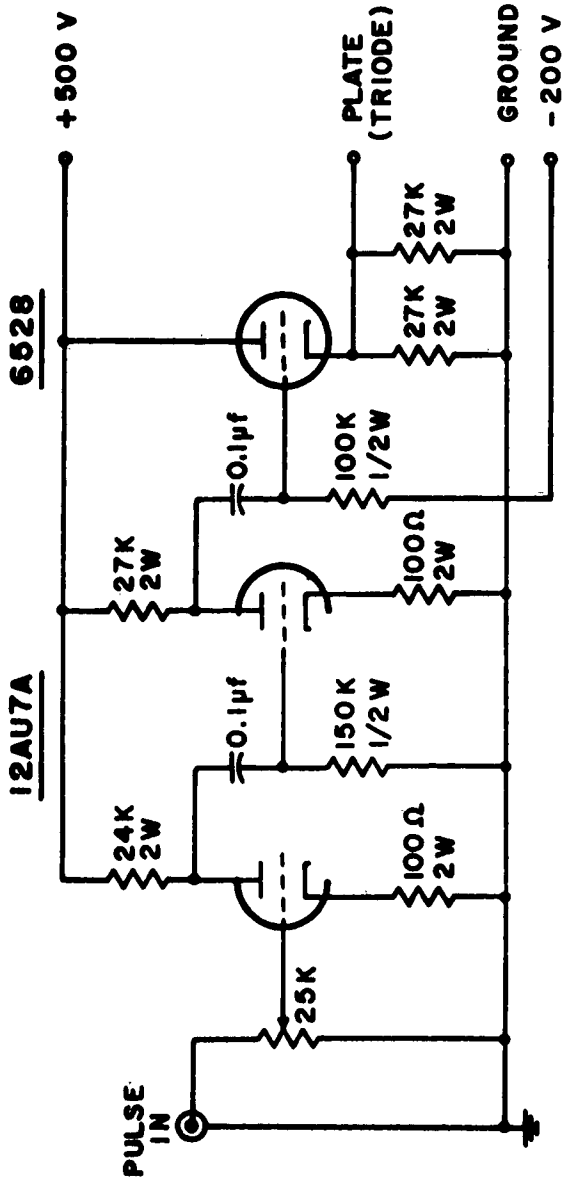

FIGURE 22: TRIODE PULSING CIRCUIT.

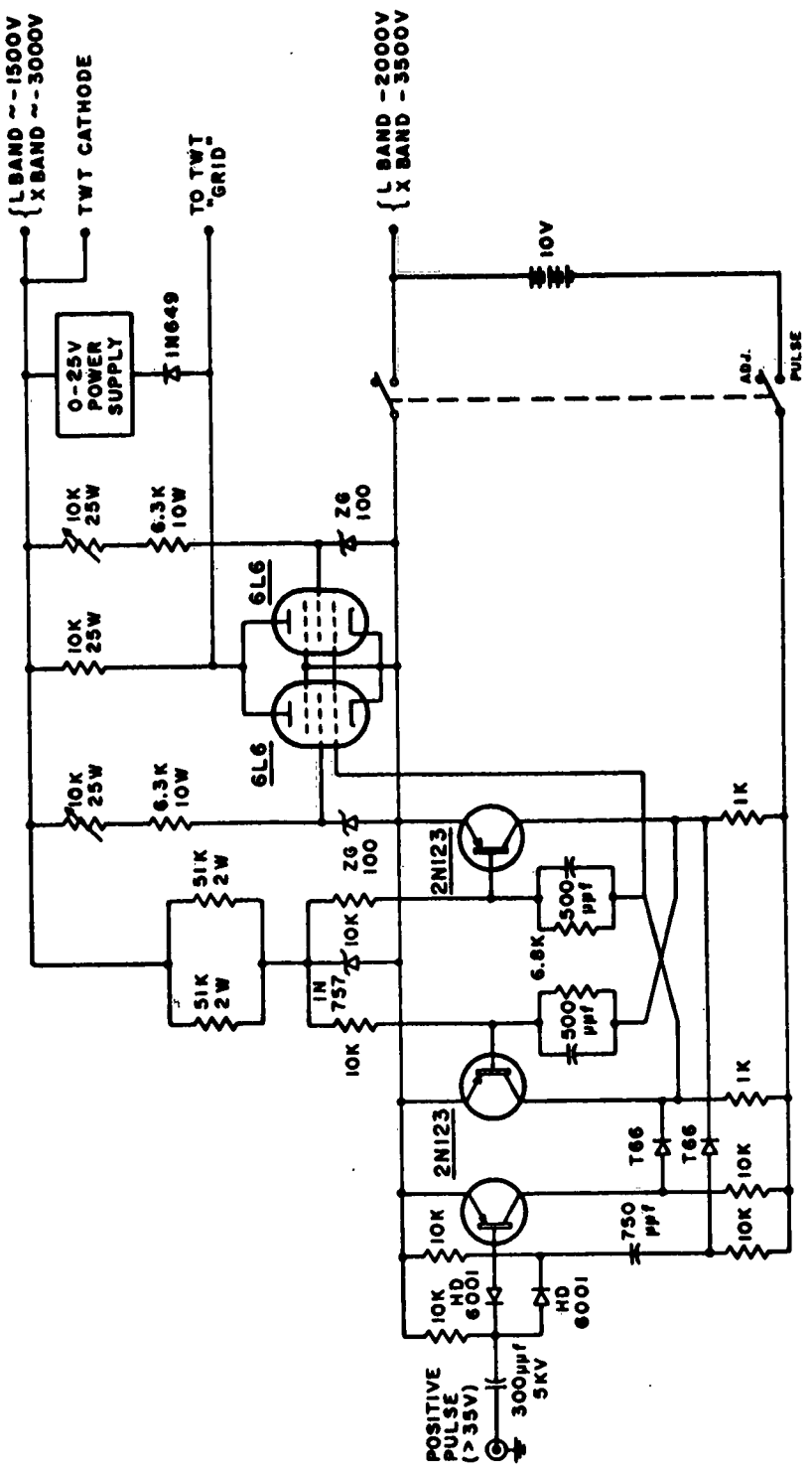

FIGURE 23: TWT PULSING CIRCUIT.

A Hewlett-Packard UHF Signal Generator (Model 614-A) could be coupled into the microwave circuit at various places for purposes of alignment.

2. X-Band

The stalo circuit shown in Figure 24 was used as the CW oscillator and as a driver for the pulsed power. Part of the output from the traveling wave amplifier tube (ITT type D-2037) was fed back to the input through a DeMornay Bonardi transmission wavemeter (type DB6-715-3). With proper adjustment of phase and attenuation, oscillation was obtained. The frequency stability of the system was not measured, but was found to be adequate.

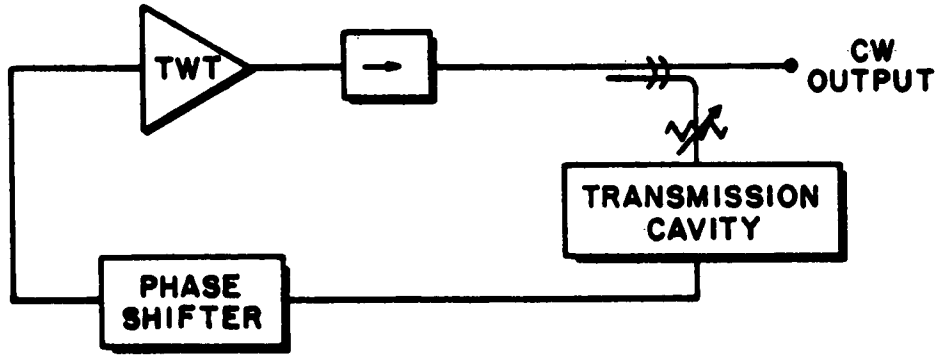

FIGURE 24: X-BAND STALO.

A Varian X-13 klystron was used as a local oscillator and was "locked" to the CW oscillator with the same arrangement used for L-Band. An additional X-13 klystron could be coupled into the microwave circuit for purposes of alignment.

An ITT traveling wave amplifier tube, (type F 6996), with an output power of approximately 10w in the frequency range 8.0 - 9.6 Gc/s, was used for the pulsed power.

B. DETECTION SYSTEM

1. Relaxation Measurements

At L-Band the microwave power was detected with a 1N21 F crystal in an unbalanced mixer (a 1N23 E crystal was used at X-Band). The output of the mixer was fed through an impedance transformer and current monitor to an IF amplifier, as shown in Figure 25. A Remanco model R-610 IF amplifier with a nominal noise figure of 2db was used. Despite the microwave bucking circuit mentioned earlier, the intense microwave pulse saturated the IF amplifier, and recovery to full gain required upward of a millisecond. To reduce the recovery time, a blanking pulse was introduced into for the cathodes of the first, second, fourth, and fifth tubes of the amplifier. It was found that the best result was obtained with simultaneous blanking of the second and fourth tubes. With this precaution the IF amplifier recovered

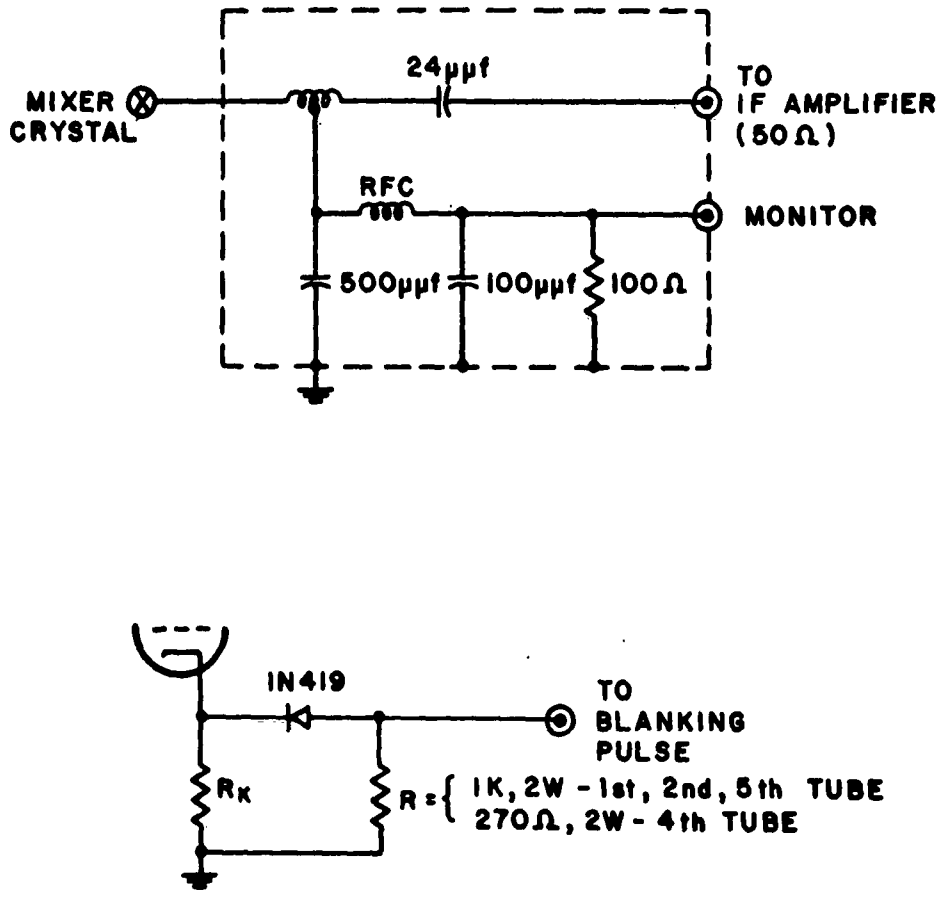

FIGURE 25: IMPEDANCE TRANSFORMER, CURRENT MONITOR AND BLANKING ARRANGEMENT FOR REMANCO IF AMPLIFIER.

long before the first measurement (~ 50 microseconds after inversion) could be taken. The blanking circuit is shown in Figure 25.

The output from the IF amplifier and second detector was passed through a low-pass filter to the display oscilloscope. A Tektronix 585 oscilloscope with a 53B or type H wide band plug-in preamplifier was used.

2. CW Measurements

A block diagram of the system used for conventional CW measurements of absorption spectra is given in Figure 26. Schematic diagrams of the components are given in Figure 27. Since this system was entirely conventional it will not be discussed further.

C. CAVITIES (46)

The cavity used at L-band was of rectangular coaxial type and was made of Hysol 4285 cast epoxy resin and silver plated (47). In this way the rapid field sweeps required for inversion could be obtained without significant eddy current losses. To reduce helium bubbles in the cavity while at the same time allowing good circulation of liquid helium around the sample, a shaped insert of foam was used to divert the bubbles away from regions of strong E field and out through holes cut in the cavity walls.

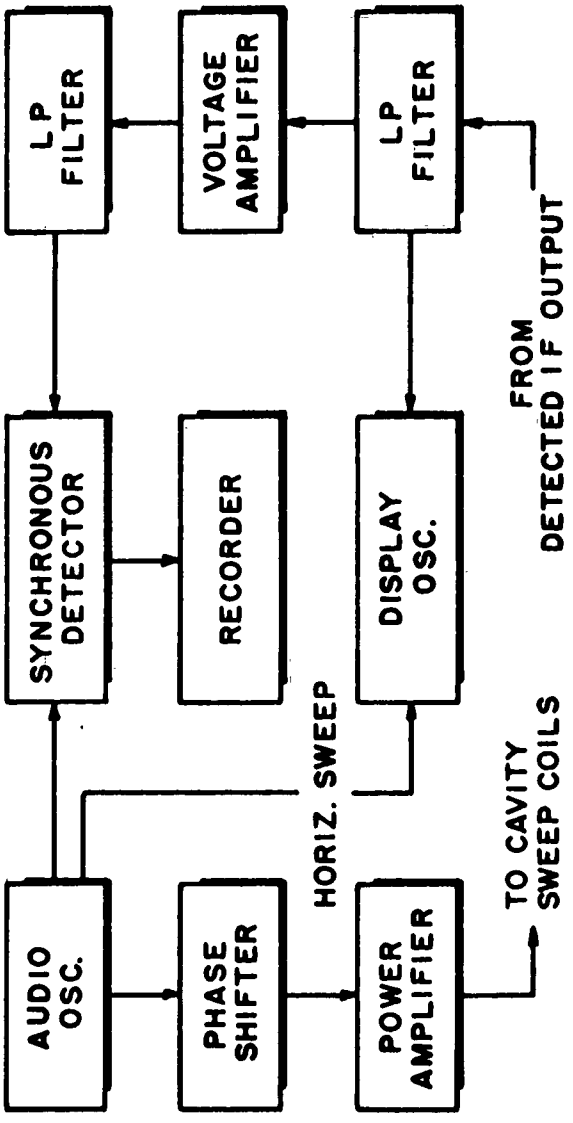

FIGURE 26: SYNCHRONOUS DETECTION SYSTEM.

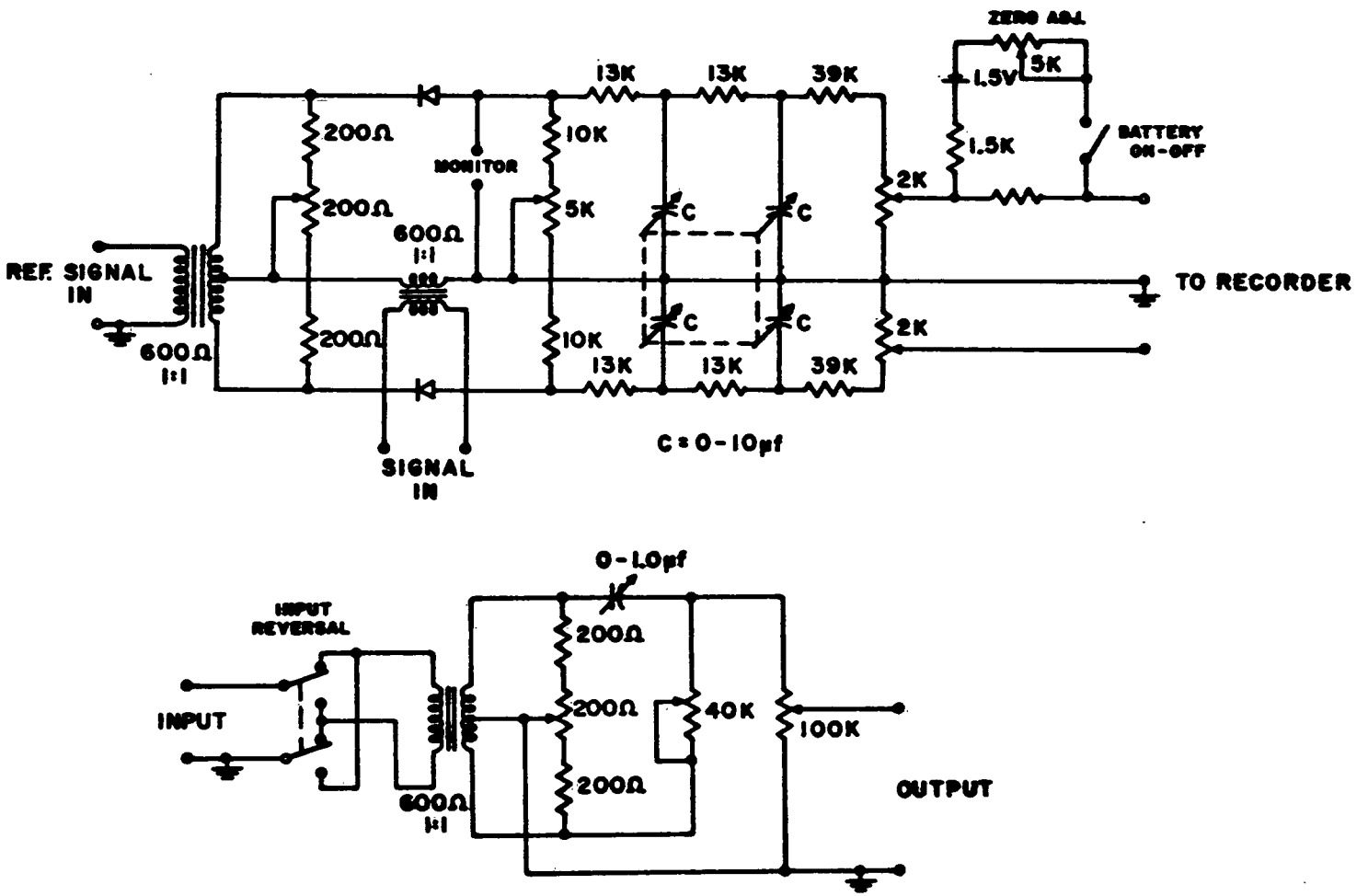

FIGURE 27: PHASE SHIFTER, SYNCHRONOUS DETECTOR AND LOW PASS FILTER.

A pair of Helmholtz coils was attached to the cavity to obtain the requisite field sweep. A current of 1/4 amp through the coils effected a field sweep of about 50 Gauss.

The cavity was resonant at 1.82 Gc/s at $4^{\circ}K$ and had provision for variable coupling. A cross-section of the cavity and Helmholtz coils is shown in Figure 28, and a photograph of the cavity is shown in Figure 29.

The X-band cavity, of rectangular type, was operated in the TE_{102} mode and was made of the same material and treated in the same way as the L-band cavity already described. The cavity was resonant at 8.535 Gc/s at $4^{\circ}K$, and had provisions for variable coupling; however, the coupling could only be changed when the cavity was outside the cryostat. Figure 30 shows a photograph of the X-band cavity.

D. FIELD SWEEP AND PULSING ARRANGEMENT

The pulsing arrangement is included in the block diagram of the spectrometer shown in Figure 5, page 35. Since most of the apparatus and circuits used were conventional, only a brief description will be given.

A Tektronix Type 162 waveform generator was used as the master synchronizing pulse generator. The output was used

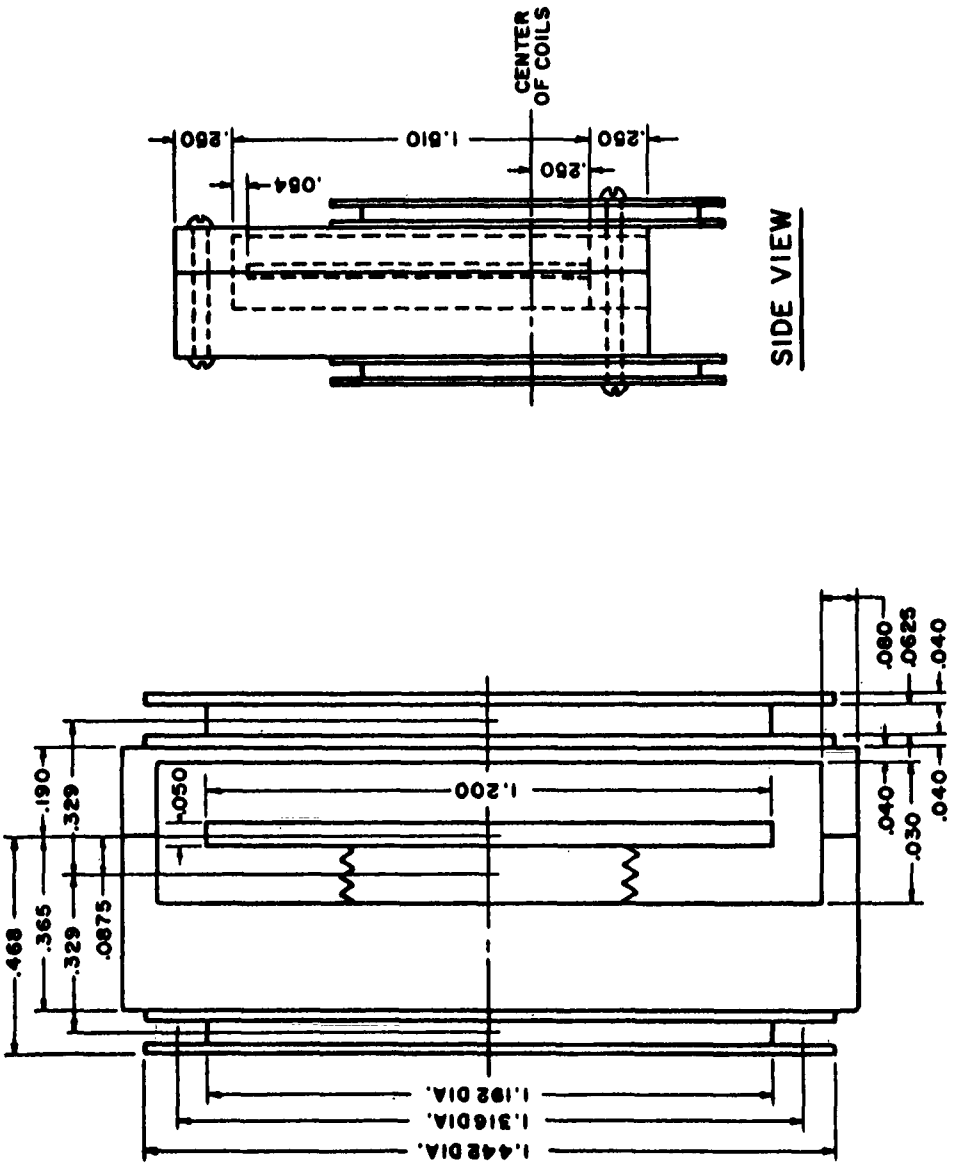

FIGURE 28: CROSS SECTION OF L-BAND COAXIAL CAVITY.

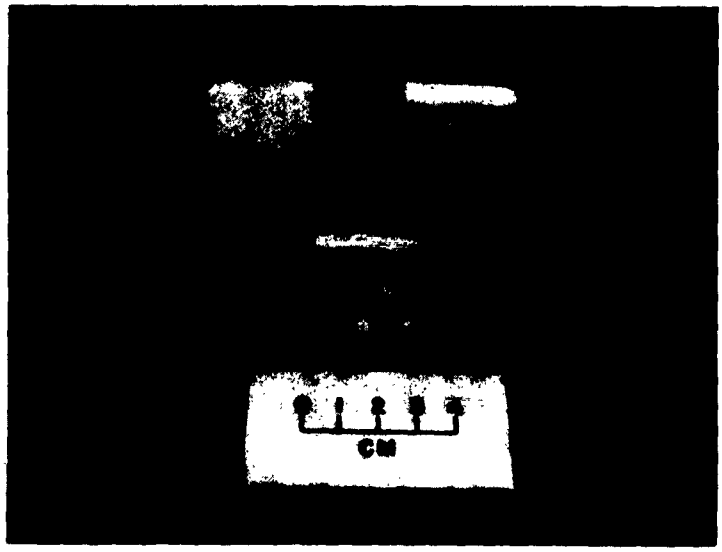

FIGURE 29: L-BAND CAVITY.

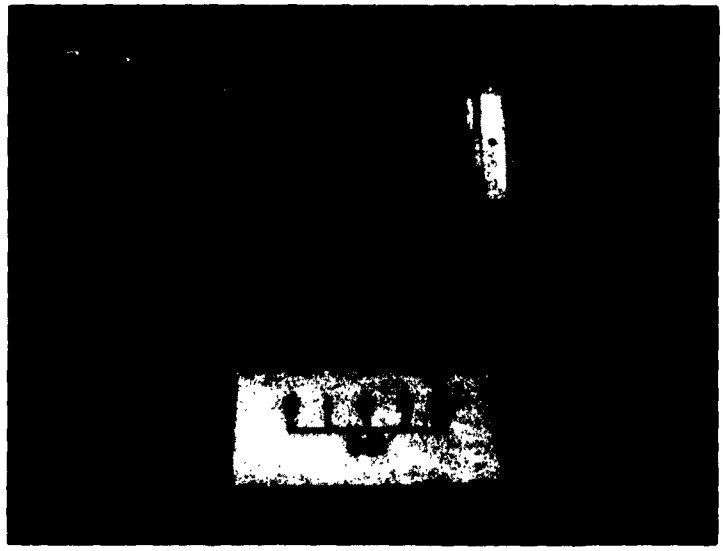

FIGURE 30: X-BAND CAVITY.

to trigger a Tektronix Type 161 Pulse Generator, used as a delay circuit, and also the display oscilloscope. The delayed trigger was fed through an N/2 divider to a Rutherford Model B-7 Pulse Generator. A Tektronix Type 163 Pulse Generator was used as the driver for the TWT pulsing circuit of Figure 23.

Another Tektronix Type 163 Pulse Generator was used as the field sweep driver and was triggered through an "or" gate, first by the master synchronizing pulse generator and second by a delayed trigger from the oscilloscope. The output of the unit was fed through an inverter, emitter follower, and a commercial constant current generator, to the field sweep amplifier. A schematic of the field sweep amplifier is shown in Figure 31.

In most cases, time was measured by means of the "delay time" calibration of the 585 oscilloscope. This instrument had been calibrated within the last year by the manufacturer. For spin-lattice times exceeding 10 seconds, time was measured from the repetition rate of a Tektronix type 162 waveform generator. This time base agreed with that of the oscilloscope to within 2%.

E. MAGNET

A Varian 12 inch Electromagnet (Model V-4012-3B) was used for the Zeeman field. The magnet was calibrated with a nuclear magnetic resonance Fluxmeter (Perkin-Elmer Numar Model M2). A Field Scanning unit (Varian type B-4280A) was used for CW measurements.

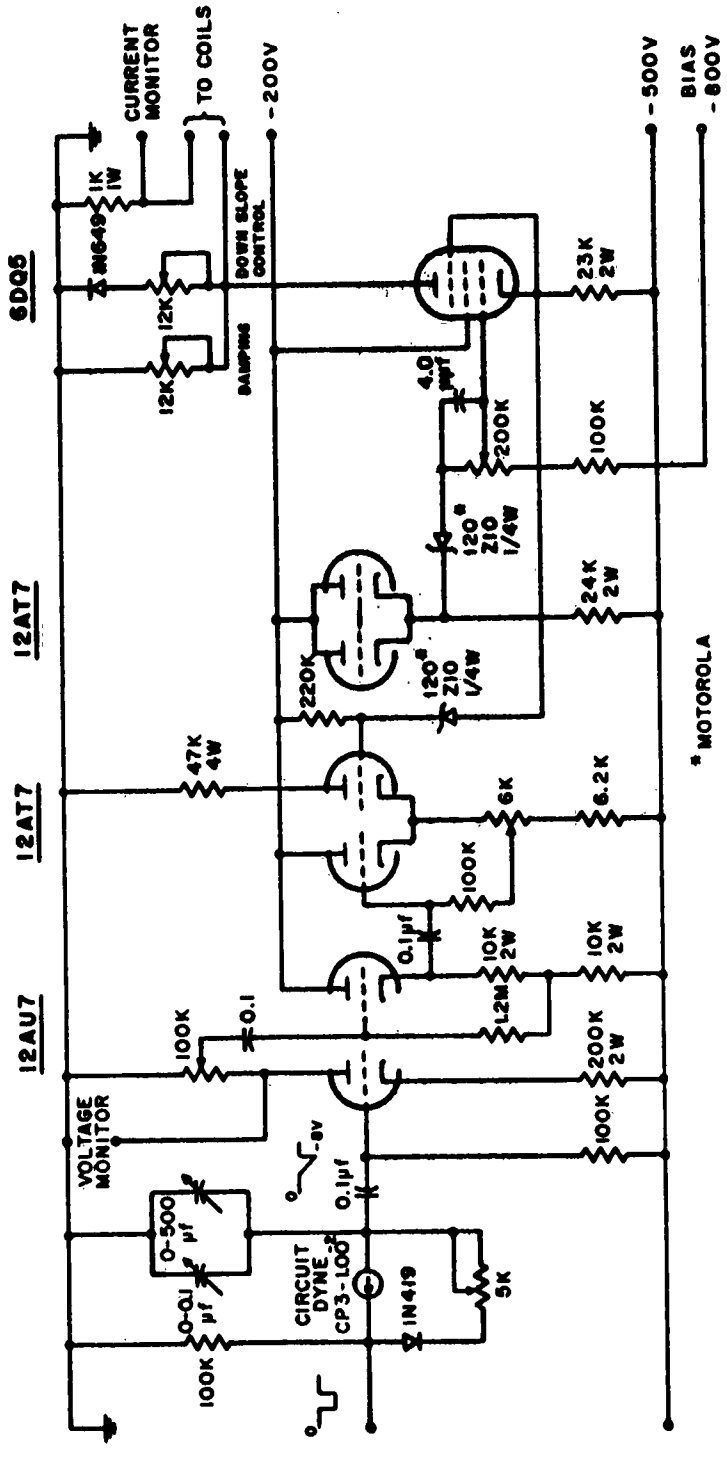

FIGURE 31: FIELD SWEEP AMPLIFIER.

F. TEMPERATURE CONTROL

A nominal 56 ohm Allen Bradley 1w carbon resistor was used as the sensor in conjunction with a modified Brown Amplifier (model 356413-1). The output from the amplifier was used to drive a servo motor that in turn drove a potentiometer. The potentiometer was used to add a controlled amount of heat to the liquid helium bath. The temperature control circuit is shown in Figure 32.

Roughly 5 milliwatts were required to achieve temperature stability in helium II; but considerably more heat was needed above the λ-point, where the limited thermal conductivity of the bath created a rather serious time lag in the control loop. It was discovered near the end of the experiment that the use of gaseous-rather than liquid-helium would allow adequate cooling for the sample. Because of the more favorable ratio of thermal conductivity to heat capacity, the gas would probably have been far superior as a heat exchange medium.

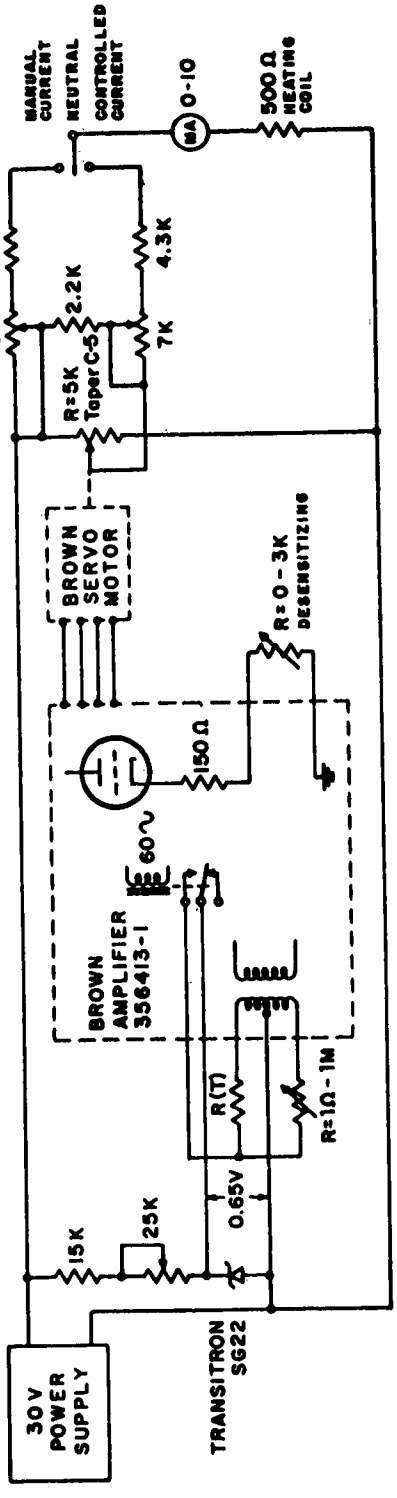

FIGURE 32: TEMPERATURE CONTROL.

BIBLIOGRAPHY

1. Zavoisky ; E., J. Phys. (USSR) 9, 211 (1945) and 10, 197, (1946).

2. Waller, I., Zeits f. Physik, 79, 370, (1932).

3. Gorter, C. J., Physica 3, 503, (1936).

4. Casimir, H. B. G., and DuPré, F. K., Physica 5, 507, (1938).

5. Casimir, H. B. G., Physica, 6, 156, (1939).

6. Kronig, R. DeW., Physica 6, 33, (1939).

7. Van Vleck, J. H., J. Chem. Phys. 7, 72, (1939).

8. Van Vleck, J. H., Phys. Rev. 57, 426, (1940).

9. Baker, J. M., Bleaney, B., and Bowers, K. D., Proc. Phys. Soc. (London) B69, 1205, (1956).

10. Bleaney, B., and O'Brien, M. C. M., Proc. Phys. Soc. (London) B69, 1216, (1956).

11. Paxman, D. H., Proc. Phys. Soc. (London) 78, 180, (1961).

12. Bray, T. M, Brown, G. C., and Kiel, A., Phys. Rev. 127, 730, (1962).

13. Artman, J. O., Murphy, J. C., Kohn, J. A., and Townes, W. D., Phys. Rev. Letters, 4, 607 (1960).

14. Honig, A., and Stupp, E., Phys. Rev. Letters 1, 275 (1958), and Phys. Rev. 117, 69, (1960).

15. Feher, G., and Gere, E. A., Phys. Rev., 114, 1245, (1959).

16. Wilson, D. K., and Feher, G., Phys. Rev. 124, 1068, (1961).

BIBLIOGRAPHY CONTD

17. Van Vleck, J. H., Phys. Rev., 59, 724, (1941).

18. Strandberg, M. W. P., Phys. Rev. 110, 65, (1958).

19. Castle, J. G., Jr., Chester, P. F., and Wagner, P. E., Phys. Rev., 119, 953, (1960).

20. Scott, P. L., and Jeffries, C. D., Phys. Rev., (to be published).

21. Ruby, H. B., Benoit, H., and Jeffries, C. D., Phys. Rev., (to be published).

22. Feher, G., Bell Tech. Jour. 36, 449, (1957).

23. Davis, C. F., Jr., Strandberg, M. W. P., and Kyhl, R. L., Phys. Rev., 111, 1268, (1958).

24. Bethe, H. A., An.d. Physik 3, 133 (1929).

25. Bleaney, B., and Stevens, K. W. H., Repts. Progr. in Phys. (London), 16, 108, (1953).

26. Bowers, K. D., and Owen, J., Repts. Progr. in Phys. (London), 18, 304, (1955).

27. Griffith, J. S., The Theory of Transition-Metal Ions, Cambridge U. Press. (1961).

28. Low, W., Paramagnetic Resonance in Solids, Academic Press, New York, and London (1960).

29. Kramers, H. A., Proc. Amsterdam Acad. Sci., 33, 959, (1930).

30. Gorter, C. J., Paramagnetic Relaxation, Elsevier Publishing Co., Inc., New York, London, Amsterdam, and Brussels, (1947).

31. Orbach, R., Proc. Phys. Soc. (London), 77, 821, (1961).

BIBLIOGRAPHY CONTD

32. Orbach, R., Proc. Royal. Soc. (London), A264, 458, (1961).

33. Finn, C. B. P., Orbach, R., and Wolf, M. W. P., Proc. Phys. Soc. (London), 77, 261, (1961).

34. Townes, C. H., Quantum Electronics, Columbia U. Press, New York, p. 392-409, (1960)

35. Singer, J. R., Advances in Quantum Electronics, Columbia U. Press, New York and London, p. 373-403, (1961).

36. Altshuler, S. A., Bull. Acad. Sci. USSR Phys. 20(11), 1207, (1956).

37. Bloembergen, N., Purcell, E. M., and Pound, R. V., Phys. Rev. 73, 679, (1948).

38. Portis, A. M., Phys. Rev., 91, 1071, (1953).

39. Bloch, F., Phys. Rev., 70, 460, (1946).

40. Redfield, A. G., Phys. Rev., 98, 1787 (1955).

41. Rannestad, A., and Wagner, P. E., Bull. Am. Phys. Soc. 7, 450, (1962).

42. Bloom, S., J. Appl. Phys. 28, 800, (1957).

43. Kiel, A., Private Communication.

44. Klemens, P. G., Solid State Physics, Vol. 7, Academic Press, New York, (1958).

45. Kiel, A., The Interaction of Paramagnetic Ions with Lattice Vibrations, The Johns Hopkins University, Dissertation (1961).

46. Chester, P. F., Wagner, P. E., Castle, J. G., Jr., and Conn, G., Rev. Sci. Instr. 30, 1127, (1959).

47. The procedure described in Millimeter Wave Research, Final Report, No. 24261-15, October 1, 1955, Bell Telephone Laboratories Inc. was used with small modifications.

BIBLIOGRAPHY CONTD

48. Rimai, L., Statz, H., Weber, M. J., deMars, G. A. and Koster, G. F. Phys. Rev. Letters 4, 125, (1960).

49. Weber, M. J., Rimai, L., Statz, H., and deMars, G. A., Bull. Am. Phys. Soc. 6, 141, (1961).

10 ASTIA
Arlington Hall Station
Arlington 12, Virginia

ASD
Wright-Patterson AFB, Ohio
1 Attn: ASAPRL
1 ASAPT
1 ASNC
1 ASND
1 ASNG
1 ASNPVD-1
1 ASNPVD-2
1 ASNR
1 ASNS
1 ASNSED
1 ASNV
1 ASNX
1 ASNY
1 ASDRC(Mr. Catanzarite)
1 ASRC
1 ASRE
1 ASRNET-3
1 ASRNGE
1 ASRNOO
1 ASRNC (Mr. Stimmel)
1 ASRNC (Major Novak)
2 ASRNCC-1
1 ASRNCC-2
1 ASRNET-1
2 ASRNCF-1
2 ASRNGW-2
1 ASRNRS
1 ASRNRS-3
1 ASROO
1 ASRSSE-2
1 ASTFPE (Captain Gregory)
1 ASOQ (Gp Captain Fletcher)

RADC
Griffiss AFB, New York
1 Attn: RAD, Dr. Irving J. Gabelman
1 RALC (J. E. Cruickshank)
1 RALSS (M. A. Diab)
1 RAUAA (John P. Huss)
1 RAUAT
1 RAUMA (C.R. Miller)
1 RAUMM
2 RAWE
1 RAWEC
1 RAWES
2 RAWI

AFSC
Andrews AFB
Washington 25, D. C.
1 Attn: SCTAN
1 SCRC (Lt. Col. Thompson)

HQ. USAF
Washington 25, D.C.
1 Attn: AFRDR-IN (Lt. Col. Pinson)
1 AFOOR-SV-ES (Lt. Col. Smith)
1 AFORQ-SA (Lt. Col. Ragsdale)
1 AFMPP-EQ (Lt. Col. Manbeck)
1 AFORQ-AD

1 USAFSS (ODC-R)
San Antonio, Texas

2 PACAF (PFESE-E)
APO 953
San Francisco, California

2 USAFE (DCS/Ops)
APO 633
New York, New York

1 3535th NTW
Attn: Electronic Warfare Familiarisation Course
Mather AFB, Calif.

1 TAC (OA)
Langley AFB, Virginia

1 DCAS (DCLMT/TDC)
AF Unit Post Office
Los Angeles 45, Calif.

SAC
Offutt AFB, Nebr.
1 Attn: DORQP
1 DOPLT

1 AFMDC (MDRRF-1)
Holloman AFB, N.M.

1 Air University Library (AUL-6234)
Maxwell AFB, Ala.

2 9AF (DOTR-FR (Capt. O. E. McCain)
Shaw AFB, S.C.

1 ADC (ADOOA)
Ent AFB, Colorado

1 Director
Weapons Systems Evaluation Group
Room 1E-875, The Pentagon
Washington 25, D. C.

10 Scientific and Technical Information Facility
Attn: NASA Representative (Code:S-AK/DL)
P.O. Box 5700
Bethesda, Maryland

1 Commanding Officer
U.S. Army Signal Research and Development Lab
Attn: SIGRA/SL-SE, Mr. I.O. Myers
Fort Monmouth, N. J.

1 Chief Signal Officer
Research and Development Division
Avionics and Surveillance Branch
Washington 25, D. C.

1 Assistant Secretary of Defense
Research and Development Board
Attn: Technical Library
Department of Defense
Washington 25, D. C.

1 Director
National Security Agency
Attn: C3/TDL
Fort George G. Meade, Md.

1 Army Ordnance Missile Command
Attn: ORDXM-RR, Hallowes, Jr.
Redstone Arsenal, Alabama

2 Commanding General
Army Ordnance Missile Command
Attn: ORDXM-RFE/Re-Entry Physics Section
Redstone Arsenal, Alabama

1 Commanding Officer
U.S. Army Signal Research and Development Lab.
Attn: SIGRA/SL-N-5, Dr. H. Bennett
Fort Monmouth, N.J.

1 Commanding General
White Sands Missile Range
Attn: ORDBS-OM-TL
New Mexico

2 Commanding Officer
Picatinny Arsenal
Attn: Tech. Information Section-ORDBB-VA6
Dover, New Jersey

1 USA Signal Electronic Research Unit
P.O. Box 205
Mountain View, Calif.

1 US Army Signal Corps School
Attn: DST, USASCS (Mr. Henry Allem)
Fort Monmouth, New Jersey

1 Chief of Naval Research
Attn: Code 427
Department of the Navy
Washington 25, D. C.

1 Commander
U.S. Naval Ordnance Laboratory
Attn: Eva Liberman, Librarian
White Oak, Silver Spring, Maryland

1 Director
Material Laboratory
New York Naval Shipyard
Brooklyn 1, N.Y.

1 Commander
U.S. Naval Missile Center
Attn: Technical Library, Code NO3022
Point Mugu, California

1 Commanding Officer
U.S. Naval Air Development Center
Engineering Development Laboratory
Attn: J. M. McGlone
Johnsville, Pa.

1 Commanding Officer
U.S. Naval Ordnance Laboratory
Attn: Code 74
Corona, California

1 Chief
Bureau of Naval Weapons
Department of the Navy
Attn: RRRE-2
Washington 25, D. C.

2 Director
U.S. Naval Research Laboratory
Attn: Code 2027
Washington 25, D. C.

1 Chief, Bureau of Ships
Attn: Code 335
Room 1532 Main Navy Building
Washington 25, D. C.

1 Airborne Instruments Laboratory
A Division of Cutler-Hammer Inc.
Attn: Library
Walt Whitman Road
Melville, Long Island, New York

1 Analytic Services Inc.
Attn: Library
1150 Leesburg Pike
Bailey's Crossroads, Virginia

2 The Johns Hopkins University
Applied Physics Laboratory
Attn: Mr. George L. Seielstad
8621 Georgia Avenue
Silver Spring, Maryland

1 Bjorksten Research Laboratories, Inc.
P.O. Box 265
Madison 1, Wisconsin

1 Cook Electric Company
Cook Technological Center Division
6401 W. Oakton Street
Morton Grove, Ill.

1 Electronic Communications, Inc.
Research Division
1830 York Road
Timonium, Maryland

1 General Dynamics/Fort Worth
A Division of General Dynamics Corporation
Attn: Chief Librarian
P.O. Box 748
Fort Worth 1, Texas

1 General Electric Company
Advanced Electronics Center
Attn: Library
Cornell University Industrial Research Park
Ithaca, New York

1 Grumman Aircraft Engineering Corp.
Engineering Library, Plant 5
Attn: M. O. Friedlander, Head Librarian
Bethpage, Long Island, New York

2 The Hallicrafters Company
Attn: Library
4401 West Fifth Avenue
Chicago 24, Illinois

1 HRB-Singer, Inc.
Attn: Library
Science Park Box 60
State College, Pa.

1 The University of Michigan
Institute of Science and Technology
Attn: IRIA
P.O. Box 618
Ann Arbor, Michigan

2 ITT Federal Laboratories
Div. International Telephone and Telegraph Corp.
500 Washington Avenue
Nutley, New Jersey

1 Jansky and Bailey
A Division of Atlantic Research Corp.
1339 Wisconsin Ave., N. W.

1 Massachusetts Institute of Technology
Lincoln Laboratory
Attn: Library
P.O. Box 73
Lexington 73, Massachusetts

1 Massachusetts Institute of Technology
Electronic Systems Laboratory
Attn: John E. Ward, RM 32-101
Cambridge, Massachusetts

1 Lockheed Georgia Company
Attn: Department 72-15
Marietta, Georgia

1 Martin Marietta Corporation
Martin Company Division
Attn: Science-Technology Library
Baltimore 3, Maryland

1 Mitre Corporation
Attn: Library
Bedford, Massachusetts

1 Motorola Inc.
Systems Research Laboratory
8330 Indiana Avenue
Riverside, California

2 North American Aviation, Inc.
Attn: Technical Library
International Airport
Los Angeles 9, California

1 Northrop Corporation
Norair Division
Attn: Technical Information, 3924-31
1001 E. Broadway
Hawthorne, Calif.

2 Radio Corporation of America
Defense Electronic Products, DSD
Attn: L. R. Hund, Librarian
8500 Balboa Blvd.
Van Nuys, Calif.

2 Raytheon Company
Attn: Librarian
P.O. Box 636
Santa Barbara, Calif.

1 Revere Copper and Brass Incorporated
Foil Division
Attn: Mr. Arthur Ferretti
196 Diamond Street
Brooklyn 22, New York

1 Stanford University
Stanford Electronics Laboratories
Attn: Security Officer
Stanford, California

1 Sylvania Electric Products Inc.
Technical Information Section
P.O. Box 188
Mountain View, California

1 The Ohio State University
Research Foundation
Attn: Dr. Curt A. Lewis
1314 Kinnear Road
Columbus 12, Ohio

1 The Rand Corporation
Attn: Library
1700 Main Street
Santa Monica, California

1 The University of Michigan
University Research Security Office
Attn: Dr. B. F. Barton, Director CEL
P.O. Box 622
Ann Arbor, Michigan

2 Thompson Ramo Wooldridge Inc.
Ramo Wooldridge Division
Attn: Technical Library
8433 Fallbrook Avenue
Canoga Park, California

1 Space Technology Laboratories, Inc.
STL Technical Library
Attn: Document Acquisitions Group
One Space Park
Redondo Beach, California

1 Unidynamics
Div. of Universal Match Corporation
Attn: Technical Library
4407 Cook Avenue
St. Louis 13, Missouri

1 Westinghouse Electric Corporation
Defense Center - Baltimore
Attn: Technical Information Center
P.O. Box 1693
Baltimore 3, Maryland